"Crosswell Seismic Amplitude-Versus-Offset for Detailed Imaging of Facies and Fluid Distribution within Carbonate Oil Reservoirs"

Final Report

Period Covered by Report: 09 September 2004 – 30 September 2008

Report authors: Wayne D. Pennington, Mohamed Ibrahim, Roger M. Turpening, Sean P. Trisch, Josh P. Richardson, Carol Asiala, and Walid Mabrouk

Date of Report: December 2008

DE-FC26-04NT15508

Principal Investigator: Wayne D. Pennington
Michigan Technological University
Department of Geological and Mining Engineering and Sciences
1400 Townsend Drive
Houghton, MI 49931

Disclaimer:

ABSTRACT

Crosswell seismic surveys were conducted at two fields in northern Michigan. One of these, Springdale, included two monitor wells that are located external to the reef, and the other, Coldspring, employed two production wells within the reef. The Springdale wells extended to much greater depths than the reef, and imaging was conducted from above and from beneath the reef.

The resulting seismic images provide the best views of pinnacle Niagaran reefs obtained to date. The tops of the reservoirs can be clearly distinguished, and their lateral extent or dipping edges can be observed along the profile. Reflecting events internal to the reef are evident; some of them are fairly continuous across the reef and others are discontinuous. Inversion of the seismic data indicates which events represent zones of higher porosity and which are lower porosity or even anhydrite plugged.

The full stacked image includes angles that are beyond critical for many of the interfaces, and some reflections are visible only for a small range of angles, presumably near their critical angle. Stacking these angles in provides an opportunity for these events to be seen on the stacked image, where otherwise they would have been unrecognized. For inversion, however, the complexity associated with phase changes beyond critical can lead to poor results, and elastic inversion of partial angle stacks may be best conducted with restrictions to angles less than critical.

Strong apparent attenuation of signals occurs when seismic ray paths pass through the upper part of the Springdale reservoir; this may be due to intrinsic attenuation and/or scattering of events due to the locally strongly varying gas saturation and extremely low fluid pressures. Signal-to-noise limitations become evident far from the source well in the Coldspring study, probably because the raw data were strongly affected by tube-wave noise generated by flow through the perforation of the receiver well.

The seismic images obtained, and interpretations of them, as assisted by Amplitude-versus-Angle studies and accompanying inversion, provide additional insight into the internal geometry of these two reefs and provide data that should be useful for reservoir management.

TABLE OF CONTENTS

EXECUTIVE SUMMARY

Crosswell seismic imaging has been tested in two fields in pinnacle reefs in northern Michigan. Conventional seismic imaging cannot provide more than an approximate extent of the reef, through the observation of an absence of reflectors due to de-tuning of events where the reef exists, and cannot provide any indication of features internal to the reef. Crosswell seismic imaging brings the seismic source and receivers closer to the reservoir, allowing for higher resolution.

The wide angles present in crosswell imaging provide additional information not present in typical surface-seismic acquisition. Instead of angles out to 30º or 40º, crosswell seismic acquisition includes angles from 35º to 90º, although the useful limit is usually less than 80º. For quite a few interfaces, this includes the critical angle. In some instances, the critical angle provides the only range in which a reflection can actually be observed above any reasonable background noise, and inclusion of these angles in a final stacked image can be very beneficial. However, beyond the critical angle, severe phase rotation of the wavelet occurs, and current processing techniques do not take this into account for Amplitude-versus-Angle (AVA) analysis. Therefore, for most detailed AVA studies, a restriction to narrower angles may be prudent.

In this study, we conducted, in essence, three tests at two fields. The Springdale site included source and receiver wells outside of the reef. These wells penetrated to much greater depths than the reef, so two experiments were conducted at once: imaging "from above" in which the seismic source and receiver locations were above the reflectors, and imaging "from beneath" with tool locations beneath the reflectors. The Coldspring site included source and receiver wells within the reef, providing much greater control over the seismic ties to well logs, in addition to gaining closer access to the target formation for imaging "from above". Both fields had been under production for many years, from undersaturated volumetric-drive oil reservoirs, in which the water table has not moved appreciably, but now highly gas-saturated in the original oil zone.

The ability to identify gross reservoir features was clearly demonstrated at both sites. The reservoir top is clear on all three data sets, and the reservoir extent is evident on both data sets at Springdale, where the entire reef was imaged between the wells, while a dipping reef top can be seen at Coldspring, where one well intercepted the reef near one edge. Many internal reflectors can be seen in all three data sets, although the image "from above" at Springdale is not as high-resolution as the one "from beneath". Inversion provides improved interpretation capability, whether conducted as "acoustic" inversion on a full-stack section or as elastic inversion on partial stacks. The full-stack inversion is, of course, not acoustic because of the wide angles involved, so the resulting image is referred to here as showing "apparent" impedances. As long as the angles included in the full stack do not include many critical angles from interfaces imaged, the resulting apparent impedance can be used as an indicator of, in these cases, porosity. That is, where the apparent impedance is low, porosity is high, and where apparent impedance is high, porosity is low, and even anhydrite plugged in the extreme cases.

Elastic inversion from partial stacks can be conducted on angle stacks that cover the full range acquired, or they can be restricted to limited ranges to avoid complexity from phase rotations beyond critical angles. The resulting images of acoustic impedance, shear impedance, Vp/Vs ratio, and density can be used to determine lithologic variations and porosity, and the results appear to be reasonable and useful for reservoir management.

The two fields were surveyed under different conditions, which led to different observations of signal-to-noise ratios. Springdale was observed from dedicated monitor wells that had no fluid flow, and the conditions were very quiet. 3000 Hz data was recorded at 2000 ft (600m) distance and final images contained 2000 Hz. The amplitudes of reflectors from within the reef were low, however, and especially so for the image obtained from above. We attribute this to attenuation and scattering of signal as it passes through the complex upper part of the reef, where gas saturation likely varies locally, reservoir pressure is extremely low, and structural complexity of the reef is evident. The image from beneath does not pass through this complexity and only experiences the gas saturation and low pressures at the upper edge of the image, allowing most of the image to be higher quality. At Coldspring, fluid flow through the perforations in the receiver well led to tube-wave noise that was high-amplitude and poorly organized, strongly affecting the quality of the raw data. After processing, the decrease in signal-to-noise ratio as distance increased away from the source well is apparent. However, strong attenuation within the reef is not observed as it was at Springdale; this may be due to in part to the higher fluid pressures at Coldspring, although that is conjectural at this time.

This study provides a significant step forward in reservoir characterization by demonstrating that crosswell seismic imaging can be used over considerable distances to better define features within a reservoir and by showing that pre-stack characteristics of reflection events can be used to reduce ambiguity in determination of lithology and fluid content. The study was conducted at a dedicated test site and at a commercial producing field, providing an example within typical commercial constraints.

In summary, the technique of crosswell seismic imaging is demonstrated to provide extremely high-quality images of reservoirs that should be useful for reservoir management. Resolution is about 40x that of surface seismic (50Hz versus 2000Hz). The top surface of the reef can be mapped and the lateral extent of the reef is evident (for images that include it); dipping layers can be identified and mapped reliably. Internal features within the reef can be observed, and, after inversion, identified as high or low porosity. Although it was not practical to observe fluid contacts in these reservoirs, such features should be resolvable in other reservoirs, particularly where these contacts are not conformable with lithologic ones.

INTRODUCTION

Purpose:

The details of the interior of oil and gas reservoirs are often unknown, and must be conjectured. In some reservoirs, the internal heterogeneity controls their productivity, and if that heterogeneity is not well-characterized, the reservoir engineer is unable to produce the field optimally. The purpose of this research was to improve the resolution within reservoirs using crosswell seismic technology, and to reduce ambiguity of lithology, porosity, and fluid content using prestack crosswell seismic data.

Reefs can be extremely heterogeneous. Geologists model reefs with many internal layers and zones, and these can provide internal barriers to flow and isolate compartments from each other. Figure 1 shows one geological interpretation of internal reef structure.

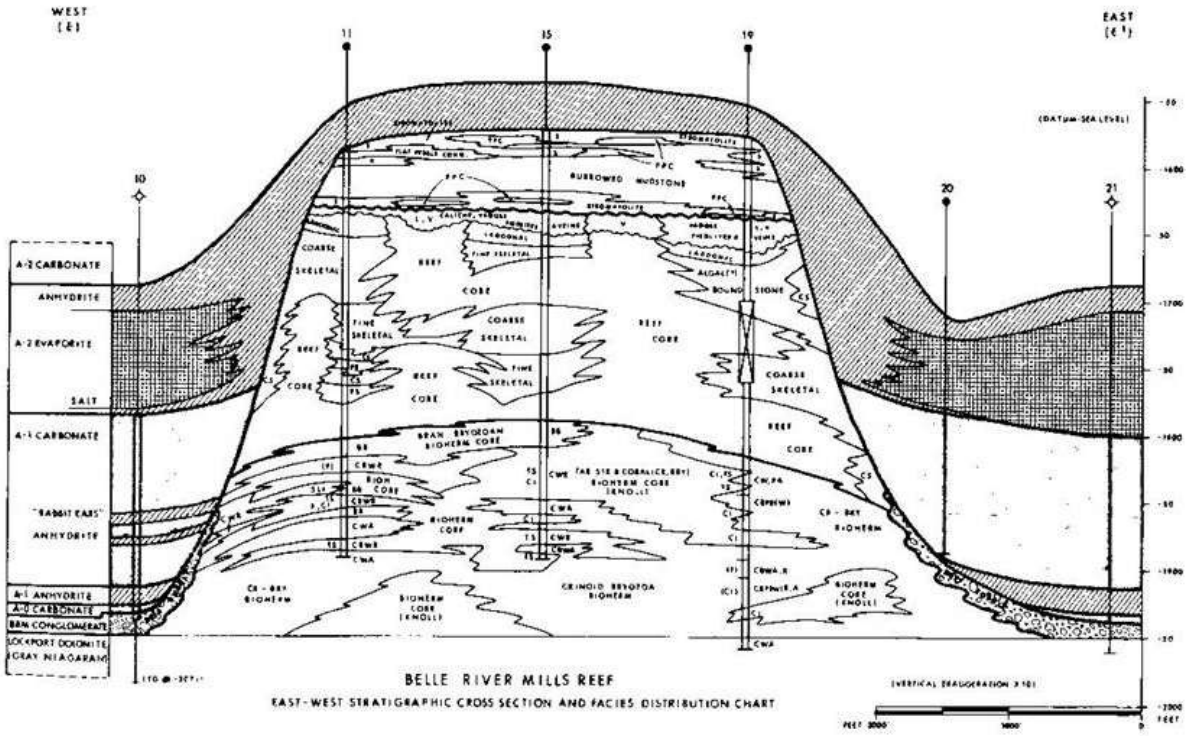

Figure 1: A typical geologic representation of a reef and its internal characteristics. Many of the facies identified are not likely to be productive in a hydrocarbon reservoir, and identification of the facies from imaging will improve the recovery of oil significantly, particularly as existing wells are sidetracked to productive zones. From Gill, 1977.

This project was designed to provide the best-possible image of the interiors of two different Niagaran reef reservoirs in Michigan, using crosswell seismology. Seismic imaging typically provides indications of contrasts in rock and fluid properties at large

scale, depending on the wavelength of the seismic signal. The wavelength, in turn, is the result of dividing the seismic velocity in the medium by the seismic frequency. For typical surface seismic data in Michigan, the highest frequencies obtainable are generally less than 50 Hz, and the seismic compressional-wave velocity for many of the carbonate layers is greater than 20,000 ft/s (6 km/s), resulting in wavelengths of 400 ft (120m). The reefs themselves are typically less than this high, and the ability to resolve any character within the reef is virtually impossible from surface data, as seen in Figure 2. On the other hand, seismic frequencies from sources located within the earth, beneath the highly attenuating surface layer (glacial till in Michigan), can result in the propagation of much higher frequencies, and therefore much smaller wavelengths.

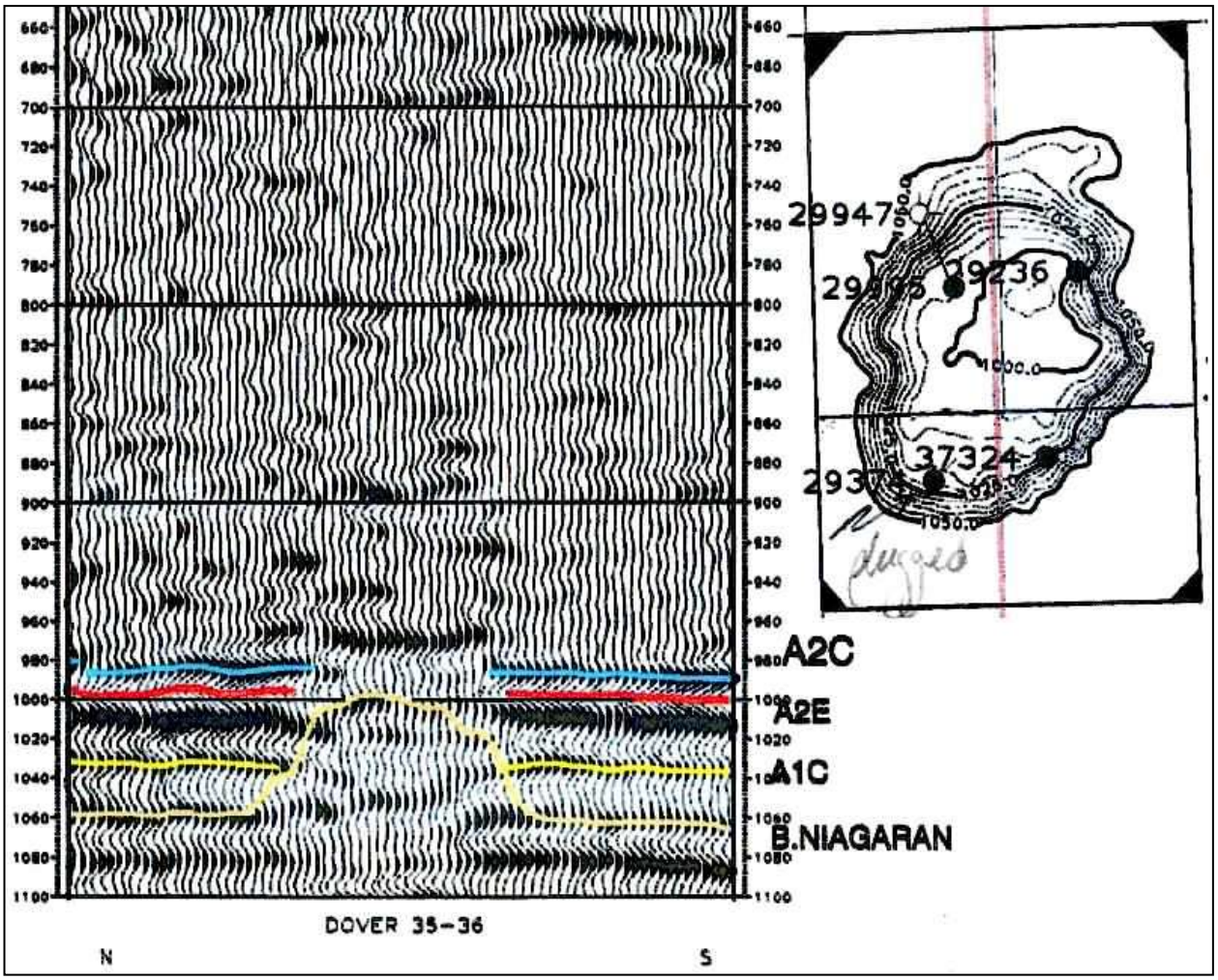

Figure 2: A cross-section and map obtained from a modern 3D seismic survey over a reef in northern Michigan (used by permission from Core Energy). Note that the presence of the reef can be identified on this section (by the absence of a reflection from the "A2E" carbonate where the reef has built up), but that no internal characteristics of the reef can be obtained.

Methods:

In addition to providing images of structures and fluid contacts, seismic data can provide indications of rock types and fluid content under many conditions. The use of Amplitude-Versus-Offset (AVO) data is fundamental to this end. This property is more properly called Amplitude-Versus-Angle (AVA) because the angle of incidence is important, not the offset; for surface data, the offset is strongly related to the angle of incidence along a specific horizon. Complete analysis of AVA data often includes both detailed study of individual reflectors in pre-stack data and inversion of partial stacks, each of which cover a range of angles. For surface seismic data, the angle ranges present are usually limited to 0º to º to 30º or, at most, 40º. For crosswell seismic data, the angles are often 40º to 80º (see Figure 3). This study was to be among the first to attempt to resolve lithologic and/or fluid information from such wide angles at such high resolution.

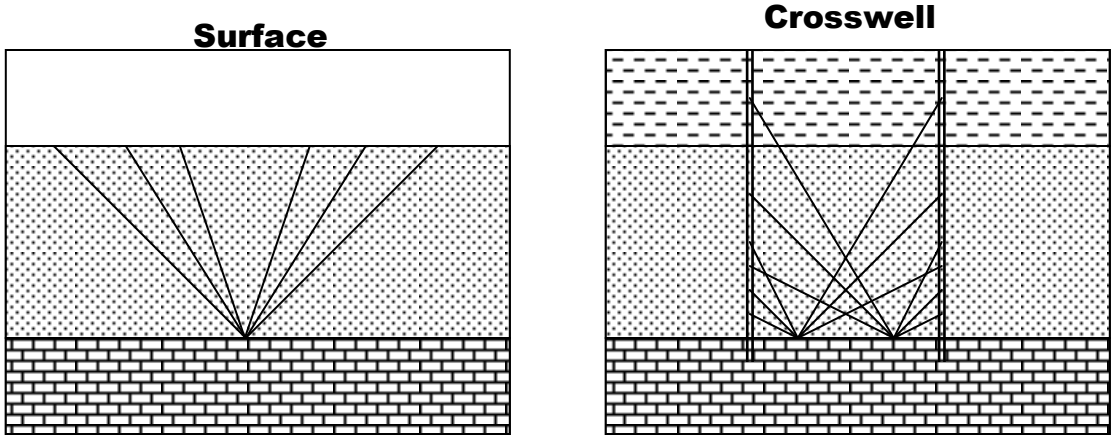

Figure 3: Comparison of surface-seismic AVO acquisition geometry (for one common depth point) with crosswell-seismic AVO acquisition geometry (for two common depth points). Notice that the crosswell configuration readily lends itself to very-wide angles of incidence, rather than near-normal angles.

Sites of the experiments:

The project was designed to conduct one survey at a test site dedicated to borehole geophysical studies, where two wells bracket a producing field, but do not intersect the reef themselves. This site is called "Springdale" in this report, and is managed by Michigan Technological University in association with the Massachusetts Institute of Technology. The production is from a well operated by Merit Energy. Following the successful acquisition and initial processing of data from this site, another site was chosen. The selection of the "Coldspring" site, also operated by Merit Energy was made in order to examine significant differences – primarily the location of wells with respect to the productive reef, and the pressure and saturation within the reservoir.

The Niagaran reefs trend around the edge of the Michigan Basin, where many wells produce. Figure 4 shows the productive wells, with the two sites selected for this project highlighted. The two sites selected for this study are typical of reefs in Michigan.

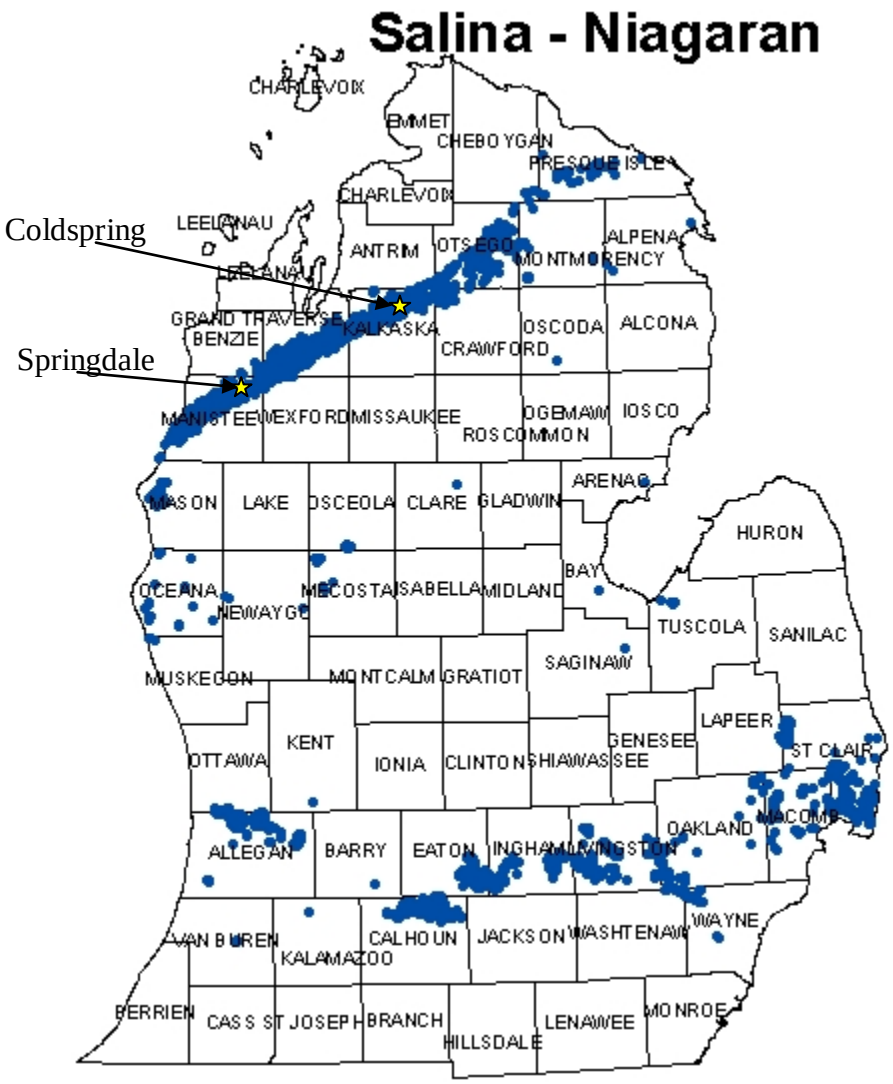

Figure 4: Niagran reef locations in Michigan's lower peninsula. The two sites chosen for this study are indicated approximately by the star symbols. Base map is from the Michigan Dept. of Environmental Quality.
(http://www.michigan.gov/images/FrmtnSalina-Niagaran_163193_7.jpg)

ACQUISITION

Planning:

The preparation for the first phase was critical to the success of the project. The immediate goal was to design a crosswell seismic survey that accomplished two tasks: (1) images the carbonate reservoir (a Niagaran reef) between two monitor boreholes in crisp detail; and (2) provide as wide a range as possible of angles of incidence for reflections of seismic waves from within the reef and at the reef's upper surface. These data would then be used to examine and demonstrate the usefulness of such data for determination of lithology, fluid content, and pressure for compartments within the producing field.

Implicit in this design was a need for coverage by transmitted seismic waves (for velocity tomography), which are used to control the seismic velocity field used for imaging the reflected waves. Thus, the survey needed to be designed for both seismic transmission and seismic reflection. These are not incompatible requirements, but could place strain on the budget of any crosswell program.

Conventional Amplitude-Versus-Angle (AVA) studies, conducted from surface seismic data, usually extend to an angle of incidence of about 30°. Special "wide-angle" or "far-offset" studies may extend to 40° or 45° at the most. Crosswell AVA starts at about 30° and extends to 90° at the limit. This will produce effects that are not experienced in conventional AVA studies, including phase rotation, radiation pattern concerns, and even phase reversal. In addition, the reflections can be observed in two directions from the same interface – from above, and from below, provided that the boreholes extend sufficiently deep beneath the target, as they do at the Springdale site. Imaging from beneath is not possible in conventional AVA studies, and will provide us with an extra degree of robustness in the crosswell environment. It will also provide us with an extra degree of quality control that is completely absent from conventional AVA studies.

The acquisition equipment consists of a single seismic source and a set of ten (10) hydrophones in a string, spaced at 10ft (~3m) intervals. The source is activated repeatedly while moving uphole on wireline. The source signal will consist of a sweep of frequencies, extending to frequencies higher than possible in other, non-borehole, environments (kHz range). This sweep will be repeated for each "source point" and stacked. Both the frequency range and the number of sweeps to be stacked would be determined from tests conducted at the start of acquisition. A cartoon view of this process, for two source points, is shown in Figure 5.

There are hundreds of source points, each of them firing into the receiver string as it is located at various depths. The detailed procedure is this: After acquisition from the source at many (hundreds) of depth points, the receiver string, which had been stationary, is then moved up the hole to a new location, immediately above the previous location. The source is then fired into it from each of the hundreds of shot points again as it (the source) is brought up the hole. The process repeats until the entire well pair is covered.

The final survey was scheduled to consist of about 5000 shot points (each with 10 shots) and 50 sets of receiver-string deployments (each with 10 receiver locations). The entire shooting sequence was anticipated to take about two days.

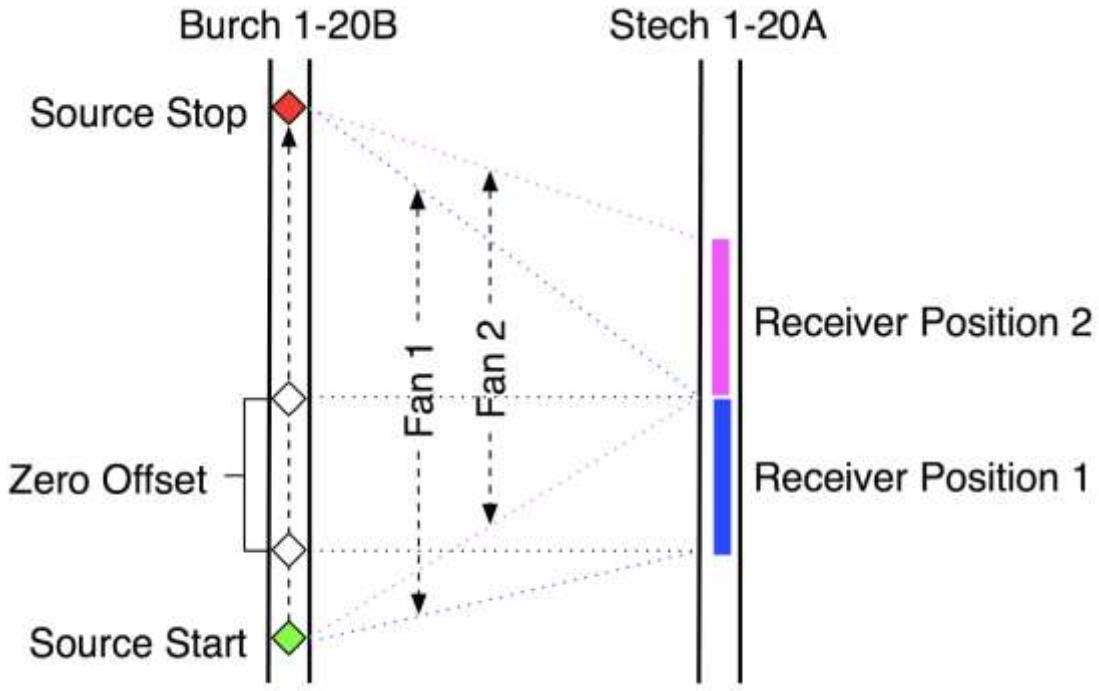

Figure 5: Graphical representation of the data collection for the conventional crosswell seismic data from a stationary receiver string and a moving source creating "fans" of data. Also shown is the zero offset survey geometry used to gather the narrowest possible incidence angles for AVA analysis. (From Trisch, 2006.)

Approach:

Our approach can be best described by referring to a few figures, typical of our survey designs. In order to visually distinguish the individual seismic rays, most of the figures shown here are drawn with extremely sparse source and receiver spacing (this is not intended to demonstrate the actual spacing; it is for visualization purposes only). Figure 6 shows the overall configuration at the Springdale test site, and a suite of sources and receivers from "Top to Bottom".

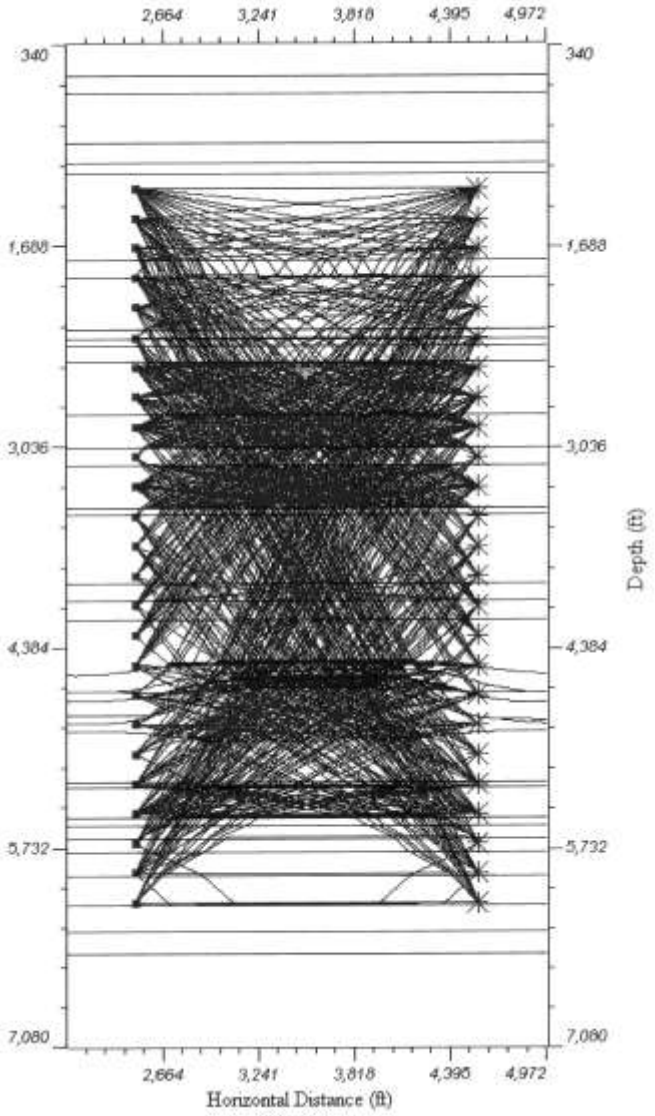

Figure 6: "Top to Bottom" survey (shown with spacings of 200 feet). The reef is the non-horizontal body shown at about 4500 ft depth. Only transmitted rays are shown; reflected rays are not shown for clarity of visualization. Scale is 1:1.

This figure demonstrates that the coverage over the reef and overlying beds will be excellent. It also helps to indicate that the angle ranges for reflected rays at the reef level will be about 30° to 90°.

Figure 7 shows a close-up, using a slightly finer spacing of sources and receivers, near the reef.

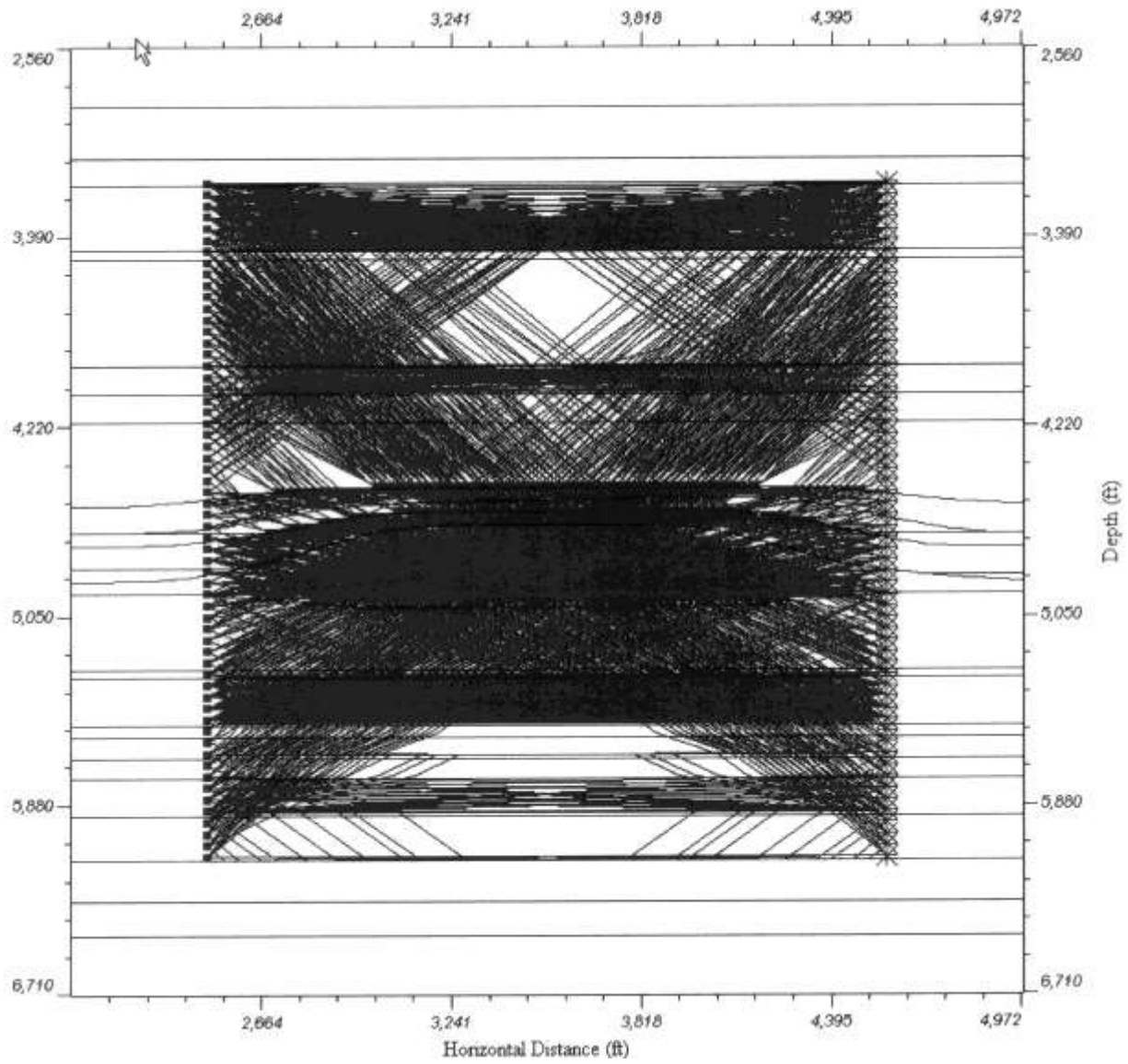

Figure 7: Close-up of reef interval, using (for visualization purposes only) a source and receiver spacing of 50 ft. This figure is not 1:1 scale, although nearly so.

The density of ray penetration into the reef is very good, and imaging can be expected to be excellent. Notice, however, that if this configuration were used, the reflections from the top and interior of the reef would be limited to about 50° to 90°, demonstrating the need for additional source and receiver locations further uphole.

Notice that the visualization of rays is difficult in certain areas, because they are so densely packed. While this is good for the survey design, it makes it difficult to interpret visually, so the previous figures used sparser spacing. Notice also that the slightly deeper location of this survey (compared with Figure 3) results in extremely poor coverage of the upper surface of the reef and the beds immediately overlying it. This is due to the velocity structure at these depths, and the sharp bending of rays. This design will not be used for the acquisition for this reason.

From the survey designs tested, it was clear that we would obtain seismic data that covers an angle range of about 30° to 90° in the limit. We should also expect to obtain reflections from above and from below at most interfaces at the Springdale site (see Figure 8).

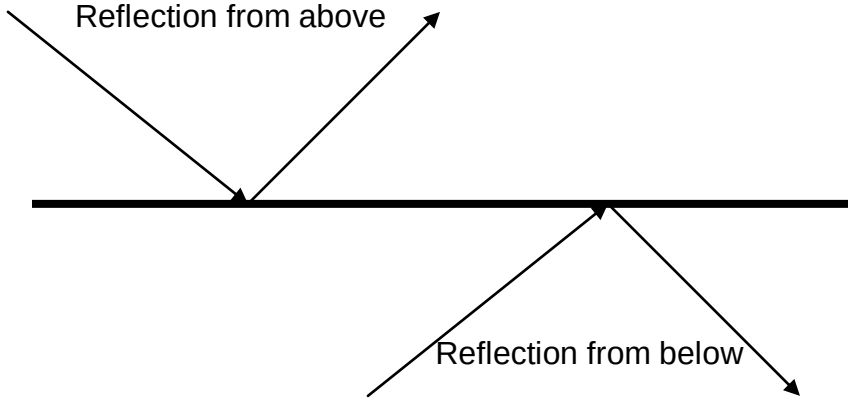

Figure 8: Cartoon view of reflections from above and below an interface.

Field Program at Springdale Site:

The first dataset was successfully collected during the summer of 2005, and initial processing for crosswell imaging was completed within a few months. Z-Seis was the contractor for both tasks.

This first crosswell seismic survey was conducted at the Springdale site, a dedicated test site, that accomplished two tasks: (1) it imaged the carbonate reservoir (a Niagaran reef) between two monitor boreholes in crisp detail; and (2) it provided as wide a range as possible of angles of incidence for reflections of seismic waves from within the reef and at the reef's upper surface. The stacked image obtained is extremely high quality, and the prestack data has been used to examine and demonstrate the usefulness of such data for determination of lithology, fluid content, and pressure for compartments within the producing field.

The survey was designed to collect transmitted waves in order to obtain a detailed velocity field through transmission tomography, and to collect reflected waves for high-resolution imaging and AVA studies. This required a thoughtful approach to the mechanics of data collection, in order to complete the survey in a timely manner.

The survey consisted of two parts. The first part, conducted over 3.5 days, was a detailed "conventional" crosswell survey, in which sources and receivers were located in positions designed to provide the crosswell transmission tomographic velocity model and the reflection data. The second part, conducted over one half-day, consisted of a suite of data,

with 10-foot spacing, in which the receivers and sources were at equal depths for all shots, and extended to the shallowest depths of the boreholes below the till. This second experiment was designed to provide data for AVA studies at any interface, including those above or below the reef, and to ensure that the widest possible range of angles was obtained for all AVA studies. Figure 9 shows the field arrangement at the source well.

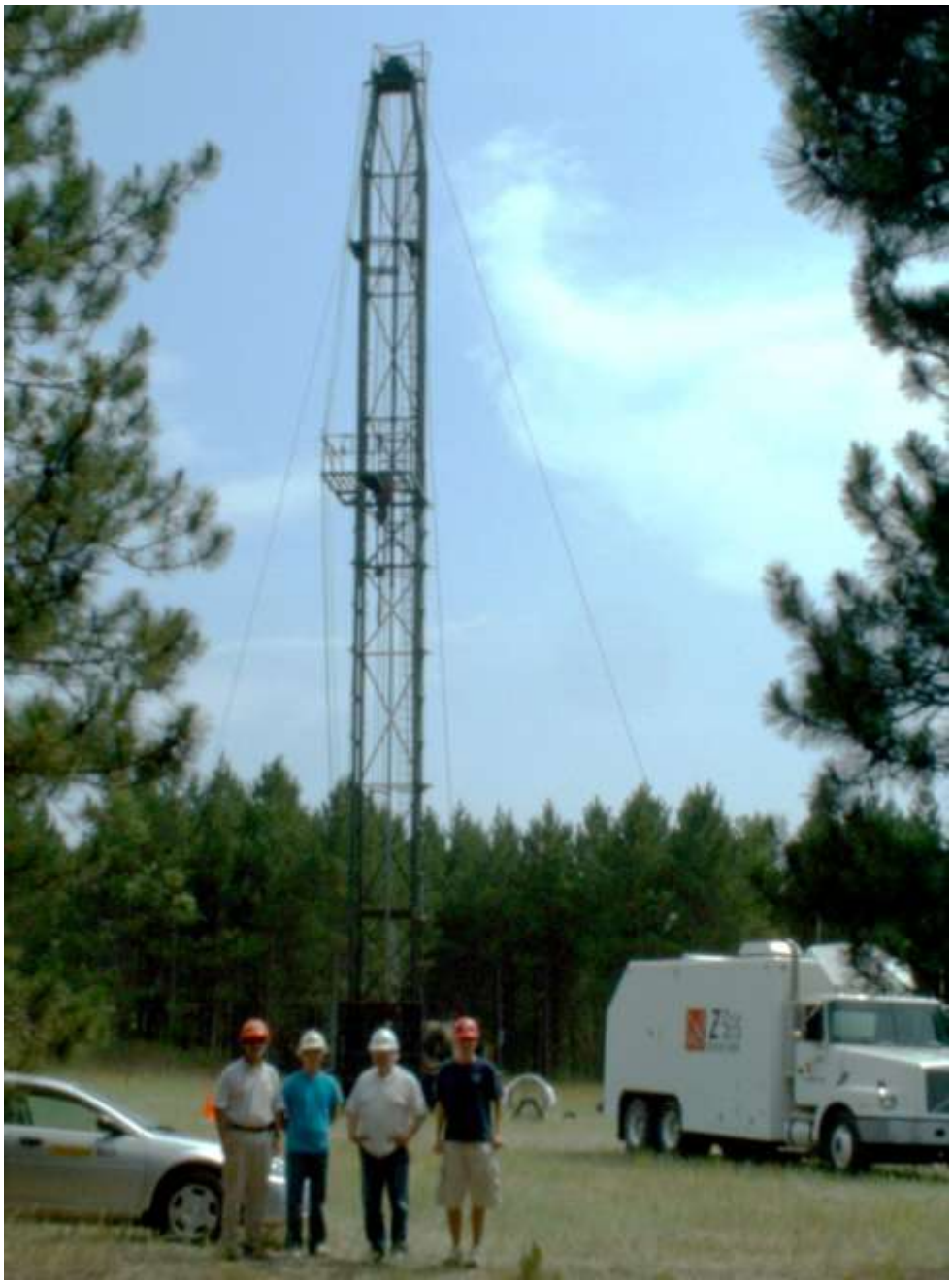

Figure 9: Picture of the Michigan Tech field crew during the experiment at the test site in 2005. From left: Wayne Pennington (PI), Sean Trisch (graduate student), Roger Turpening (co-PI), and Josh Richardson (undergraduate student). The Z-Seis recording truck is in the background, with the receiver string suspended 3500 ft below the surface of the Stech well. Photo by Josh Richardson.

The acquisition equipment consisted of a single seismic source and a set of ten (10) hydrophones in a string, spaced at 10-ft intervals. The source was activated repeatedly while moving uphole on wireline. The source signal consisted of a sweep of frequencies, up to 3000 Hz. This sweep was repeated 8 times for each "source point" and stacked. The signals received at most receiver stations showed that 3000 Hz data was easily obtained at the spacing of these boreholes (about 2000 ft).

The Springdale test site is well-characterized, as shown in Figure 10. The reef is currently at extremely low pressure, 25-50 psi (1.2-2.4 kPa), and contains water, oil, and gas.

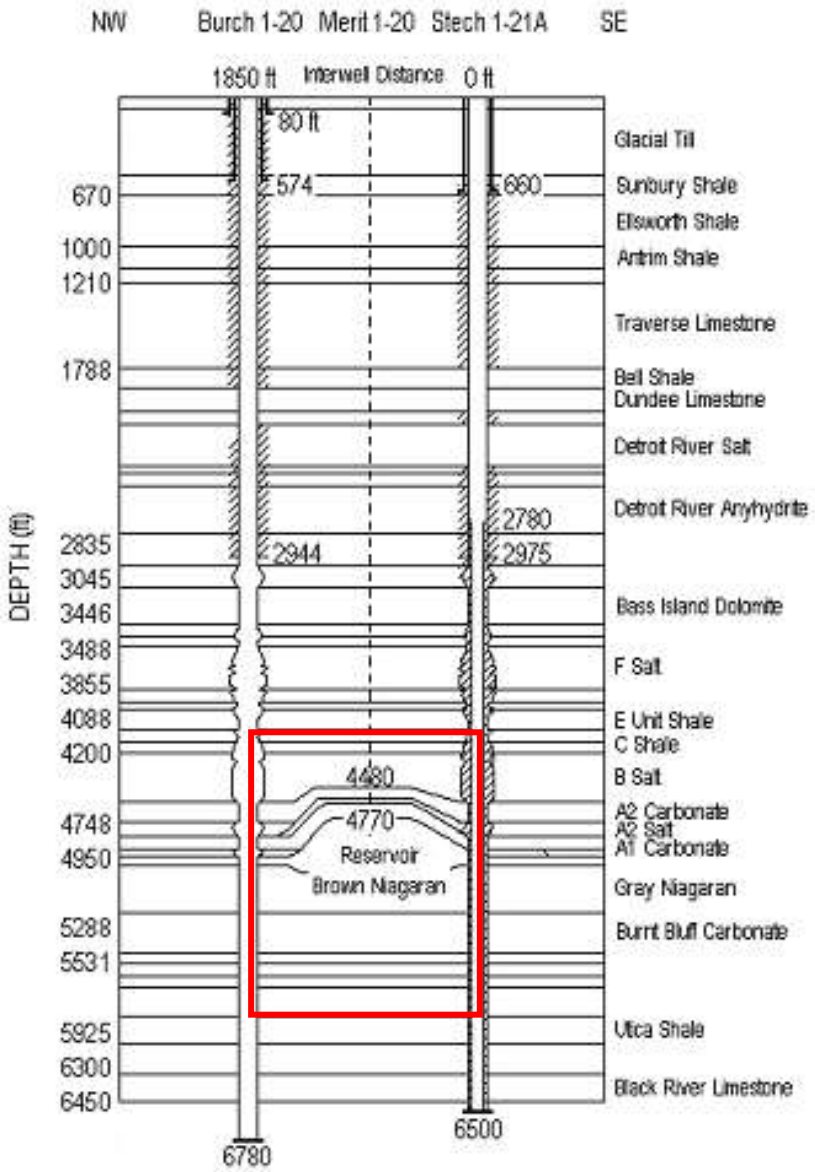

Figure 10: schematic cross section of the dedicated test site used in phase 1. The area included in the image of Figures 11 and 12 are approximated by the rectangle.

The processed image provided by Z-Seis is shown in Figure 11, and an interpreted version is shown in Figure 8. Details of the acquisition and processing immediately follow.

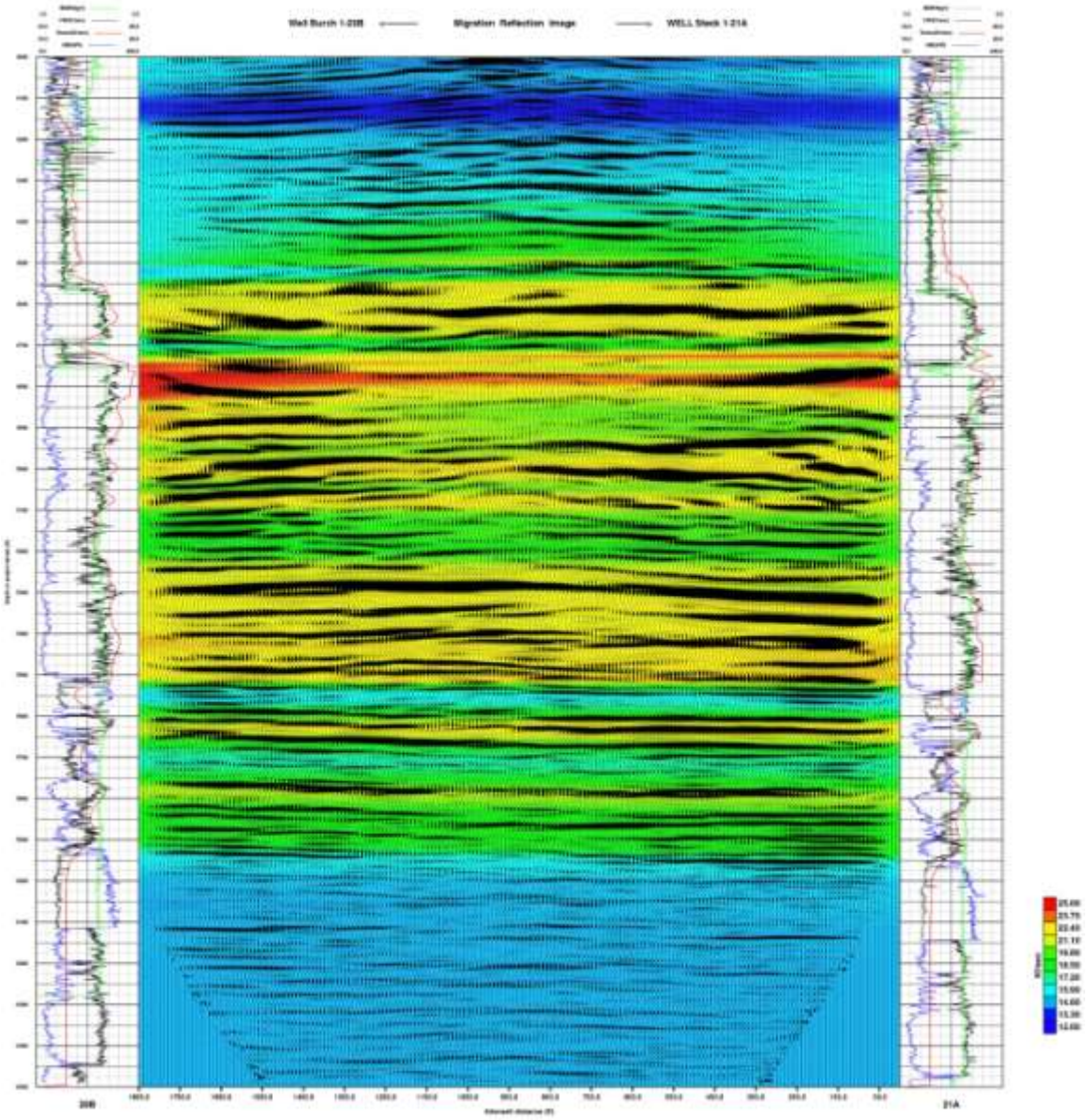

Figure 11: Processed seismic crosswell image as produced by Z-Seis. Color background represents velocity model determined by crosswell transmission tomography (errors can be large near the wellbores at the edge of the image). Wiggle traces are the migrated seismic data from crosswell reflection imaging using the velocity model to provide transformations and migration. Various logs are displayed along the edges, at the locations of the Burch (on the left) and Stech (on the right) boreholes. Vertical axis is depth (not time). An interpreted version of this image is provided in the next figure.

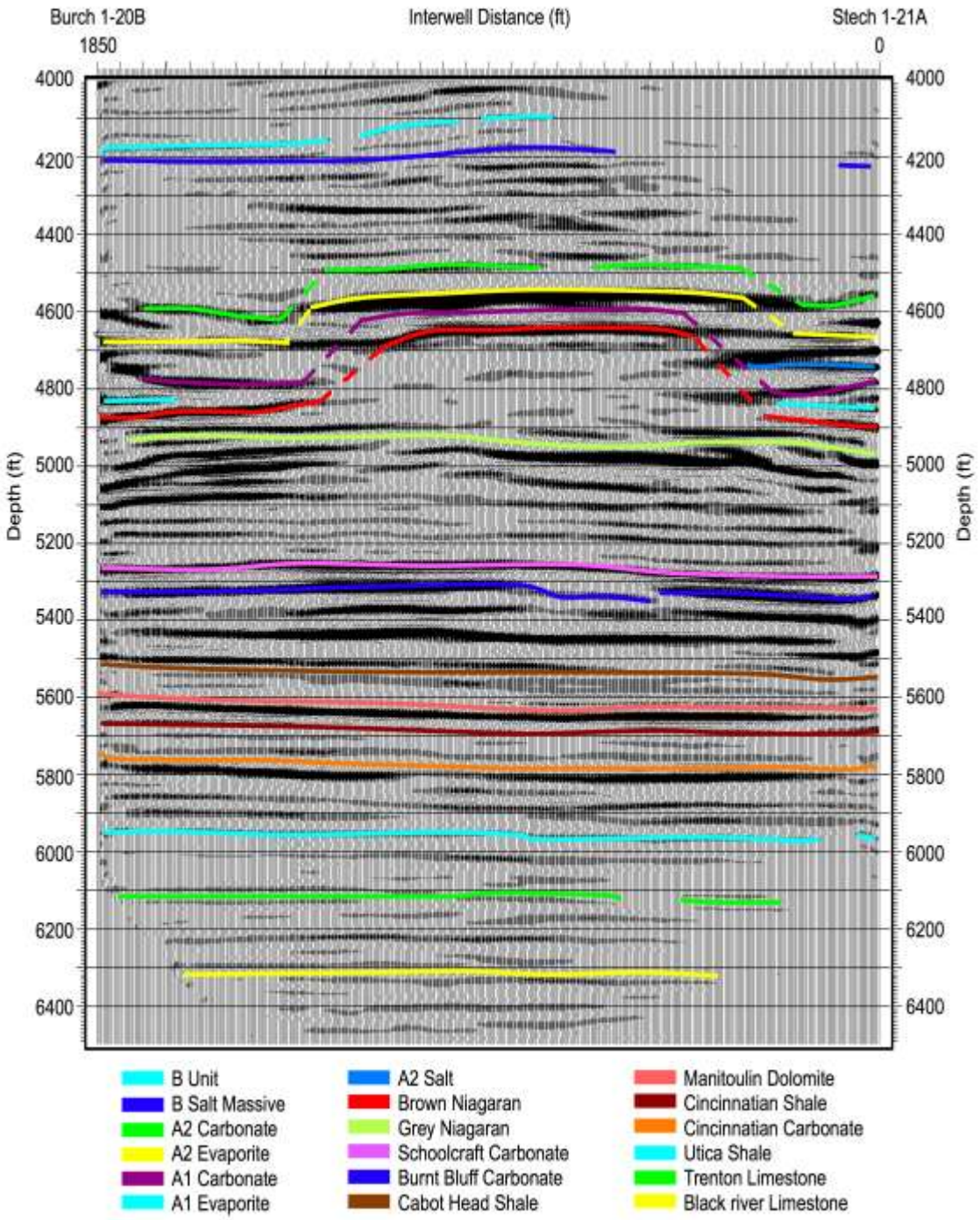

Figure 12: Interpreted (reverse polarity) migrated crosswell reflection image, using both reflection image and tops picked from well data. The observable events were directly interpreted while the flanks of the reef were inferred and drawn in with dashed lines. The geometry of the survey prevents direct imaging of the flanks of the reef and layers draped over it. The layer tops are described in the key at the bottom of the figure and increase in depth from top left to bottom right. This stacked image is based on angle gathers from 55 to 65 degrees. (From Trisch, 2006.)

The detail present in figures 11 and 12 can be contrasted with that found in a 3D (surface) seismic survey conducted over the site in 1983, as shown in Figure 13.

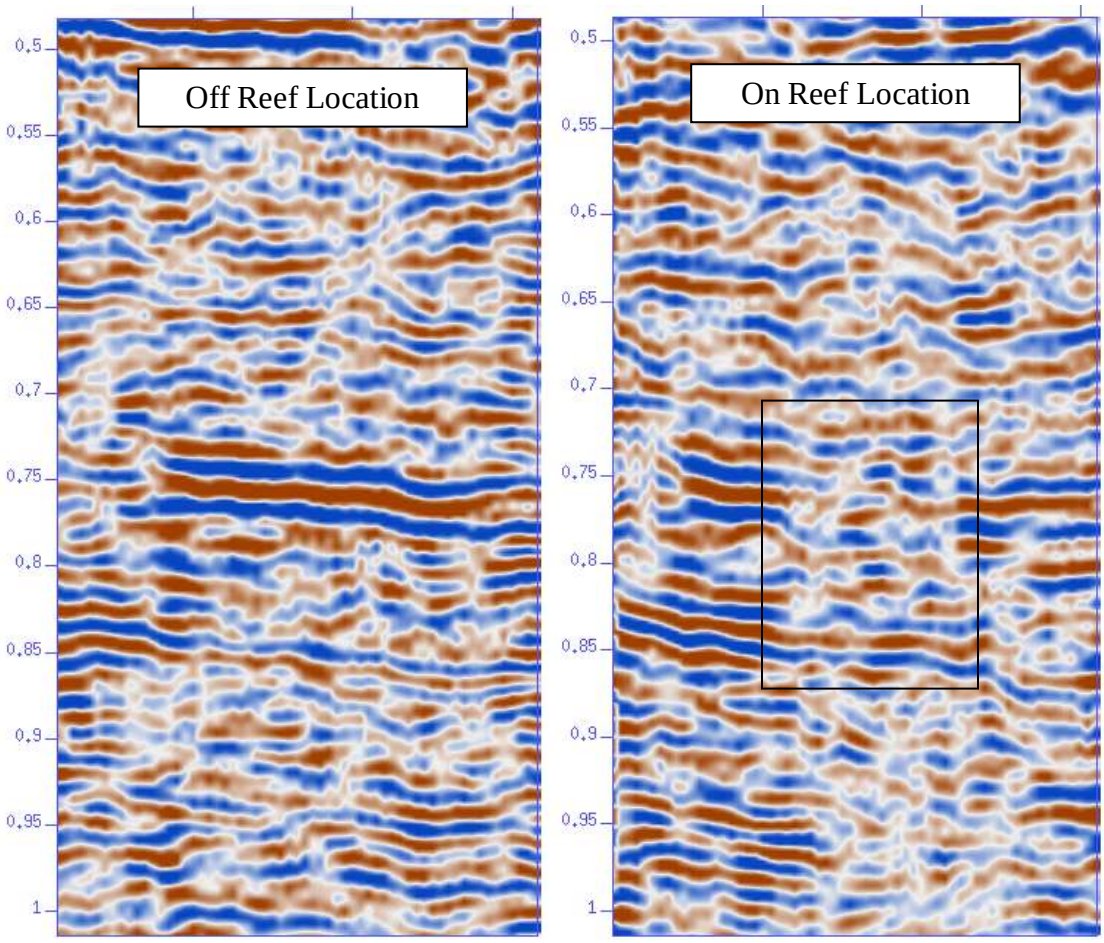

Figure 13: Two seismic lines extracted from a 3D survey conducted over the Springdale site in 1983. The line on the left is from an area that does not include the reef, and the line on the right includes the reef. The presence of a salt layer causes a large reflection where there is no reef, evident in the image at the left. The substitution of an anhydrite layer instead of the salt directly over the reef results in a de-tuning where the reef exists. The typical result is the more-chaotic reflection image shown at right. The area covered by the crosswell surveys shown in Figures 11 and 12 is indicated approximately by the rectangle.

The details of data acquisition are now discussed. Data were collected for the main survey using source and receiver locations, every 10 ft, from about 2600 ft depth to about 6000 ft depth. A 0.35s sweep from 100 Hz to 3000 Hz was stacked 8 times at each depth. This geometry yielded coverage of the reef zone with reflection fold of over 200 and angles of incidence ranging from about 30° to 90°. A summary figure from ZSeis is shown in Figure 14, providing additional details.

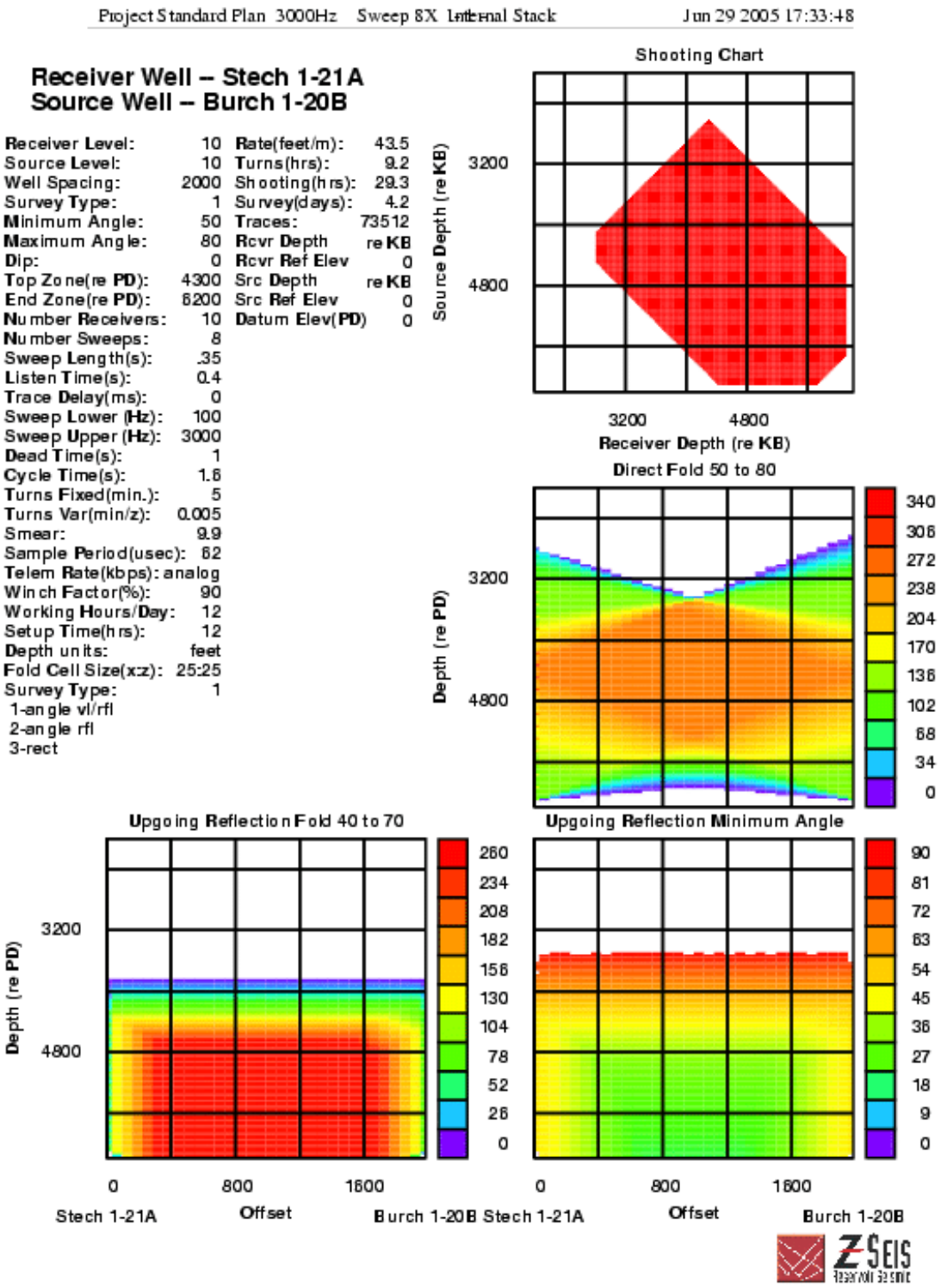

Figure 14: Summary of data acquisition provided by Z-Seis.

The source was suspended in the Burch well, while the receivers were in the Stech well. The Burch well is cased only down to 2944 ft, and is open below that. (The Burch well

needed to be cleaned out prior to running the survey, to remove salt that had precipitated in casing.) For each "fan" of shooting, the receiver string is held at a constant depth (using 10 receiver groups at 10-ft spacing for a total span of 100 ft) while the source is moved up the borehole, firing as it is moved. 8 shots, all within a 10-ft interval, are stacked for each source point. When the source has reached its shallowest point, it is returned to depth, and the receiver string repositioned for the next "fan" of shooting.

One example of a common-receiver gather is shown in Figure 15, with a power spectrum for the entire gather.

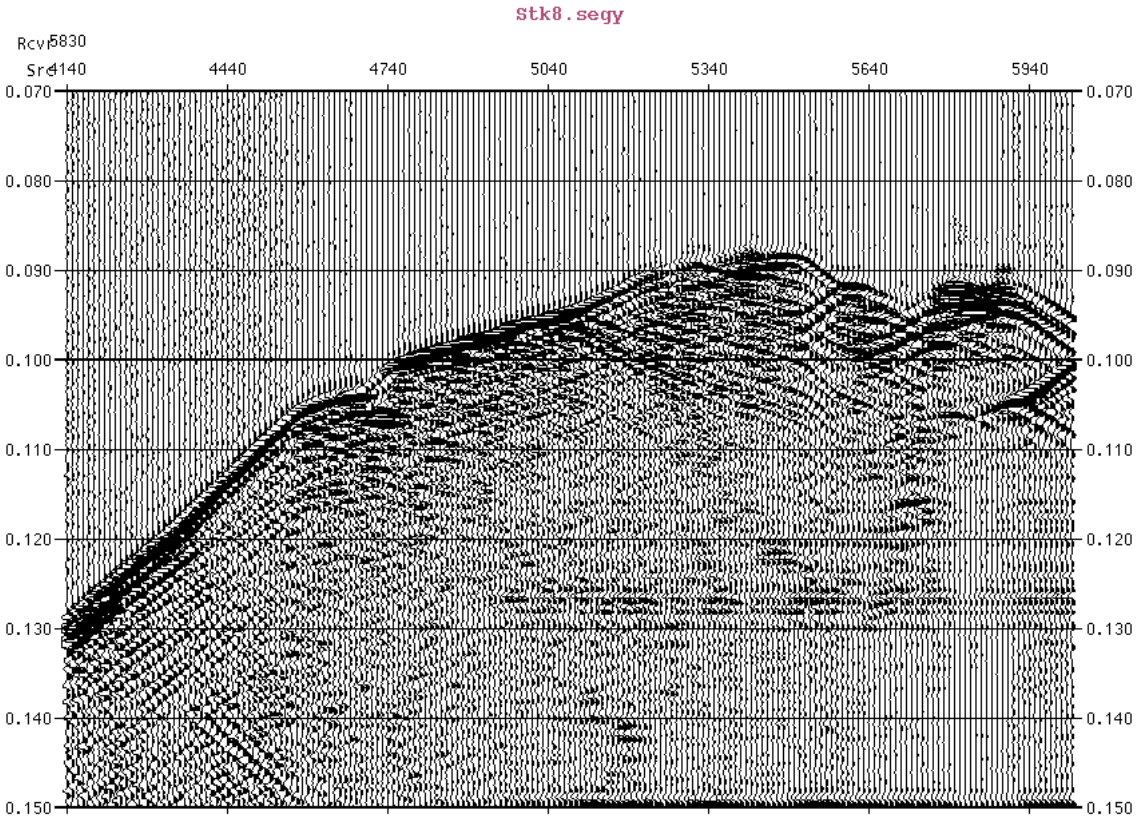

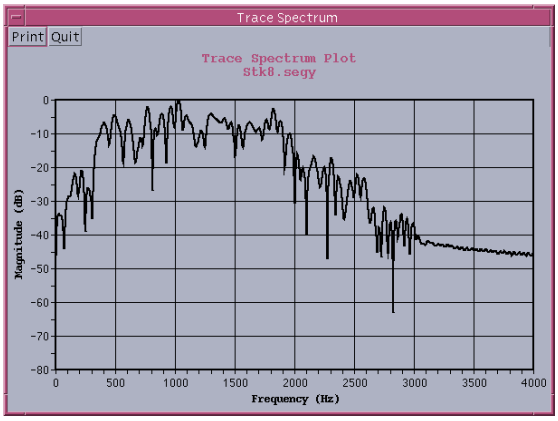

*Figure 15 :*Common-receiver gather and spectrum for a receiver at 5830 ft depth, and sources ranging from 4140 ft (at left edge) to 6000 ft (at right edge). The arrivals are clear and distinct, and reflections and converted phases are apparent even in this gather, prior to stacking. Notice that there is a set of arrivals with constant time (clearly visible at 0.126 s) when the source is deeper than about 5000 ft.

The origin of a source-generated noise (seen as the constant-time arrivals visible in Figure 10) was of some concern in the field, and several small experiments were

conducted to ensure that it was truly due to seismic (or pressure) waves in the formation or well. This noise is an unusual form of tube-wave noise. As all tube wave noise, it is easily removed, but is worthy of study in its own right – it appears to have been caused by electromagnetic propagation of the source pulse through the earth and conversion to seismic energy at or near the receiver well. Figure 16 shows a common-source gather for a single source depth, with the noise clearly visible.

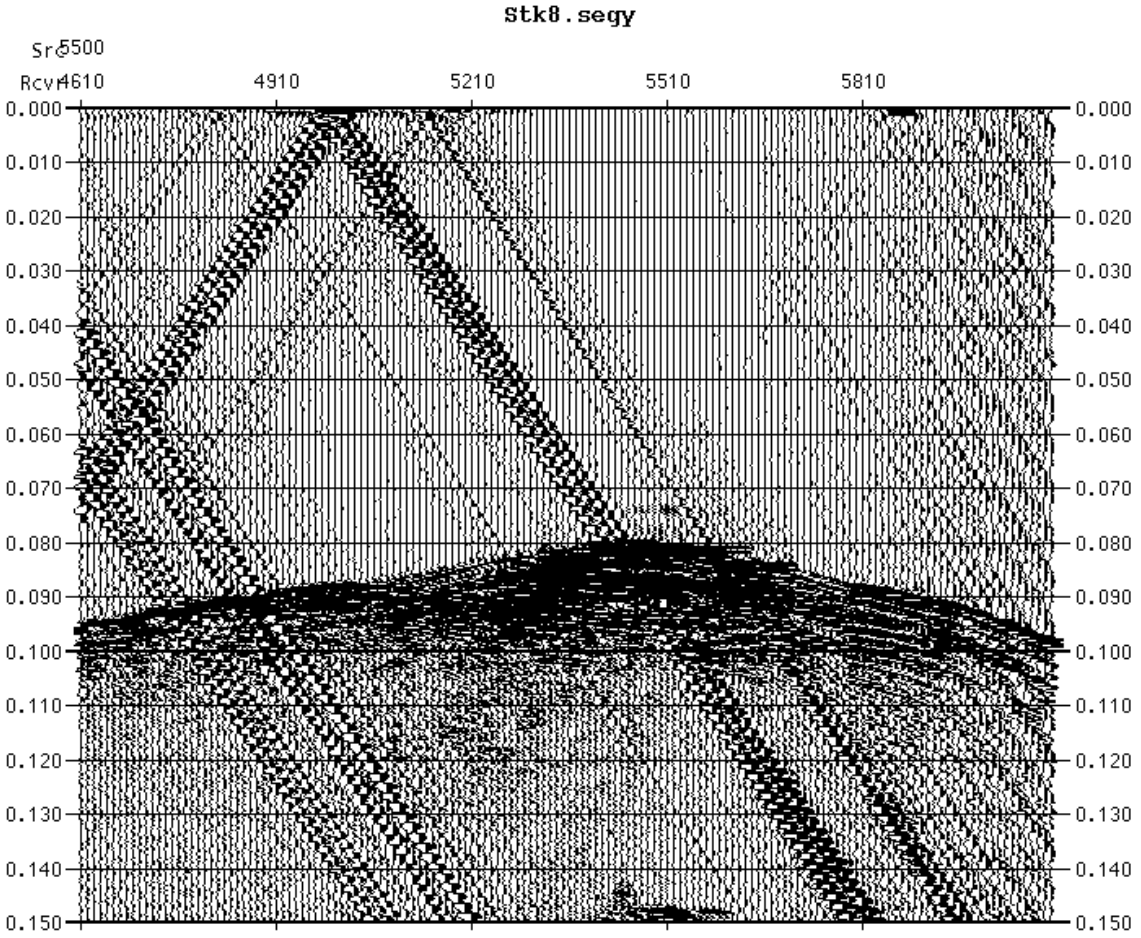

Figure 16: Common-source gather for a source at 5500 ft depth and receivers from 4610 ft to 6000 ft depth. The noise that was "flat" with time in the common-receiver domain is clearly seen to be traveling with tube-wave velocities in the common-source domain. These tube waves start at zero time at specific depths in the borehole.

The noise is seen to consist of tube waves which originate at zero time in certain locations in the wellbore. The fact that they are initiated in the receiver well at the time that the source is fired, and not at the time that the P-waves arrive at the well, indicates that they travel from the source well to the receiver well nearly instantaneously. In a separate study, we (ZSeis and Michigan Tech) are investigating the possibility that these waves travel as electromagnetic waves from the source well, where the wireline cable is suspended below casing in open hole, and convert to tube waves upon arrival at the receiver well. We suspect that the long wireline cable acts as a sort of antenna

The tube-wave noise is easily removed from the data by standard array techniques such as median filtering, radon transforms, and f-k filtering. While it presents an interesting case study in its own right, it does not affect the data quality at all.

We note that the tube-wave noise only appears when the source is at depths greater than about 4500 ft. Figure 17 shows an example of a common-source gather at 3780 ft, showing no apparent tube waves.

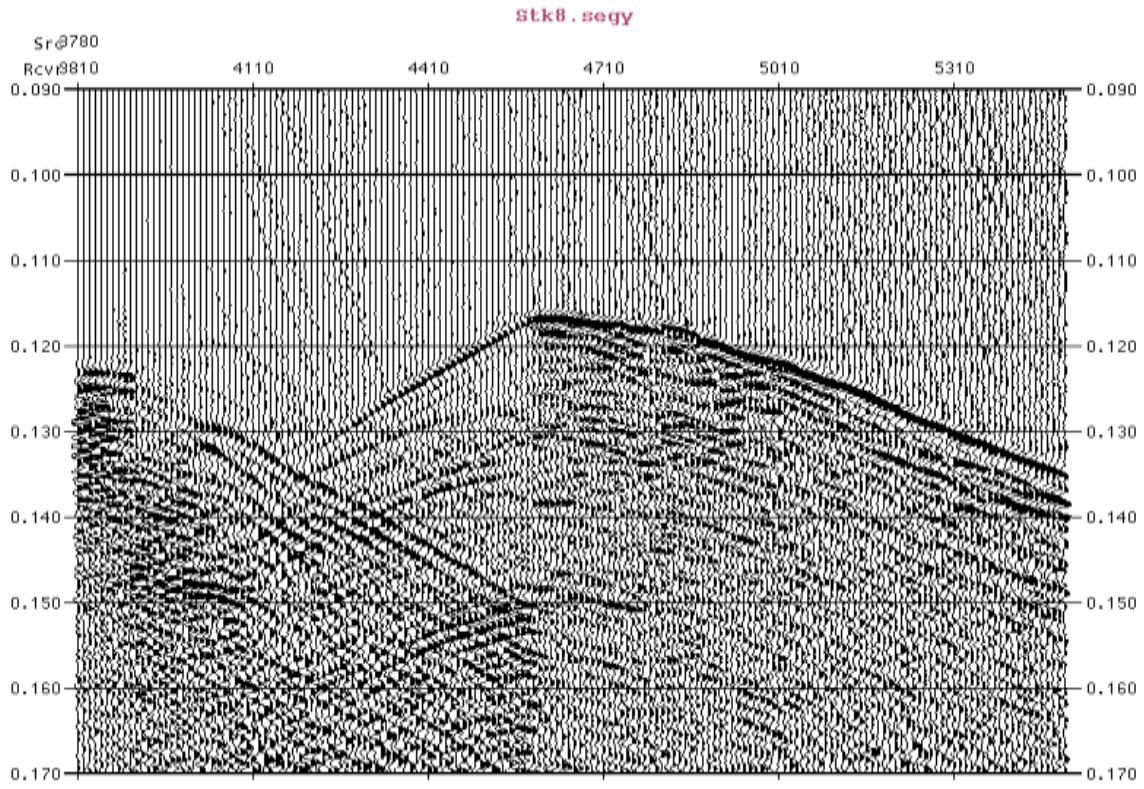

Figure 17: Common-source gather with a source depth of 3780 ft and receiver depths from 3800 ft to 5500 ft. Note that the large tube waves evident in Figure 8 are almost completely absent, suggesting that the long cable length in open hole is required to produce these large events.

A common-receiver gather is shown in Figure 18, at a receiver depth of 3810 ft (comparable to the source depth of Figure 16) with a power spectrum indicating that frequencies up to 3000 Hz were well-recorded. This gather was collected for a receiver depth in a thick salt layer. At this site, the carbonates and shales are so competent that salt is slow in comparison, resulting in the later arrivals in the middle of this gather, and refracted arrivals evident on either side. The tube-wave noise (again, with origin time of zero) is apparent for all source depths greater than about 4500 ft depth.

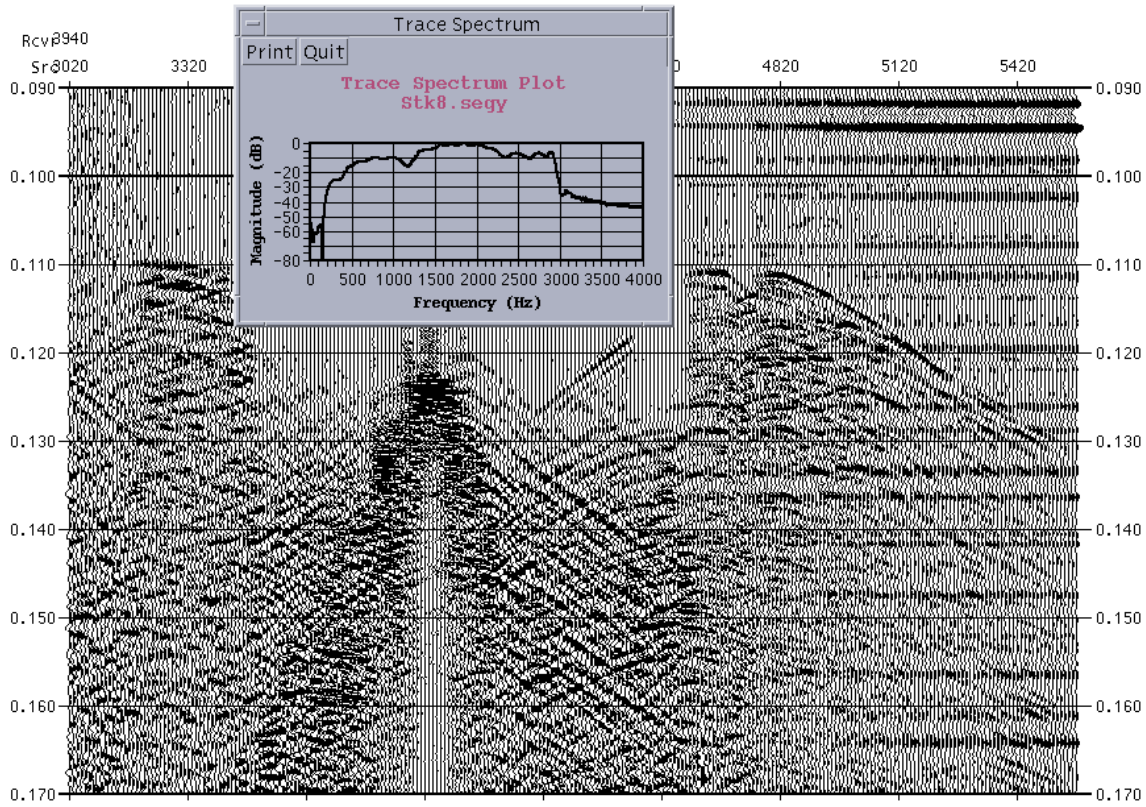

Figure 18: Common-receiver gather and spectrum for a receiver at 3810 ft and source depths from 3120 ft to 5500 ft. The spectrum is from a single trace with source depth of 3810 ft.

One additional data set was acquired, in order to ensure that we obtained the smallest-possible reflection angles of incidence. This consisted of what is called zero-offset data, for the entire well depths. In crosswell terminology, offset refers to differences in depths of receivers and sources, not to well separation. (See Figure 19 for a cartoon describing terminology.) Thus, zero-offset data refers to data collected with sources and receivers at the same depth. In this case, the source was moved up 100 ft, with 8 shots stacked every 10 ft, while the receiver string remained stationary with one receiver (group) located at the depth of the first shot. Then the receiver string was moved up 100 ft and the process repeated. Thus, we essentially collected a number of "fans" containing zero-offset data every 10 ft as well as offsets of 10 to 100 ft for each fan (every 100 ft). The zero-offset data will provide the narrowest-possible angles of reflection for reflectors beneath (or above) the depth of the source and receiver, while the "fans" associated with each shot point will allow the separation of upcoming and downgoing reflections.

NOTE: Because "offset" refers to differences in depth, we will use the term amplitude-versus-angle (AVA) rather than amplitude-versus-offset (AVO) in reference to the pre-stack amplitude studies in crosswell domain.

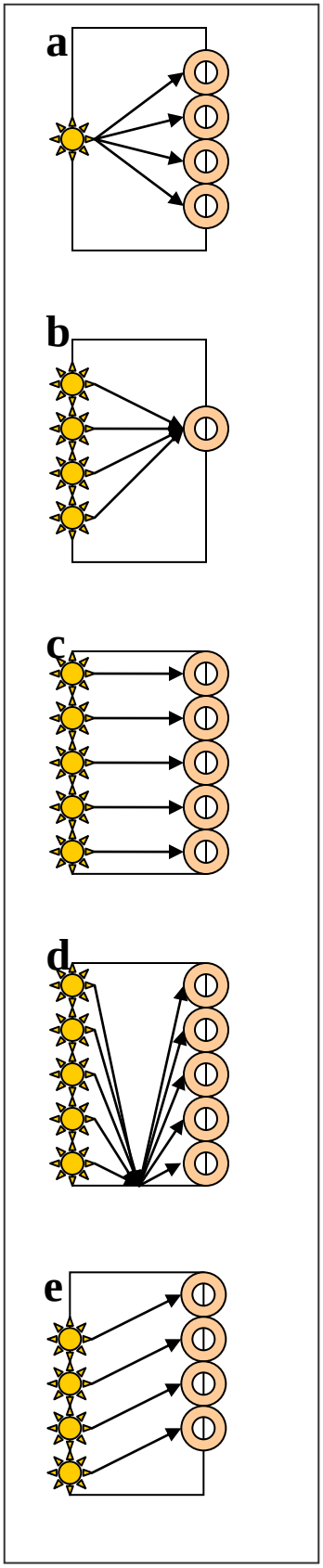

Figure 19: Cartoon clarifying terminology for crosswell data.
(Starbursts are sources, rings are receivers.)

a: Common-source gather. Direct ray paths are shown.

b: Common-receiver gather. Direct ray paths are shown.

c: Zero-offset gather. Direct ray paths are shown.

d: Zero-offset gather. Reflected-wave paths are shown for a single deep reflector. Note that the angle of incidence decreases for increasing differences in depth between the source-receiver location and the reflecting horizon.

e: Constant-offset gather. Direct ray paths are shown.

Figure 20 shows a field display of the zero-offset dataset. Because the data have not been filtered for upcoming or downgoing reflections, the direct arrivals dominate. (Note the tube-wave noise present below 4500 ft depth.)

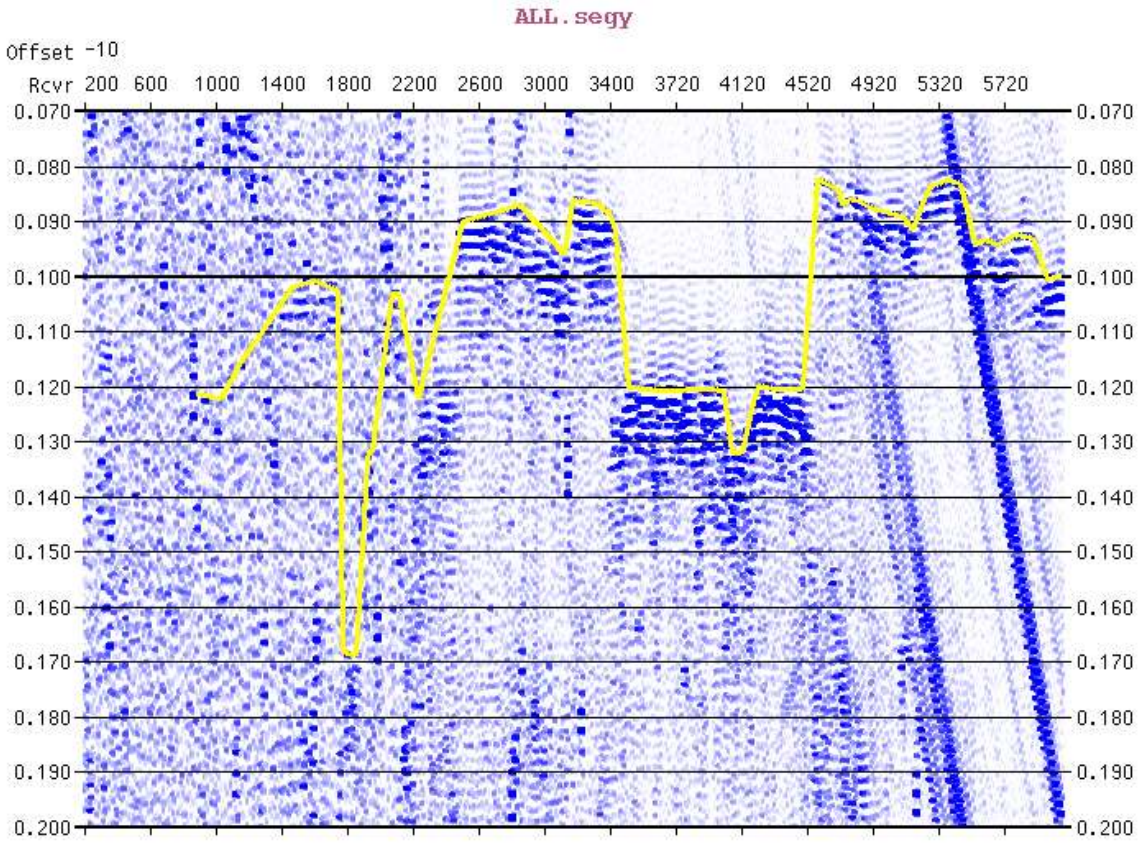

Figure 20: Zero-offset (actually, this display is for a constant-offset of -10 ft), with (direct) first-arrivals indicated by the yellow line. Note the tube waves below about 4500 ft depth. This dataset has not been filtered for upcoming or downgoing waves, so the section is dominated by direct arrivals. Processing will bring out the AVA character of the reflections.

The variations in angle of takeoff at the source and angle of incidence at the receiver are important because these angles vary so greatly in the crosswell geometry. The source is a piezo-electric transducer, with a strength that varies with angle. The strongest radiation is emitted perpendicular to the axis of the tool; in this experiment, the tool is vertical, and the strongest radiation is in the horizontal direction. The strength varies, to a first-degree approximation, in a sinusoidal manner. Figure 21 shows the source strength as a function of angle of takeoff, with a long-diagonal path used for demonstration.

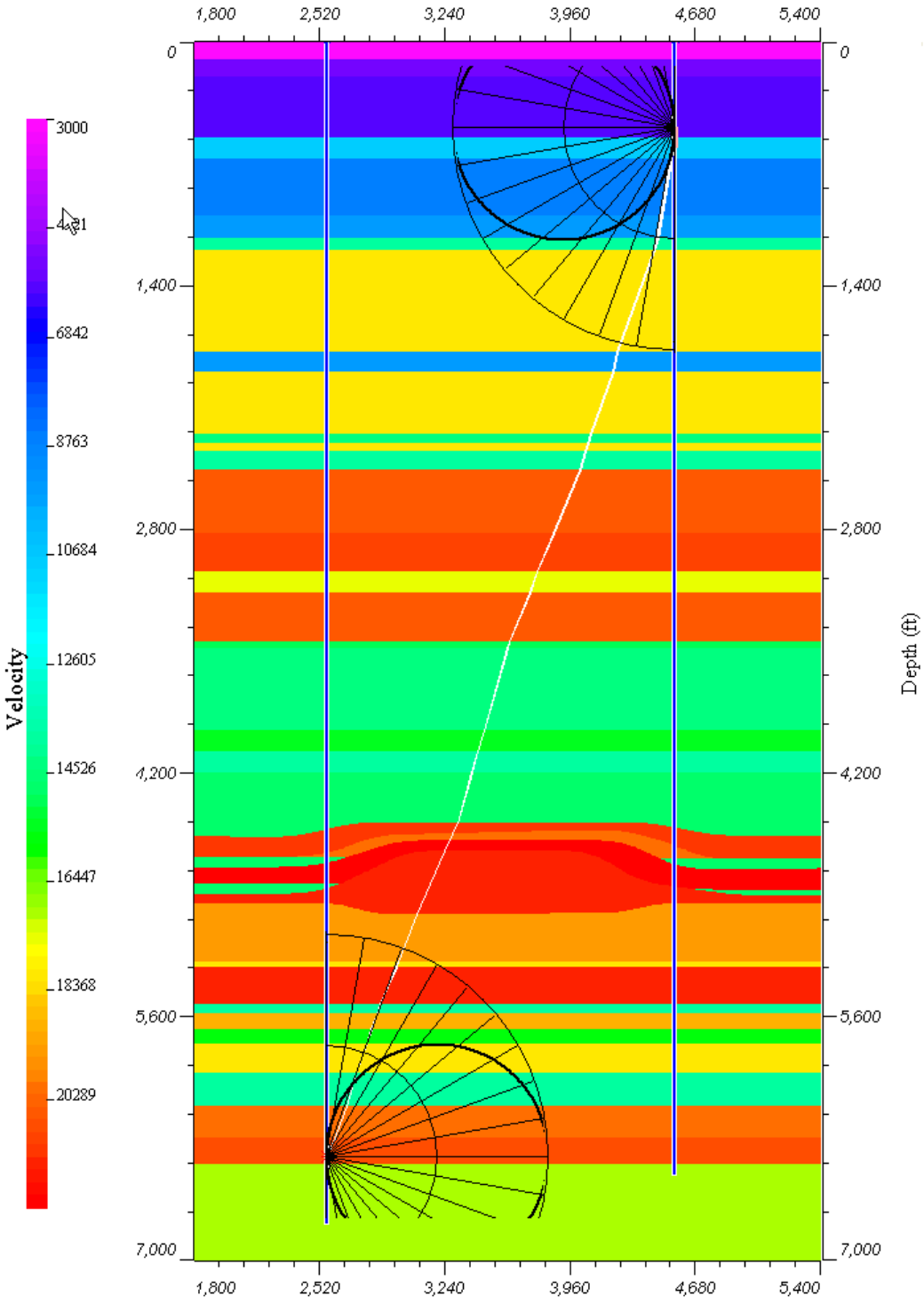

Figure 21: schematic diagram showing radiation pattern (energy is proportional to length of dark circles) and long ray path tested between 500 ft and 6500 ft. The dark circles show the amplitude of the signal; the light circles are simple protractors superimposed in order to provide a visual indication of angles of takeoff and incidence.

The image shown in Figures 11 and 12 was derived from a stack of all (upward) reflections with angles of incidence within a certain range. The partial-stack images of Figure 22 demonstrate some of the effect that AVA can exert. This data provided us with enough experience to begin to plan the second acquisition program, while additional processing and analysis of the Springdale data set progressed.

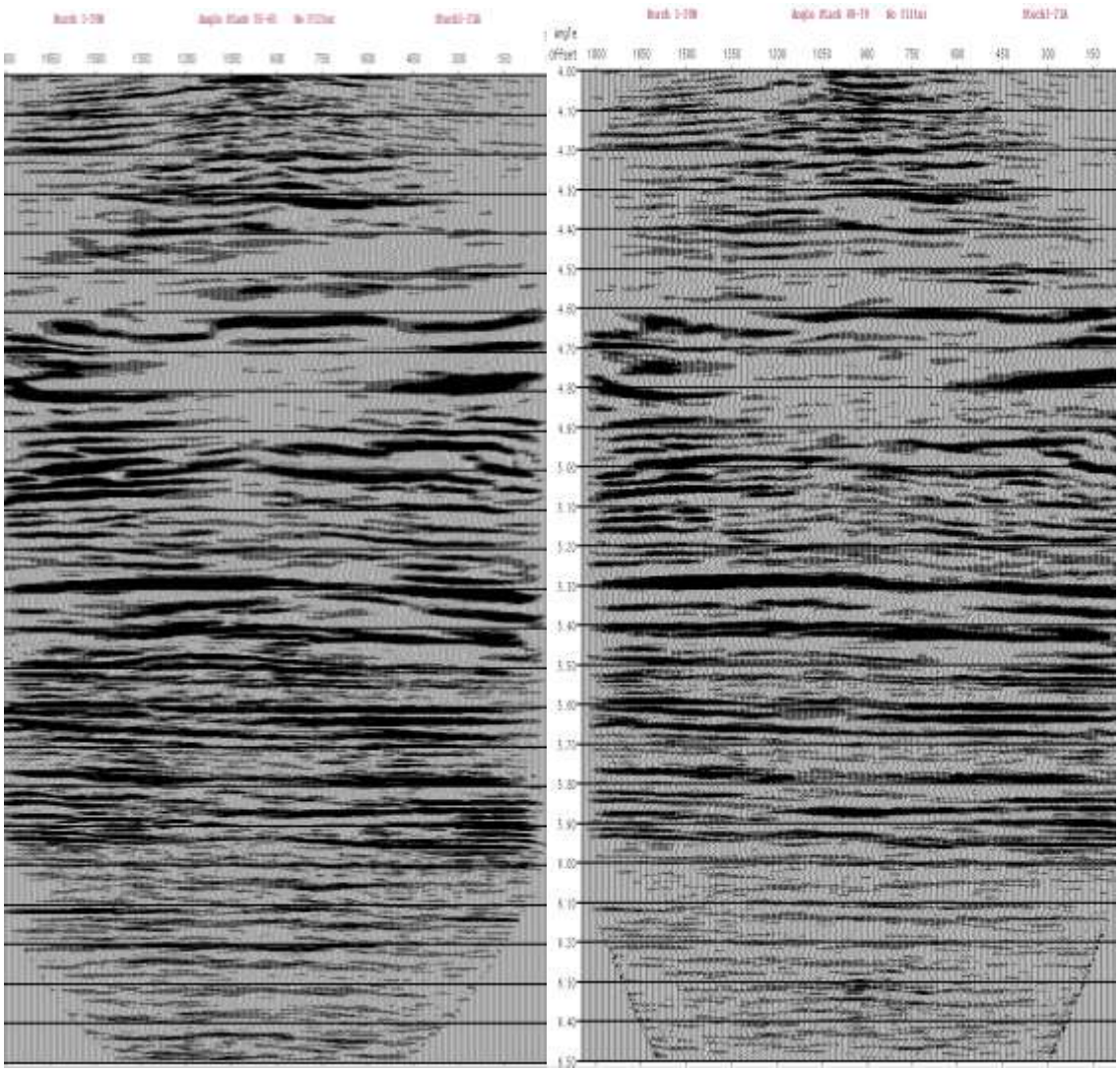

Figure 22: Two stacks of the data. The image on the left was stacked using angles that ranged from 55° to 65° and the image on the right included all angles from 40° to 70°. The differences are due largely to differences in AVA response. (Vertical scale is depth in thousands of feet.)

Field Program at Coldspring Site:

The second data set was acquired in September 2006, after a delay caused by a lack of rig availability; again, ZSeis was the contractor for the acquisition and initial processing. The data were acquired in a field near Kalkaska MI (see Figure 1) operated by Merit Energy of Dallas TX. Both wells were within the reef itself, although they did not penetrate deep beneath the reef as at the dedicated Springdale test site for the first data set. This reef is at higher pressure, about 1000 psi (50 kPa) , but still below bubble point. It also contains a significant amount of carbon dioxide that had been injected, along with flue gases, for EOR purposes. It is likely that there exists an oil rim that can still be produced. Figure 23 shows the acquisition parameters for the study.

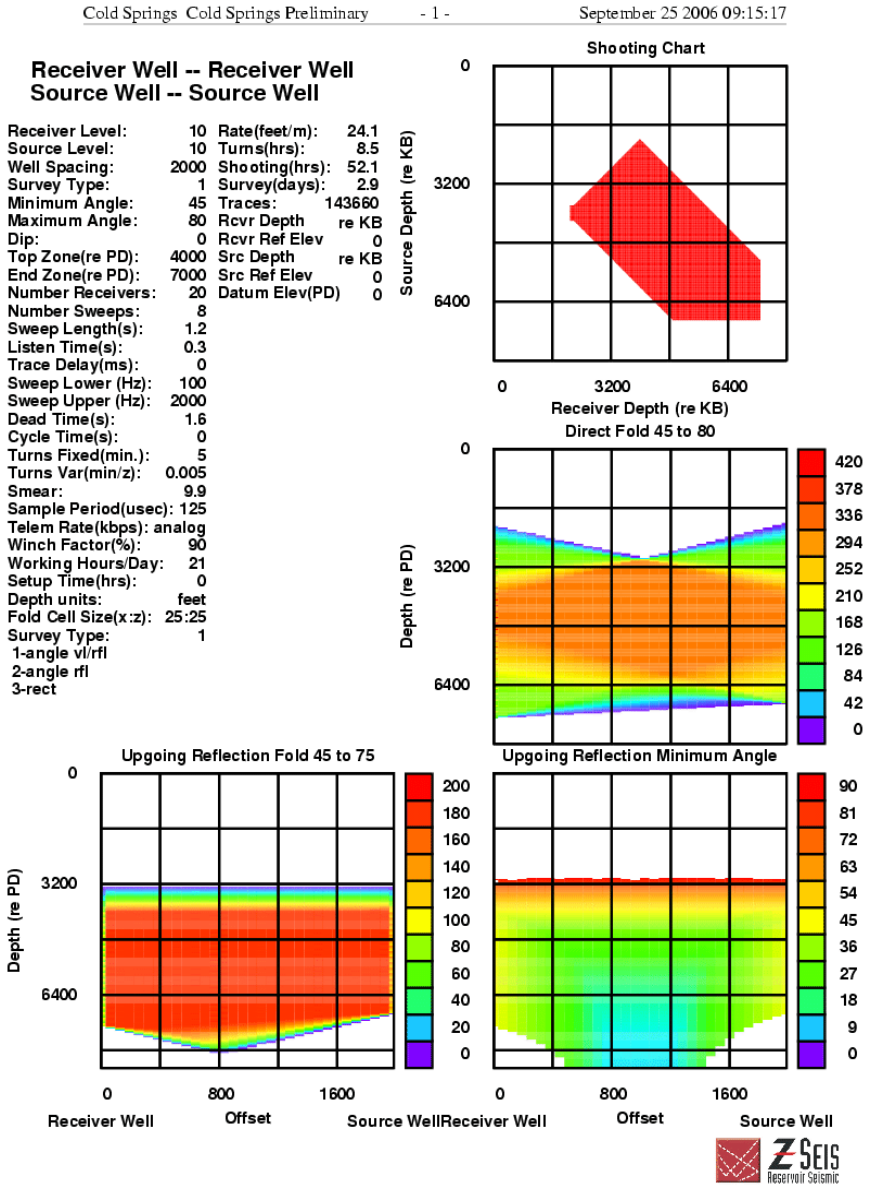

Figure 23: acquisition parameters for the second data set.

Sample seismic gathers are seen in Figure 24.

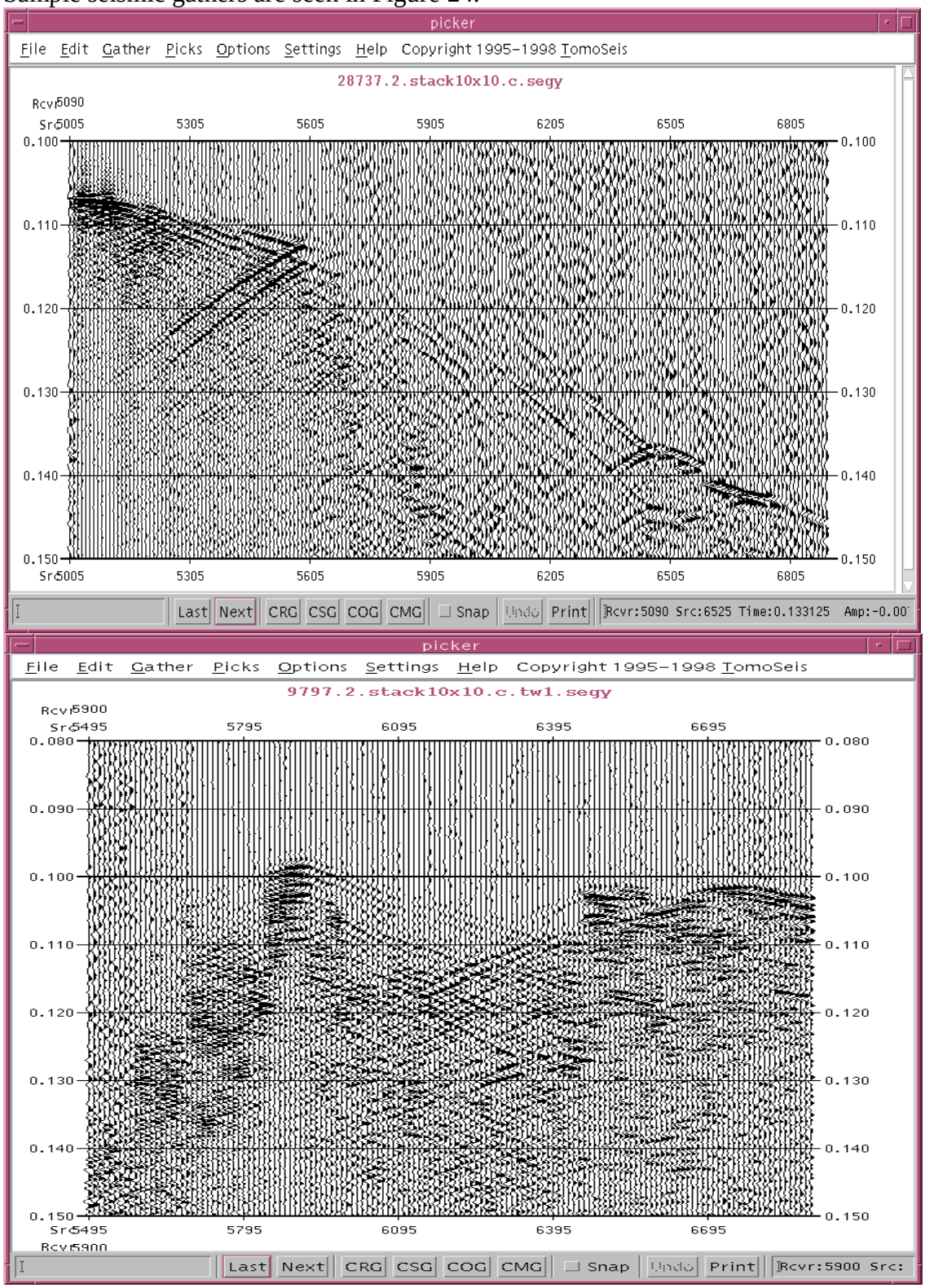

Figure 24: Sample seismic gathers from the second data set prior to any processing.

Because the two wells used for the seismic source and receiver string were also used for production, they are open to the formation through perforations. The wells had to be "killed" by adding water to prevent the flow of hydrocarbons, but this also led to the flow of water into the formation through the perforations. This, in turn, generated seismic noise in the form of conventional tube waves. This caused the data to be of somewhat lower quality than the first data set, in part because the tube waves were not as well organized as those at Springdale, and were therefore a bit more difficult to remove, but the data set is still excellent, and is probably more typical of that which can be expected under "normal" commercial operation.

The Coldspring dataset was obtained in a field with slightly better well coverage within the reef itself than at Springdale, and within a reef that exhibited a significantly higher pressure with a variety of fluid phases. An initial image of that dataset is provided in Figure 25, with the reef area indicated by the arrows; in this case, the reef extends across the entire image because the wells are both within the reef.

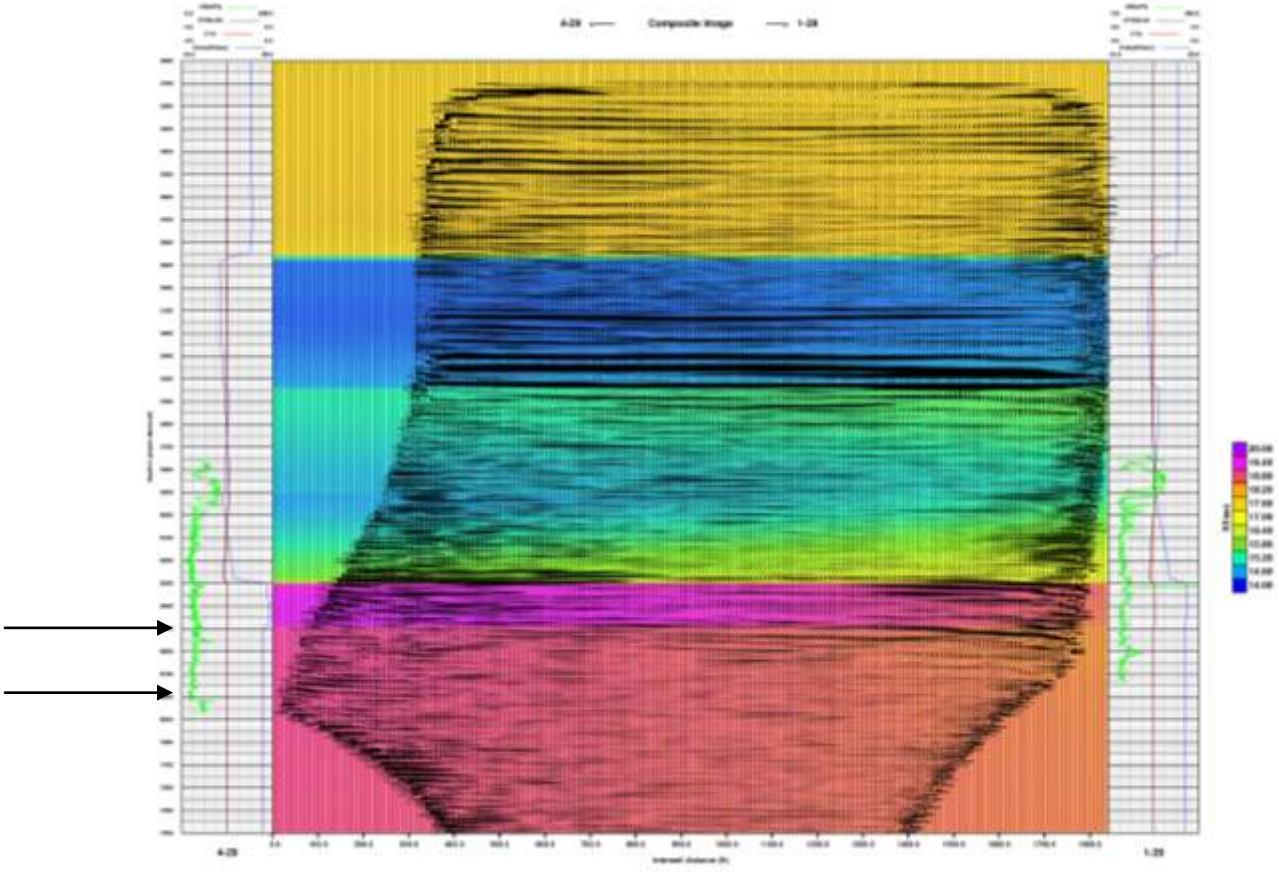

Figure 25: Initial stacked image, provided by ZSeis, for the Coldspring site. The arrows indicate the approximate location of the reef, which extends fully across this image. Colors indicate the tomographically derived seismic velocities, and the wiggle traces are the stacked seismic data over a wide range of angles.

ANALYSIS

Background on Wide-Angle Reflections:

Whereas most surface seismic data (and all standard analysis techniques) are used over reflection angles of 30° or less (at most 45°), almost all of the data within a crosswell seismic set is in the angle range of 40° or greater. It has been the experience that the processing that yields optimal images for crosswell data consists of narrow-angle gathers – as close to 40º as practical; this is probably due to the wavelet distortion that occurs at wide angles, and selecting too broad an angle range will tend to stack wavelets of different phases as well as including multiple reflections and refractions, which are difficult to separate at these angles (e.g., Smith, 1993). For a seismic wave impinging on an interface across which the velocity increases, refraction results in a "critical angle" for the reflected wave, beyond which the reflection is nearly total (the reflection coefficient has an amplitude approaching 1). However, the phase of the seismic signal is distorted, in a way that can be predicted. Figure 26 shows the amplitude and phase of the reflected signal for such a seismic wave, from the complete (not approximated) solution to Zoepprittz equations.

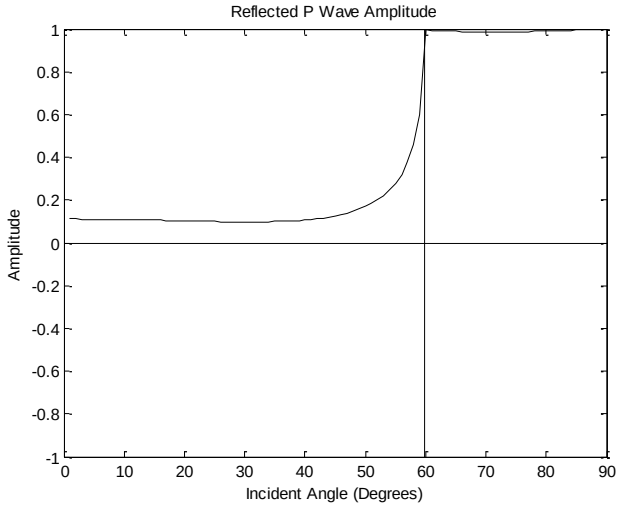

Figure 26a: Amplitude response of P-wave reflections as a function of angle for a typical reflection in the sequence encountered within the reef play. In this example, the critical angle is seen at about 60º.

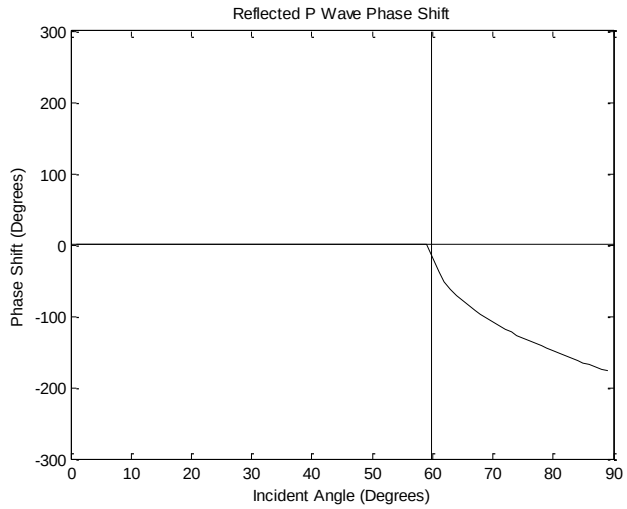

Figure 26b: phase shift for the case shown in (a). Note the large phase shifts at angles greater than about 60° in this case.

In some environments, it is possible to observe direct indications of hydrocarbon content from AVA analysis. Usually, this is accomplished by noticing changes in the AVA and/or zero-offset reflection character along a given horizon – it may be observed to exhibit certain characteristics when the interface is underlain by a water-saturated formation, and different characteristics when the underlying formation contains light hydrocarbons. In order for this technique to work, the interface must separate rock units which are themselves relatively homogeneous, or vary in a reasonably predictable manner. In addition, the contribution that the fluid content of the pores makes to the seismic velocity of the rock is important – in general, less compressible (faster) rocks, show less dependence of velocity on fluid content.

The reef environments in which we conducted this study are poorly suited for direct detection of hydrocarbons because the limestone and dolomite comprising the formation are highly incompressible and their velocities are very weakly dependent on fluid content. In addition, they are quite low porosity – a few percent at most – and the amount of hydrocarbon that may be present is therefore a tiny fraction of the total formation volume. However, there is one opportunity to observe hydrocarbons directly at very wide angles: Within the reef, we might expect to see gas-oil (or gas-water) contacts, within a given lithologic unit. We investigate the response that we could expect for this contact in a competent carbonate rock here.

The solution to Zoeppritz equations for the idealized simple case of an overlying gas-saturated limestone (density = 2.6 g/cc; Vp=20,000 ft/s; Vs=12,000 ft/s) with a reflection from its interface with an oil-saturated limestone (density=2.7 g/cc, Vp=21,000 ft/s; Vs=12,000 ft/s) is shown in Figure 27.

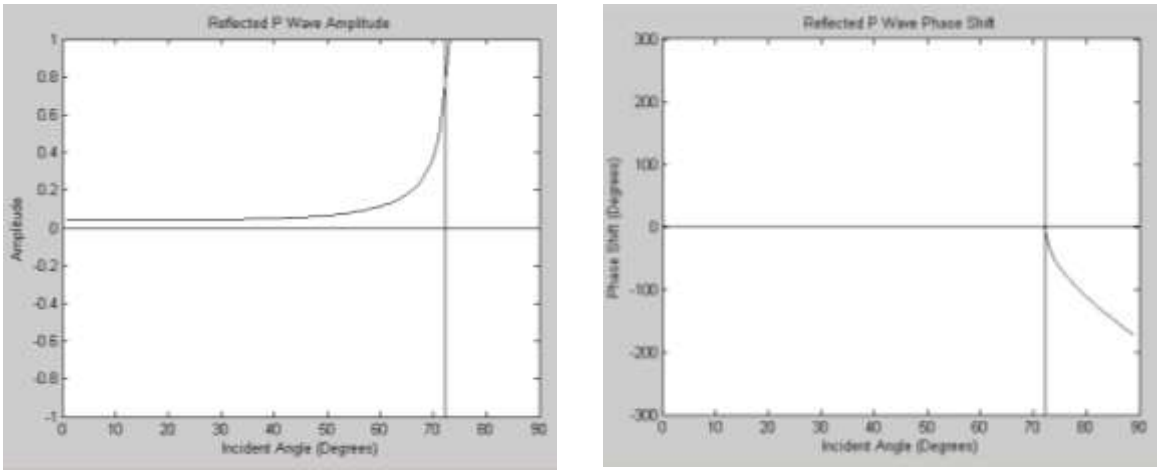

Figure 27: Zoeppritz solutions for the case of an idealized gas-oil contact within a limestone reef with low porosity.

Notice that the critical angle is 74°, well beyond the range that can be collected from surface seismic methods. Notice also that the amplitude of the reflection is vanishingly small for the range 0°- 60°, and would likely be imperceptible on surface seismic data.

On the other hand, the amplitude is extremely large within the typical stacking range for crosswell seismic imaging, particularly so within the range of 60° - 70°. Beyond 70°, the amplitude of the reflected P-wave is close to 1, but the phase shift slowly increases to 180° at 90° angle of incidence. Thus, we may expect to see fluid contacts within the reef if they exist at a scale visible to crosswell observations.

The modeling demonstrates that reflections from subtle contrasts, such as fluid contacts in competent rock, may be visible on wide-angle data from crosswell surveys, even though they would be invisible on surface seismic data. Phase shifts are important and their effect cannot be ignored beyond critical angle.

Presentation of AVA Data in 3 Dimensions:

Crosswell data is inherently 2D, unless a network of wells is employed. Because we can readily visualize in 3D, an opportunity exists to use the third dimension to display AVA character. We loaded the seismic data into a seismic-interpretation suite (Geographix by Landmark) and treated the data set as if it were 3D: vertical is depth (not time); one (inline) horizontal direction is distance along the profile measured from one of the wells; and the other (crossline) horizontal direction is angle of incidence. The processing sequence for creating a stacked image relies on first obtaining velocities through tomographic analysis, and then using that velocity field to determine appropriate times and locations of all seismic paths from all sources to all receivers. This, implicitly, finds the angle of reflection for any point in any seismic gather. The data are then re-sorted to "angle gathers" of traces at half-degree intervals, using a modified form of the VSP-CDP transform (details can be found in Lazaratos, 1993).

We can select and display any slice through the new seismic "volume". If we select a horizontal slice, we are viewing the amplitude-versus-angle behavior at one particular depth for all points along the line connecting the two wells. If we select a vertical slice in the "inline" direction, we can view the amplitude at any given angle of incidence along the line connecting the two wells. A view perpendicular to that provides an image of the angle gather for a given point between the wells. We can also "track" a specific reflection if the normal flattening allowed some residual moveout to remain in the gather, and display the AVA character along that event as it extends between the wells. Figure 28 shows a sample of these selections in three dimensions, while Figure 29 shows an angle gather for a specific location.

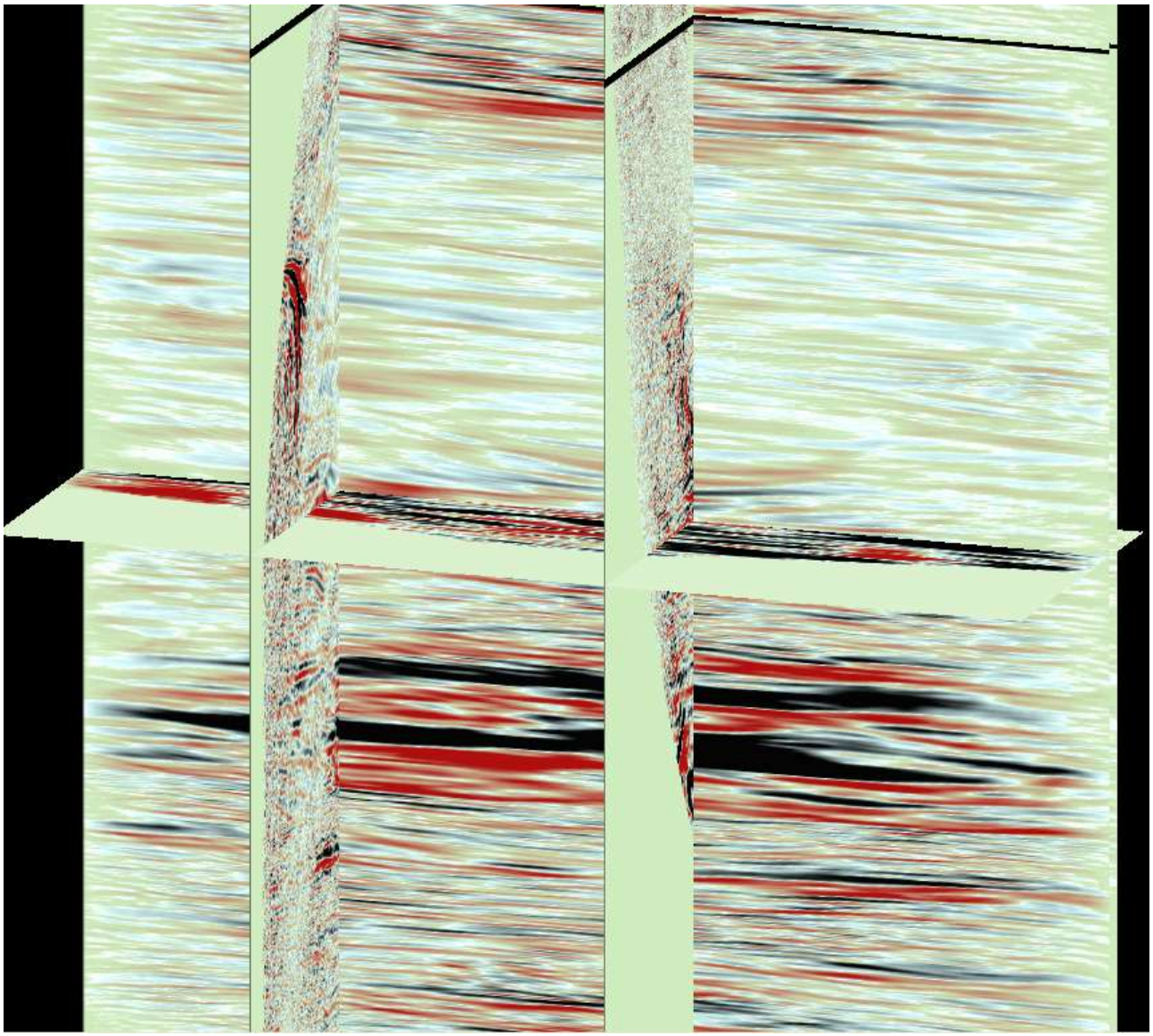

Figure 28: slices from a 3D volume of crosswell data, in which the "y" direction (here, into the paper) is actually the angle of incidence for the reflection. One of these slices is also shown in Figure 29.

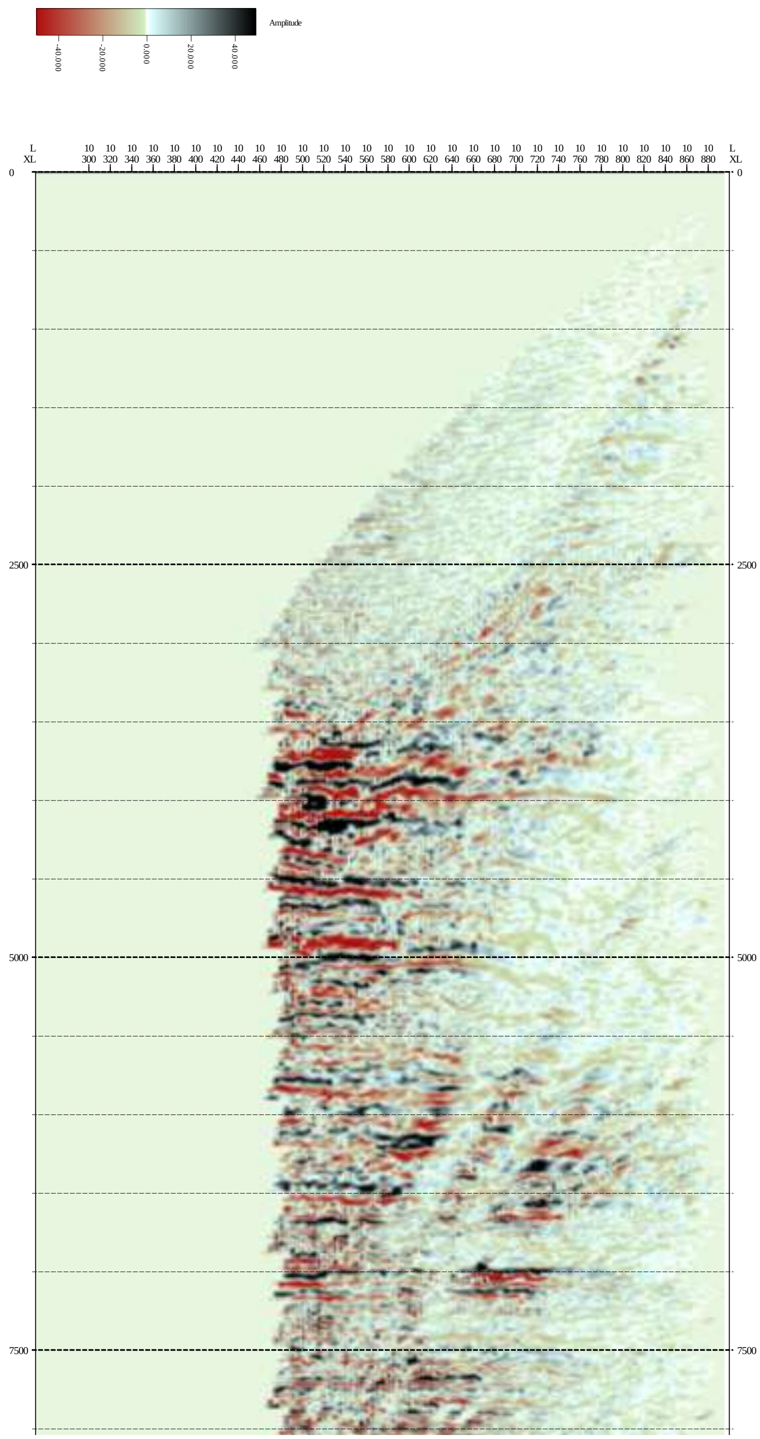

Figure 29: An example of the gather of seismograms (for the 10th cdp point away from the Stech well). The horizontal axis is Angle of Incidence. One can see some sources of “noise” or interference (probably processing artifacts, required to remove other features not of interest) and indications of amplitude variation with angle.

Springdale Site:

The stacked image (e.g., Figure 11) obtained from the crosswell survey is excellent, and shows the interior of the reef at a resolution that has not previously been practical. We can make several observations, and detailed discussion of them will follow.

(1) The interior of the reef contains very low-amplitude reflections, in stark contrast to the major lithologic boundaries outside the reef. There are two possible explanations for this: (1) the lithologic and fluid contrasts within the reef are very small; and/or (2) the highly variable saturations expected within the reef result in high attenuation and scattering on a local scale. We suspect that both mechanisms are in play here.

(2) The AVA character of beds within the reef are unremarkable, as may be expected if saturations do not change across interfaces, and the lithology varies by only a minor amount. If this is the case, then the interior of the reef may be drained in a very systematic manner. However, the reflections from within the reef are limited to narrow angle ranges, and the AVA character may simply not be well defined; this limitation may be due to low-amplitude reflections that are only apparent at near-critical angles.

(3) The AVA characters of well-defined bed boundaries beneath the reef are striking, and exhibit properties expected for reflections at or near the critical angle, consistent with modeling. However, the variations of this character along strike, where no lithologic variations are expected, provide a clue to the nature of the reef above the reflector. It appears that reflections whose ray paths pass through the reef itself are low-amplitude and somewhat incoherent, while those reflections whose ray paths pass outside the main body of the reef are more coherent, with the predicted behavior near critical angle.

(4) The images created from source and receiver locations beneath the reef ("imaged from beneath") contain higher-frequency data within the reef, and appear to exhibit reflections that are more continuous than those imaged from above. This may be due to a general trend of increasing velocity with depth, which would result in fewer reflectors with critical angles from beneath.

Amplitudes:

First, we will look into the general amplitude character within the reef, as imaged from above. There were two separate studies performed on this attribute. One was conducted largely by ZSeis, and has been published in a proceedings volume (Carrillo et al, 2007). In that study, they concluded that the apparent attenuation within the reef is real, and can be quantified. The other study was conducted largely by Michigan Tech, and is reported here.

In order to understand the character of the reflections within the reef, we must examine the raypaths for those reflections. Figure 30 shows another display of a stacked image from the Springdale site. The reef is readily visible as a low-amplitude region.

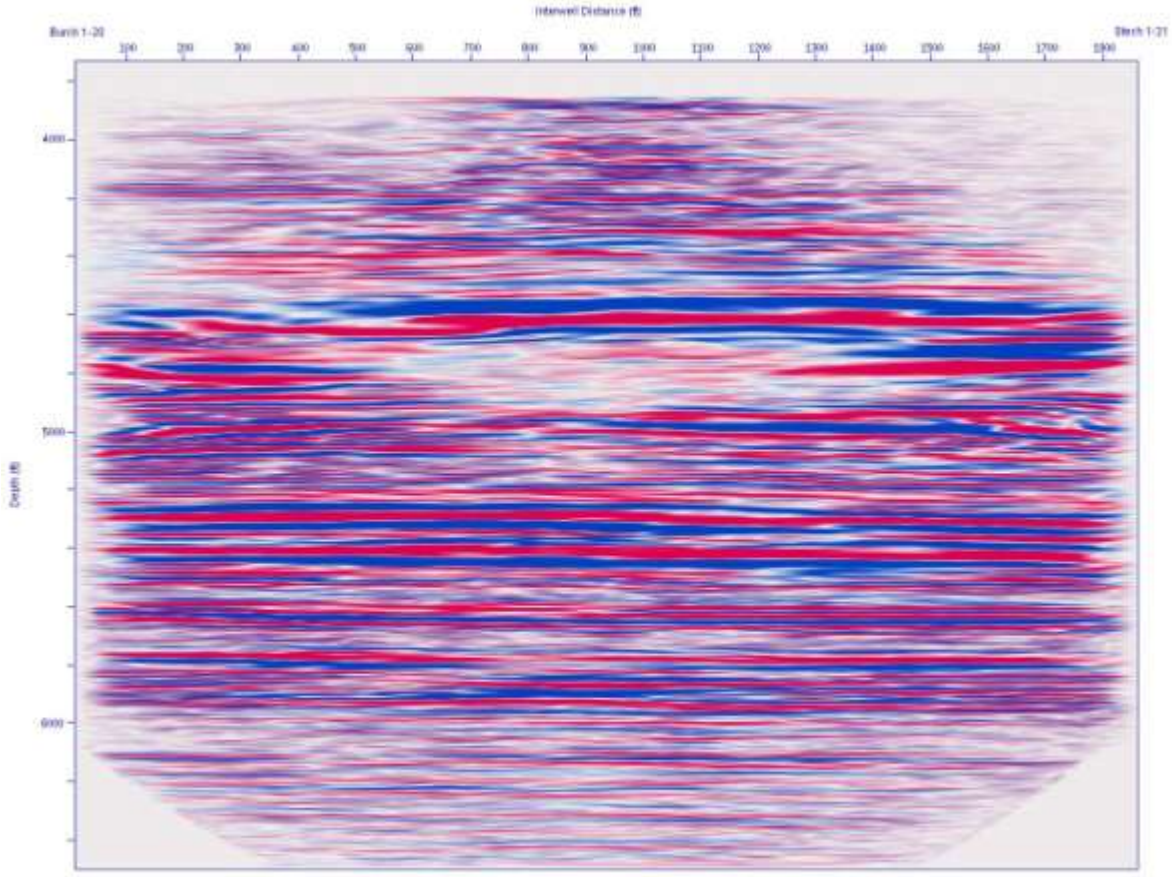

Figure 30: Stacked image of Springdale crosswell data, with amplitudes held at constant gain across the entire image. The reef is readily visible as the low-amplitude region at depths of about 4700 to 5000ft (1.4-1.5km), near the center of the image. Low-amplitude reflections can be seen within the reef.

It is important to understand that the flanks of the reef cannot be imaged directly from the aperture of seismic sources and receivers used in this study. Due to the dip of the flanks, sources and receivers would need to be located within the same well, or both in the well and at the surface, for a reflection from the flank to be visible in the data. Nonetheless, we can see the termination of the A1 anhydrite at the sides of the reef (reference the schematic geologic profile in Figure 10), and the appearance of the A2 anhydrite over the crest of the reef; these are the strongest reflectors apparent in the image.

Our initial studies of amplitude effects were centered on gross effects, including source- and receiver-location effects and transmission effects. Figure 31 shows a sample gather of seismograms gathered from one receiver location and many source locations (a common-receiver gather). The receiver location chosen for this figure is one that is barely below a major salt bed. First arrivals are evident on this gather, but the slow salt

beds (the formations in this part of Michigan are all very fast, so salt is considered slow in this environment) show both a "direct" arrival and a refracted arrival which arrives first. The direct arrivals are shown by the red line, used in the tomographic imaging process. This sort of plot can be generated for hundreds of source and receiver gathers, but only one example is shown here, in Figure 31.

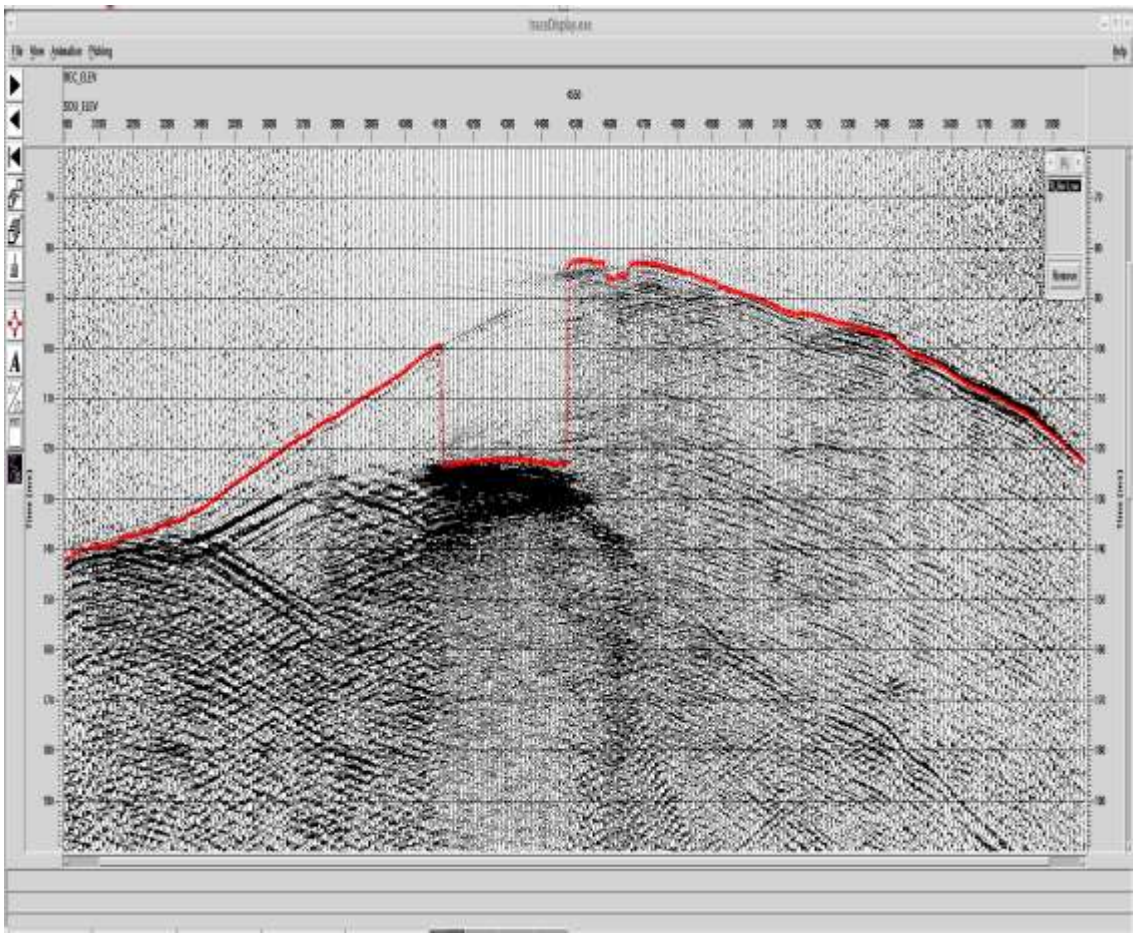

Figure 31: A gather of seismograms from many source locations and one receiver location. The red line shows the timing of the arrivals of "direct" waves, which are not always the first to arrive.

We used the direct-arrival times (not necessarily the first-arrival times) for all source-receiver pairs to study the amplitude and frequency content of the direct arrivals.

Figure 32 shows a perspective view of the amplitudes of all direct arrivals for all source-receiver pairs, while Figure 33 shows the same data viewed directly from "above".

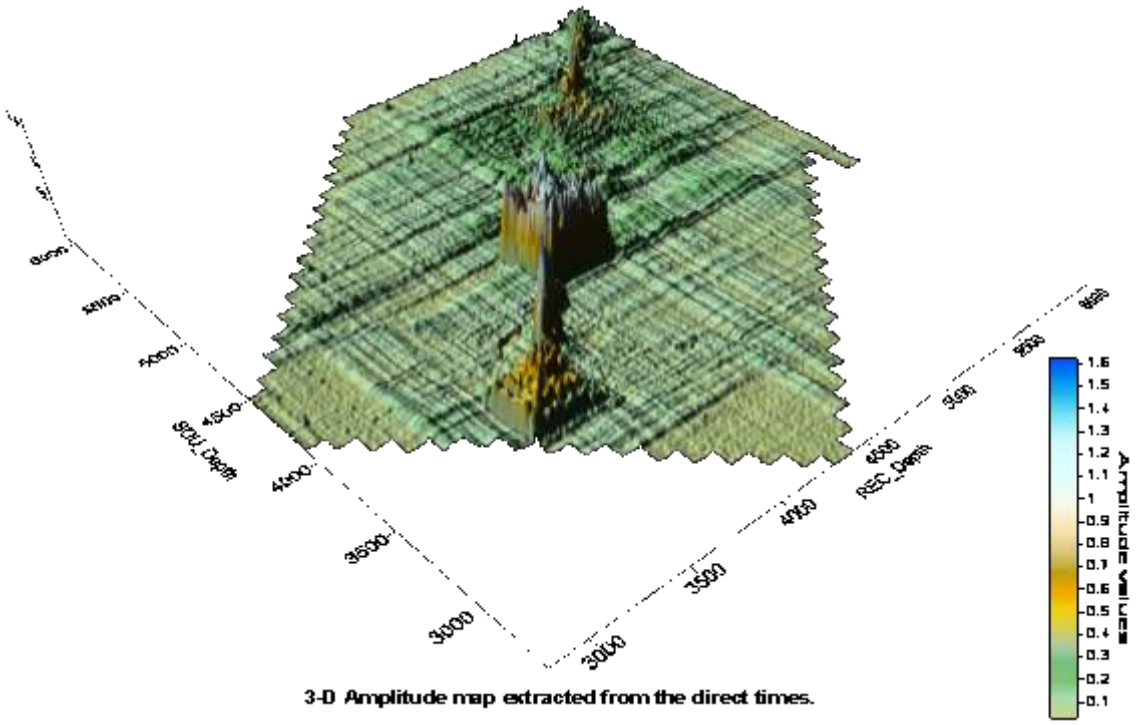

Figure 32 (above): A perspective view, showing the amplitude of the direct arrival for each seismogram, as indicated by source and receiver locations. Height and color both indicate amplitude of the arrival. *Figure 33* (below) shows the same data viewed directly.

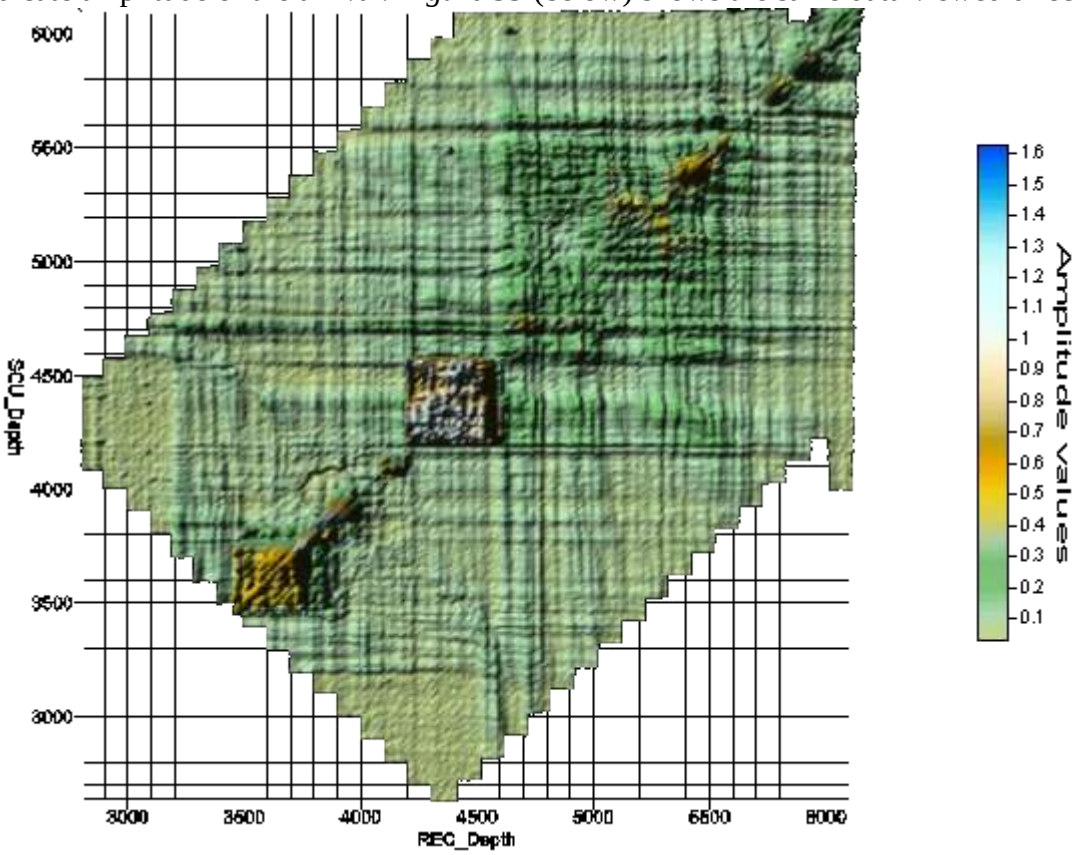

On this plot, seismograms that demonstrate "zero-offset" between source and receiver depths (that is, the source and receiver are the same depth) lie along the diagonal that runs from lower left to upper right. Seismograms that are recorded from a common source location are along horizontal lines, while seismograms that are recorded from a common receiver location are along vertical lines. Seismograms that have a "common-mid-depth" – that is, those whose mid-point between source and receiver locations are the same – lie along diagonals that would run from upper left to lower right; the location of that mid-depth is the depth at the point where this line crosses the main "zero-offset" line. These relationships are indicated in Figure 34 below.

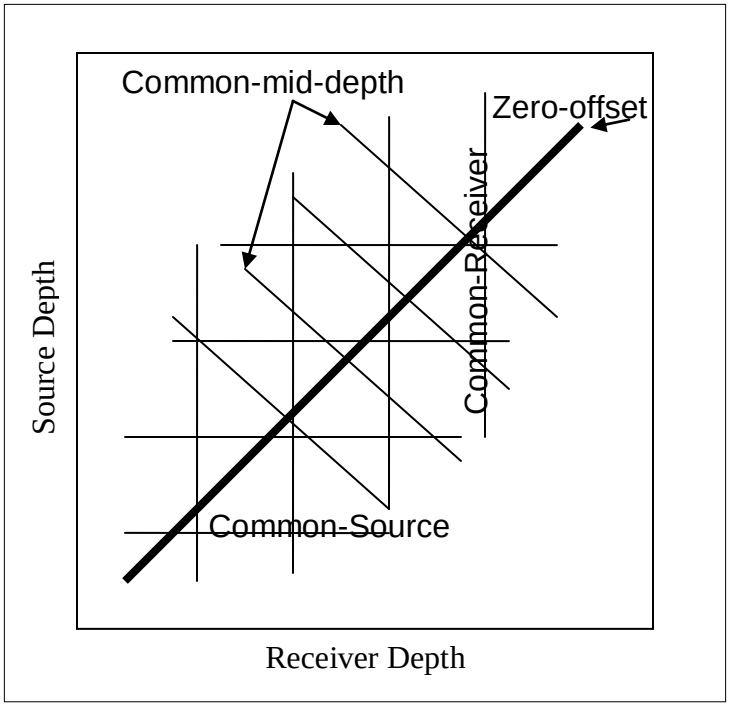

Figure 34: Schematic of source and receiver locations for the displays of Figures 32-33.

The most-obvious features in all three previous figures are related to the salt beds. The later arrivals (in Figure 31) are large amplitude, due to the focusing nature of the slow salt formations. In addition, salt is extremely homogeneous, and little or no scattering is expected within the salt beds. Figures 32 and 33 show the extremely large amplitudes associated with salt, for example as seen at depths of ~4200 to ~4600 ft, where the sources and receivers both lie within the massive "B" salt (reference Figure 10 for formation locations). The direct arrivals are "trapped" within the B salt for these source and receiver locations, and are very large as a result. Similar effects can be seen for other salt beds.

Less-obvious features are found at other depths. When the source is at depth 4750 ft, a larger amplitude signal is seen at all receiver locations. (This is evident by the strong horizontal line seen on Figure 32 at that depth.) Because the receivers were held stationary while the source was moved up the well, we cannot assume that this was due to a particularly "hot" source firing. Instead, we see that for each of the dozens of times that

the source occupied this depth interval, the amplitudes recorded at all of the receivers was larger than other nearby depth intervals. We conclude that this is the result of some sort of near-source, or source-coupling, effect. At this location, the amplitude was apparently affected by the washout seen on the caliper logs (shown schematically in Figure 10); the larger borehole at this depth allowed the source signal to be larger-amplitude when it entered the formation (there are several possible mechanisms for this).

While there are many other small amplitude effects of interest, we will not discuss each detail here; instead, we concentrate on the evidence relating to passage of seismic waves through the reef area. Using the plot of Figure 34, we would expect seismic rays that pass through the reef at, say, 4720 ft depth, to be indicated by source-receiver locations that map roughly along diagonal lines, the common-mid-depth lines, running from upper left to lower right, and passing through 4720 ft. We do not see any profound amplitude effects in the display on Figure 32 corresponding to seismic rays that have a common mid-depth at 4720 ft. It is important to recall, however, that the seismic rays bend through the varying velocity structure, and a seismic ray with a common mid-depth of 4720 ft does not necessarily pass through that depth at the midpoint between the source and receiver wells. Nonetheless, there is no obvious pattern of lower amplitudes that seems to correspond with rays that should have crossed through the reef, other than a slight effect seen at common mid-depths of about 5200 ft, a bit deeper than the reef.

While amplitude effects can be due to a number of things, including source or receiver coupling and focusing of seismic rays, the preferential attenuation of higher frequencies is more strictly related to intrinsic properties of the material and/or finer-scale seismic scattering. In order to investigate this phenomenon, we use a plot similar to that for amplitudes, but showing the predominant frequency within the first couple cycles following the "direct" arrival. These plots are seen in Figures 35 and 36.

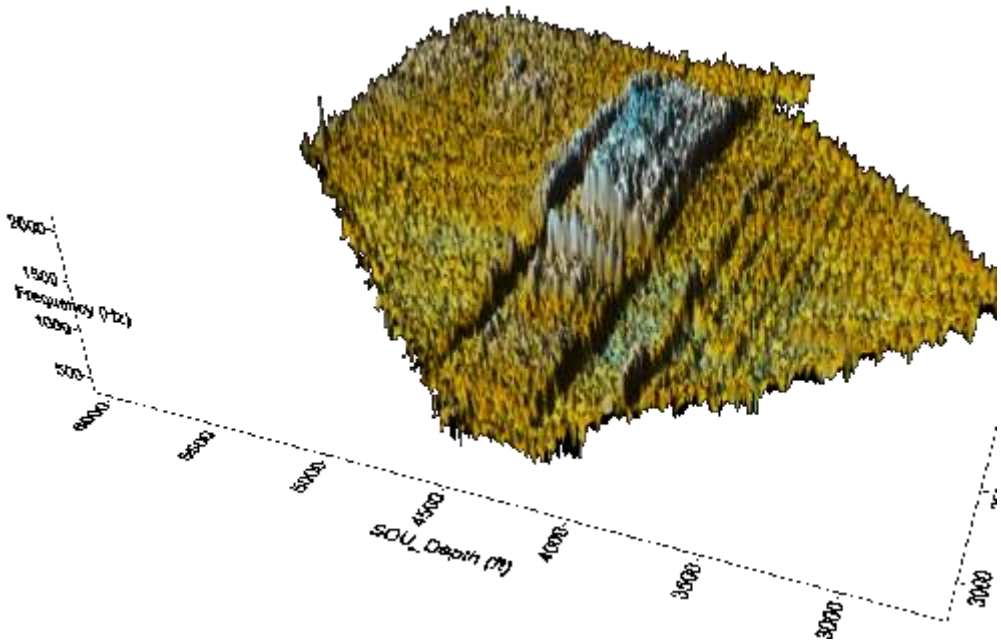

Figure 35: Perspective view of predominant frequency of the direct arrival.

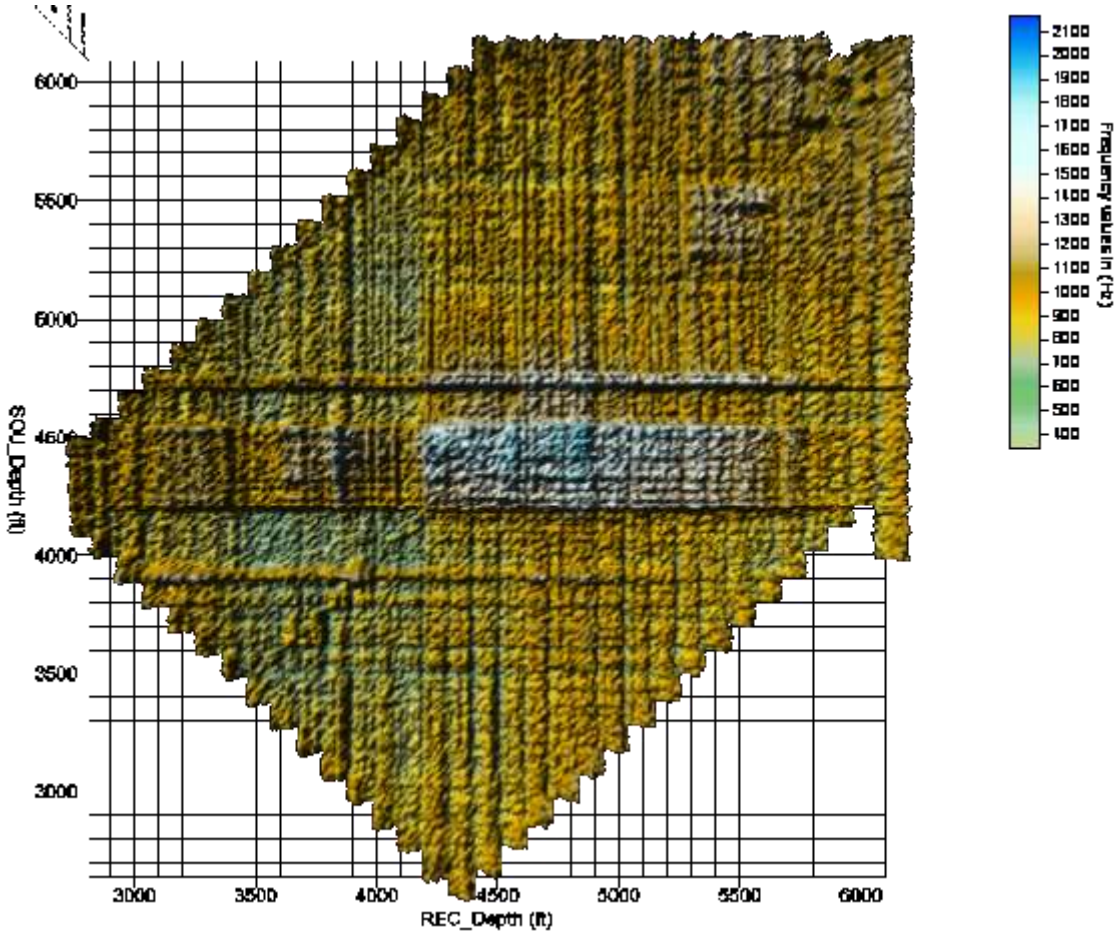

Figure 36: Same as Figure 35, but viewed directly without perspective.

The first thing to notice is that the frequency content is, to a first order, controlled by the source location alone. When the source is in a washed-out borehole associated with a salt bed, the seismogram recorded contains higher-frequency direct arrivals. If the receiver is in that same salt bed, or below it (but not above it), the frequency is the highest. Because the source borehole was uncased (at the depths of interest), while the receiver borehole was cased with a liner, we suspect that the borehole size is more significant than the fact that the formation contains salt.

There is no obvious effect on frequency associated with passage of a seismic ray through the reef depth zones, as evident from Figures 9 and 10.

In order to fully investigate the possible effect of attenuation in this data set, true amplitude and frequency tomography should be conducted. Such a study was performed by Carrillo et al (2007). They found that there is a significant attenuation of seismic waves that have passed through the reef, summarized in Figure 37, taken from their publication.

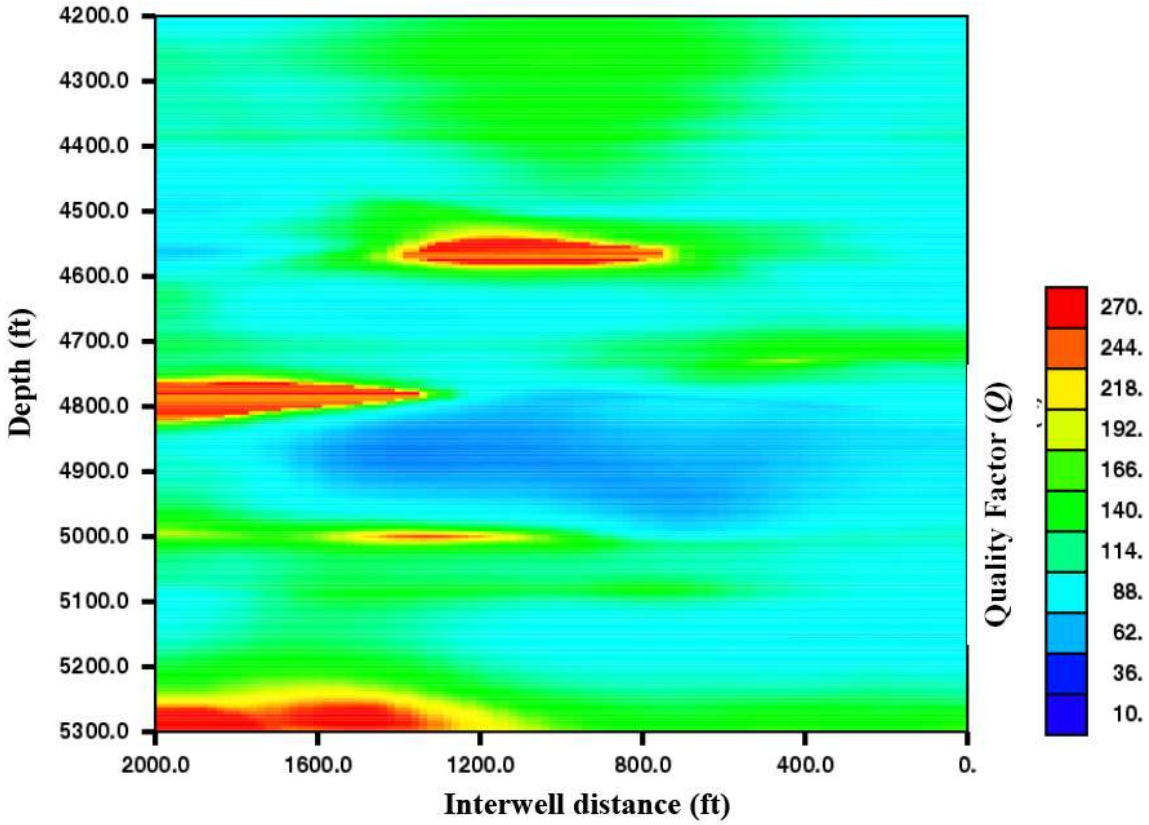

Figure 37: Q-factor for the profile between the wells at the Springdale site. Q-factor is the property that results in efficient transmission (high values) or poor transmission (low values). The reef is located at the site of the blue (low values) feature below 4700 ft, indicating that seismic waves which pass through the reef are attenuated, particularly in the higher frequencies. The high-Q regions above the reef and neighboring the reef correspond to anhydrite and salt layers, respectively. (Figure 5 from Carrillo et al, 2007.)

We have also investigated the possibility that the quality of the stack for reflected events is degraded when the seismic ray passes through the reef. If this were the case, we would expect to see incoherent reflections within the reef on pre-stack gathers. Instead, as the example shown in Figure 38 demonstrates, the reflections are small in the pre-stack domain, confirming that the stacking process is not responsible for the low amplitudes.

The stack of a crosswell image is constructed by stacking partial angle ranges. The angle ranges used are defined in Figure 39, where it is clear that the stacked traces represent a "fan" of angles. In Figure 40, we show six different, overlapping, angle range stacks. Notice the high-quality of the shallow reflections at small angles, and the high-quality of the deeper reflections at large angles.

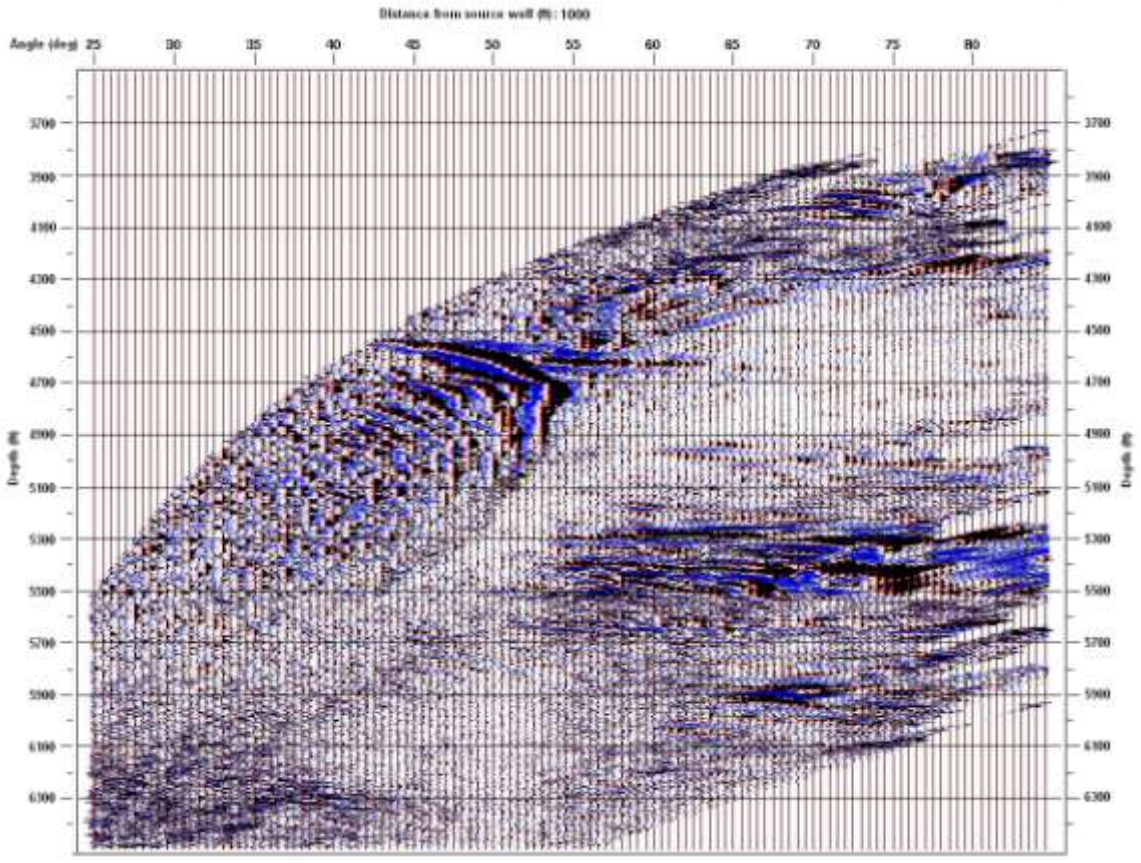

Figure 38: After mapping from a VSP domain to a CDP domain, the data are gathered at each interwell point with varying angles of incidence. This diagram shows one AVA gather. The data at angles greater than 55 degrees are most reliable at this location (determined by geometry of acquisition). We see that the depth interval corresponding to the reef location (4700-5000 ft) is indeed a zone of very-low-amplitude reflections, as is the region just over the reef at larger angles of incidence.

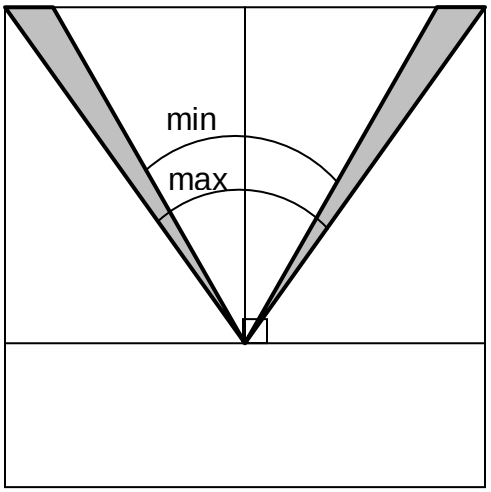

Figure 39: The angles used in stacking represent a range from a minimum angle (the inner limit of the fan) and a maximum angle (the outer limit of the fan).

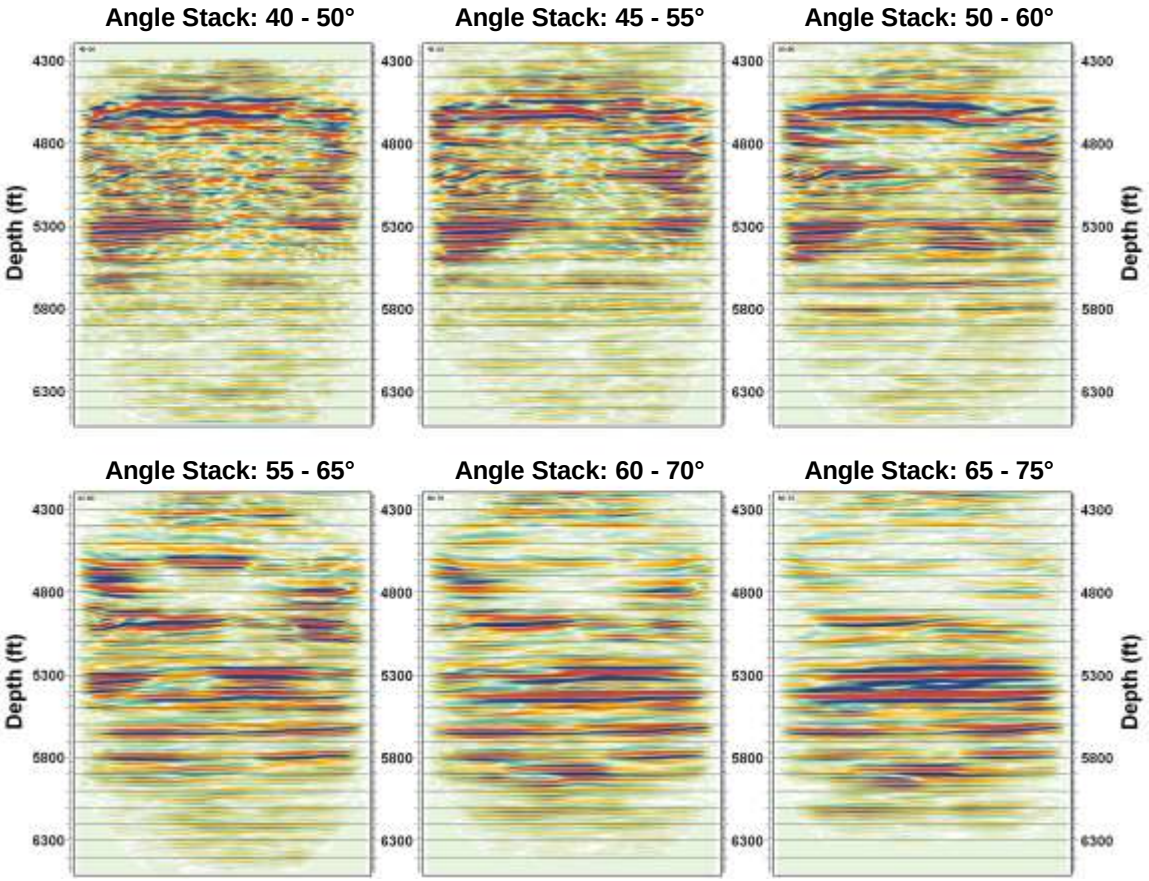

Figure 40: Six angle range stacks of the complete seismic section, illustrating the changing nature of reflectors with differing angles. Each image covers same depth range and all are approximately 1:1.

The character of the reflected events can be seen to change as the angle ranges used for stacking changes. In particular, the shallower layers are larger amplitude and more continuous at smaller angles, while the deeper events are larger and more continuous at greater angles. Figure 41 shows the same angle stacks as Figure 3, but with the approximate fan of angles represented, sketched on each section for a reflection from the center of the image, below the reef.

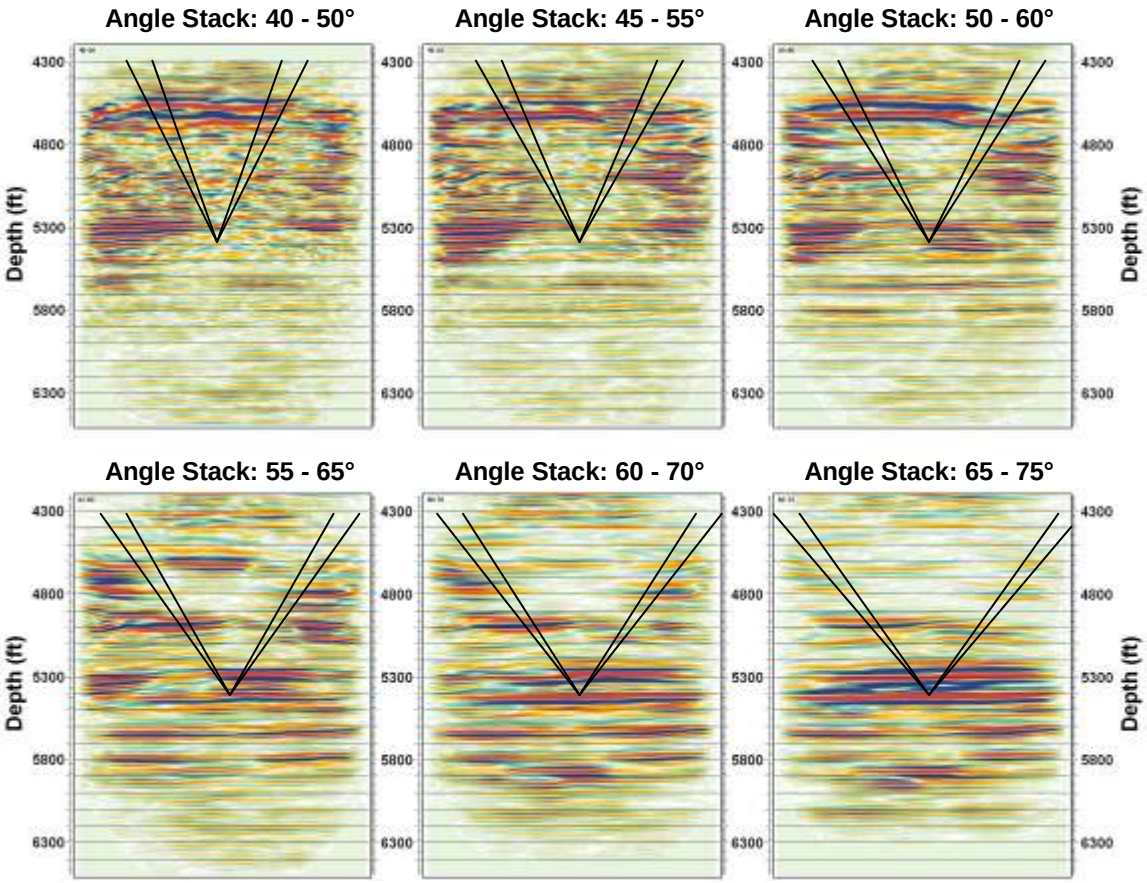

Figure 41: Six ranges of angle stacks of the complete seismic section, illustrating the changing nature of reflectors with differing angles. Each image covers same depth range and all are approximately 1:1. Approximate Angle wedges are drawn in for visual reference.

Figures 40 and 41 clearly demonstrate the effect of angle of incidence on the quality of the stacked image for reflectors on a large scale, particularly surrounding (above and below) the reef. Figure 42 shows the same gathers, but over a limited depth range, selected to provide a clearer image of the reef itself.

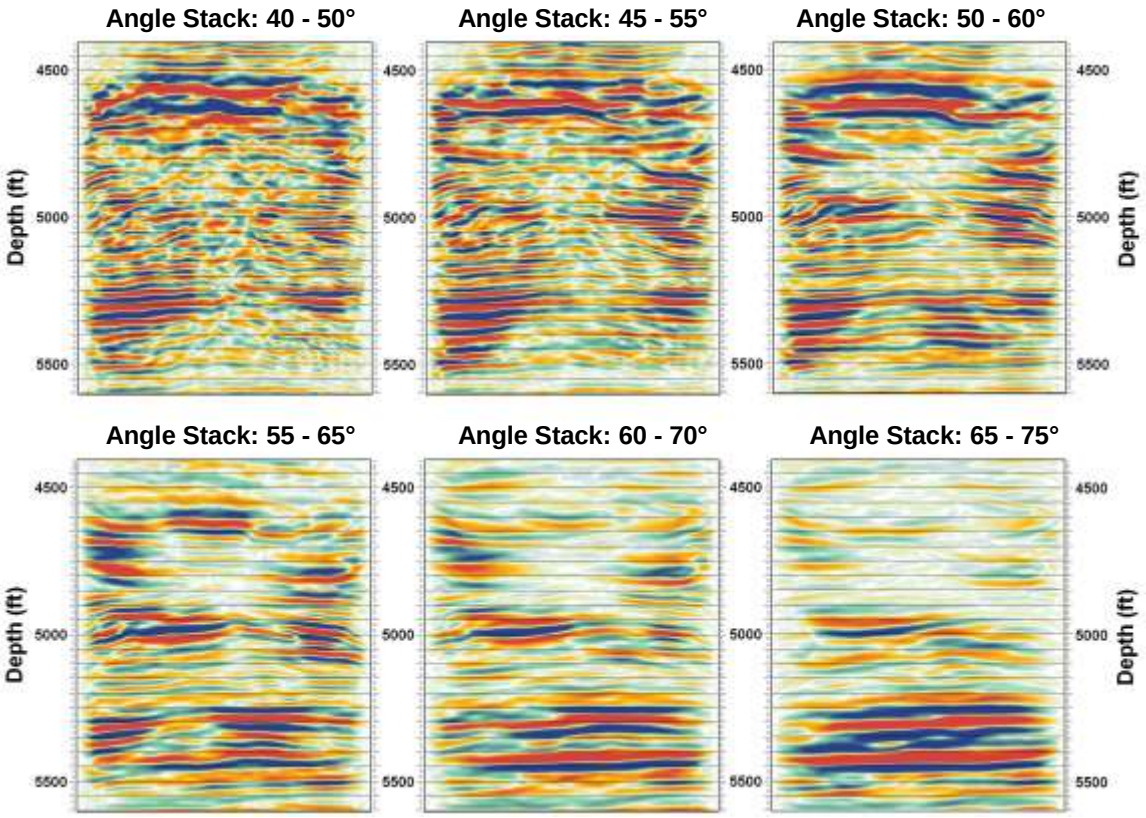

Figure 42: Six of the angle range stacks for a 1000' section nearly centered on the reef, which illustrates the changing nature of the internal reef reflectors with angle. The Reef lies approximately between the depths of 4700' – 5000'.

The images in Figures 40-42 show the effect of reflection character caused by the angle of incidence. While some of the variation is due to changes in attenuating properties of the medium through which the seismic ray has travelled, some of it is due to the nature of the interface itself. We now investigate the AVA behavior of select reflectors within the Springdale crosswell data set.

AVA Character of Reflectors:

We start by examining the reflection character at one interface beneath the reef, using reflections obtained from sources and receivers above the reef. The target in this case is the top of the Burnt Bluff carbonate. Figure 43 shows the location of three reflection points along the profile between the two wells, while Figure 44 shows that the coverage provided by the acquisition program should not be expected to have affected the AVA character in any meaningful way.

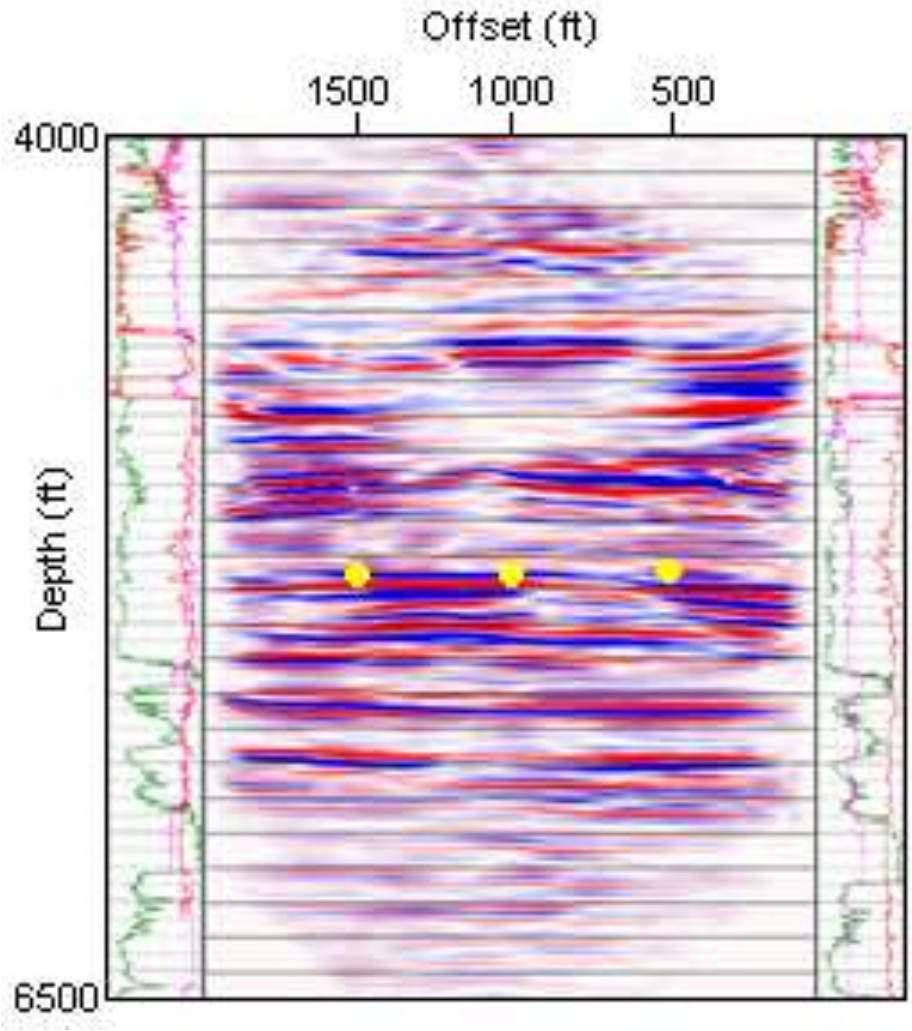

Figure 43: Stacked unmigrated reflection image. Yellow dots correspond to distances from the receiver well later used in AVA analysis. The reef is in general an area of low reflection amplitude at depths of 4700' to 5000', but coherent reflections are apparent within it.

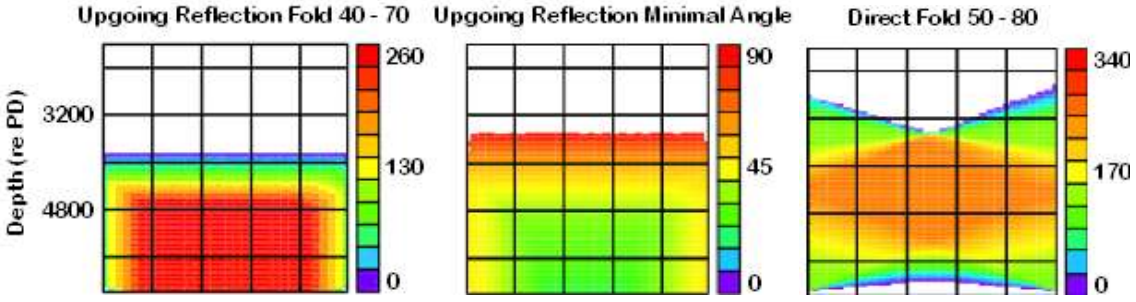

Figure 44: Crosswell survey acquisition parameters (data provided by ZSeis, Inc.)

One feature of acquisition, unavoidable in crosswell geometries, is the range of angles present within different portions of the interwell region. The middle diagram of Figure 44 hints at this, but a more meaningful example is provided in Figure 45, which shows the complete crosswell angle gather at three locations between the wells. The varying angle ranges makes it difficult to provide exact comparisons of AVA behavior at different locations.

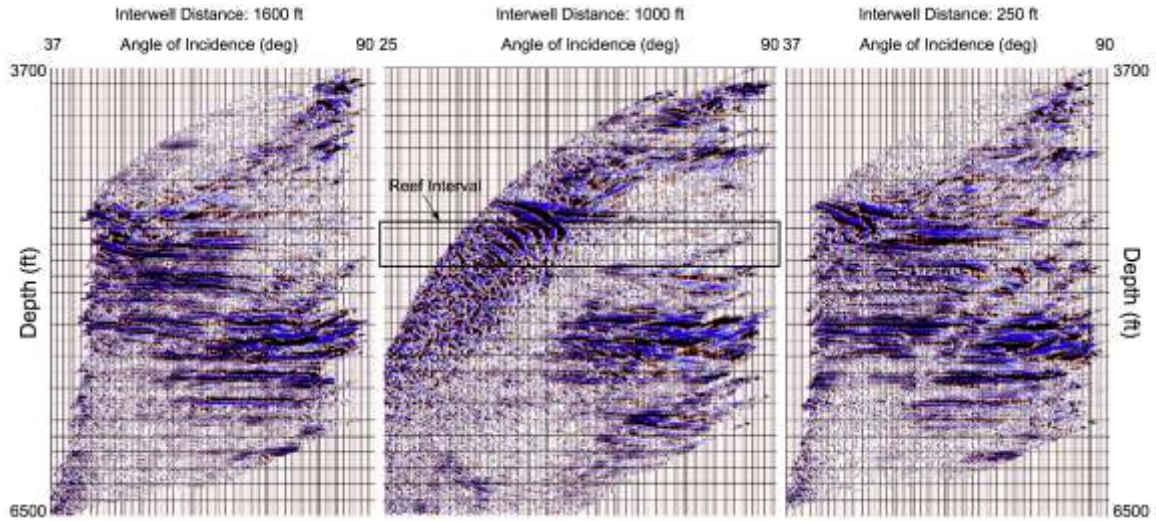

Figure 45: Various full angle data gathers at differing interwell distances as measured from the receiver well. Note the changing AVA character between interwell distances and varying angle ranges available, making the interpretation of the same interface difficult at these different locations. (Trisch, 2006.)

Let us first look at the AVA character of deep reflection that can be well-characterized by its logged properties. The reflection amplitude for the event associated with the Burnt Bluff carbonate is modeled in Figure 46, using the complete Zoeppritz equations.

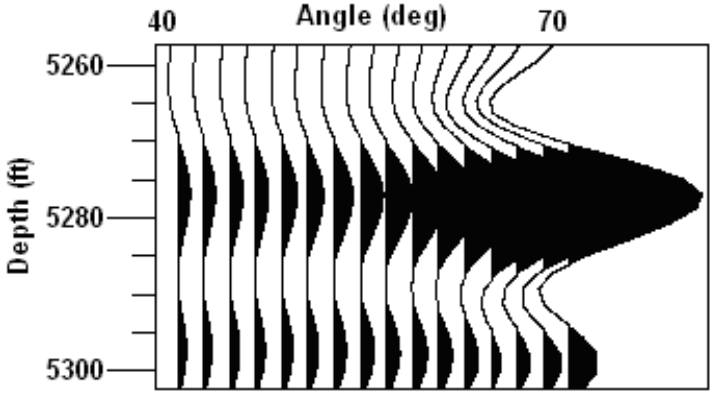

Figure 46: Synthetic reflection gather for the reflection from the top of the Burnt Bluff carbonate at approximately 5280 ft, using a 2000 Hz Ricker wavelet.

The first interface in this study is a strong reflector at approximately 5280 feet deep. This reflector is the interface between the Gray Niagaran and the Burnt Bluff carbonate, based on well log data. Three interwell distances, at approximately equal intervals, were chosen to represent this interface. The AVA character can be observed to change depending on the interwell location, despite the apparent homogeneity of the interface as indicated by the well log curves at each well. The variation in AVA character at the different interwell distances is apparently due to ray path effects and can be observed in Figure 47. The angle ranges available at different locations varies greatly, limiting the range available for comparison at the different interwell locations. Figure 47 shows the seismic gathers for the three locations indicated by dots on Figure 43. It also shows the measured amplitudes and the predicted amplitudes.

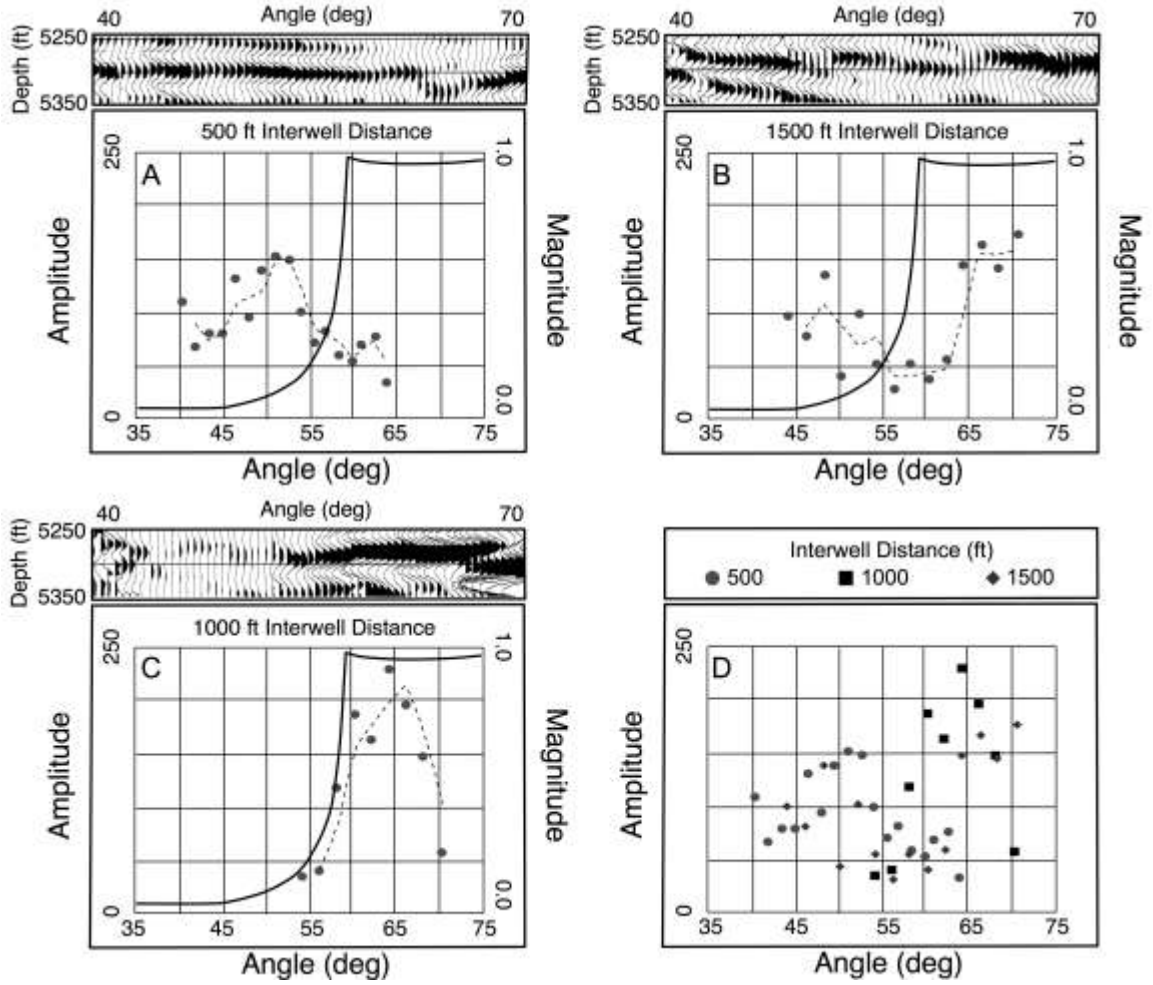

Figure 47: AVA character for three interwell distances along the Gray Niagaran to Burnt Bluff Carbonate interface. Above each figure is the angle gather reflection used for amplitude extraction. Data points are plotted with gray points (left axis scale), while the thin dashed line is the moving average of the data to help show data trend. The heavy black line is the modeled Zoeppritz reflectivity solution (right axis scale) for the interface. Data are plotted together in D for comparison. Scales for each figure are the same.

Now we turn to the comparison of this data with a predicted AVA model response over the full angle range for each location. The modeled Zoeppritz solution for this interface between the Gray Niagaran and the Burnt Bluff Carbonate is shown in Figure 47. The expected amplitude from the Zoeppritz solution (Figure 47) is near zero at angles less than the critical angle. Around this angle there is a small range of angles from which good amplitude data can be extracted before the phase rotation affects the wavelet and becomes a problem. The expected angle range over which to analyze the data is very small and at most perhaps 15 degrees when the amplitude is strong enough to be observable, but before it exceeds the critical angle. In Figure 22 the reflection is seen to change as a function of angle on the seismogram plotted above each graph at the different interwell distances. The different angle ranges available for each interwell distance are due to the geometry of the crosswell environment. There is a similar trend in AVA response among the angle ranges at the various locations. In the gather locations flanking the reef, 500 ft and 1500 ft from the receiver well, the amplitude increases from 40° to 50°, declines near 60°, but then increases for the gather that includes at larger angles due to approaching the critical angle. The 1000 ft offset gather has the same trend of increasing amplitude approaching the critical angle and then decreasing post critical, perhaps due to phase distortion.

At extremely large angles, the amplitudes may decrease not only as a result of the phase rotations, but also as a result of the filtering required to remove the direct and refracted waveforms. Smith (1993) observed that crosswell reflection time and moveout both approach the direct arrival travel time as the incidence angle approaches 90°, and these events are filtered out (Lazaratos, 1993). However, it is not apparent from the observations made here that these effects are present at angles as low as 70°.

We also investigated other locations within the profile. These are shown in Figure 48.

In order to avoid the complications that result from seismic wave propagation through the reef, we will investigate a reflection from an interface above the reef. In order to avoid the possible critical angle problems and local heterogeneities, we select an interface that is fairly continuous and represents a slight decrease in acoustic impedance at the interface. Figure 49 shows the AVA character for an interface at approximately 4615 feet deep. This interface appears as a good reflection over approximately 500 feet of horizontal distance between wells, directly over the central portion of the reef. This reflector is interpreted to be one of the many thin bedded interfaces draped over the top of the Brown Niagaran carbonate reef, based on well log data.

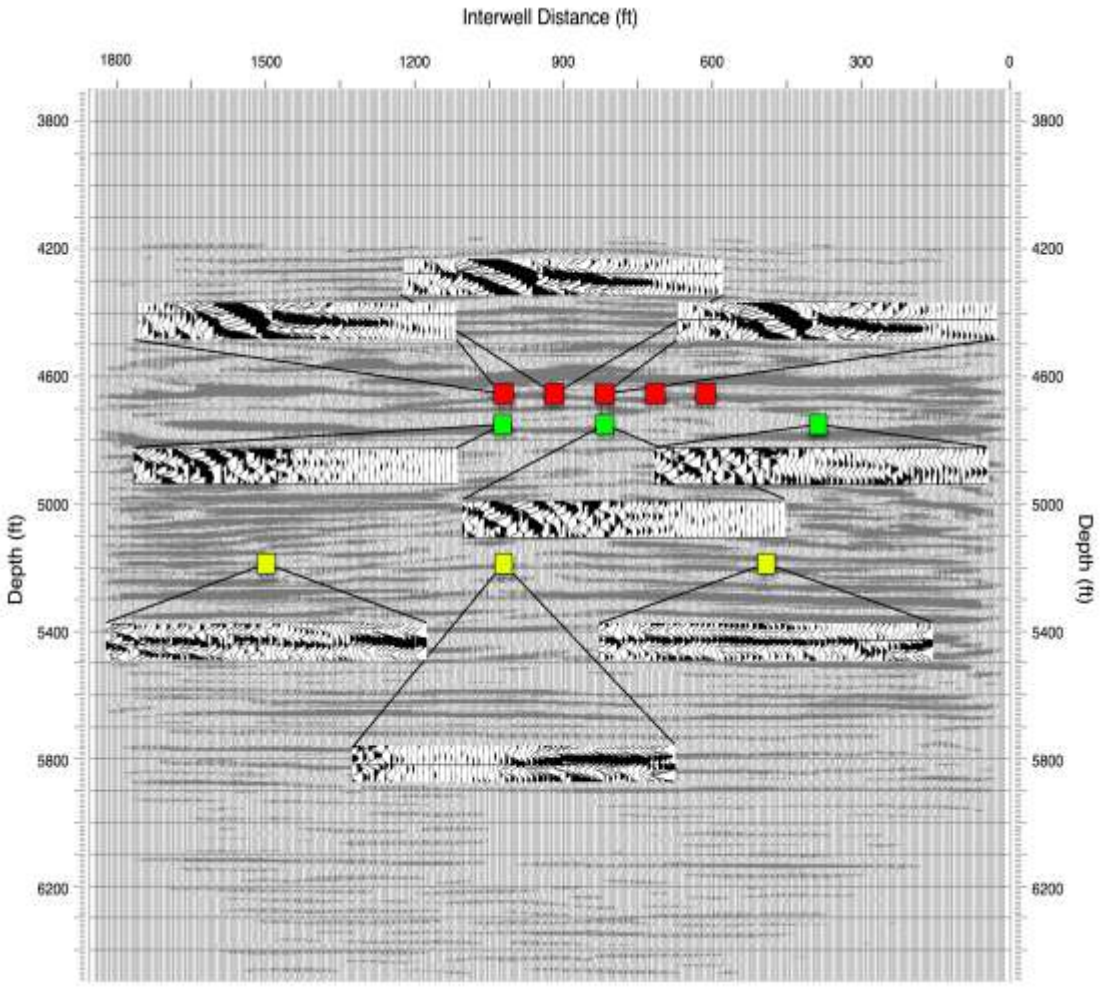

Figure 48: The locations of example AVA studies presented here. The gray-scale image is the stacked seismic section, for reference. The colored dots present the locations of specific study locations; the sites represented by the yellow dots were also presented in Figure 47. The black-and-white overlays show the prestack seismic data at those locations, with increasing angle to the right. (Trisch, 2006.)

The gathers shown in Figure 49 consistently exhibit a reflection with amplitude decreasing rapidly with increasing angle beyond 55° or 60°. Because the gathers start at 53°; with only small angle ranges available, definitive interpretations of the interface are difficult from only one location. However, some detailed differences in amplitude and overall AVA character between the gathers from different interwell distances, a consistent trend is apparent from the combined plot in the lower right of Figure 23. The overall trend is one of high amplitude decreasing to zero with increasing angle of incidence. Because we have independent knowledge of the nature of this interface we can compare this behavior with model predictions.

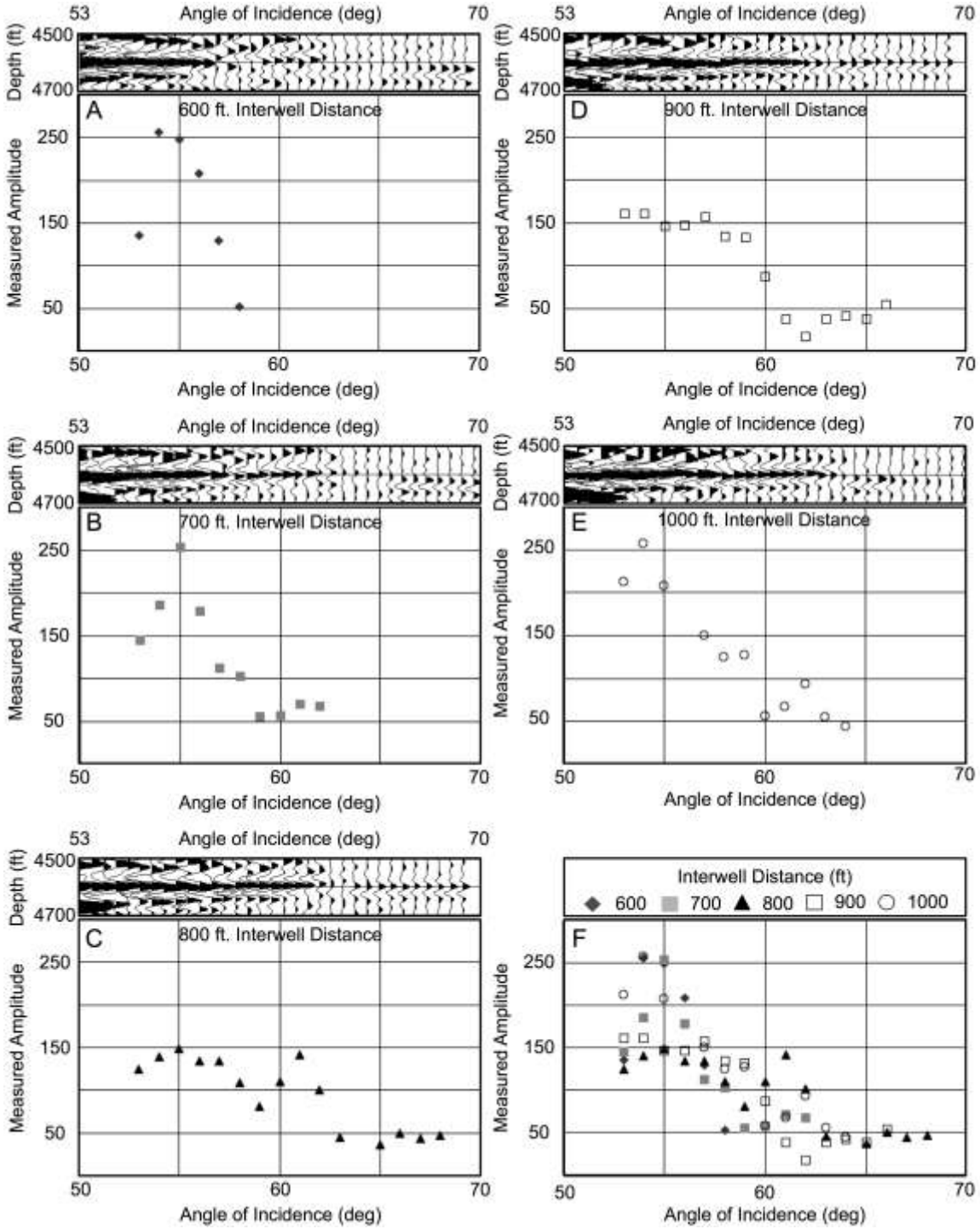

Figure 49: AVA character for five interwell distances for the interface near the top of the Niagaran reef (red dots on Figure 48). The reflection character for each offset is shown in the box above the amplitude plots. The lower right plot (F) is the amplitude plot of all five offsets overlaid together to show the changes and similarities in AVA character. Reflection events were flattened to 4600' from a depth of near 4615' for interpretation and amplitude extraction purposes. (Trisch, 2006.)

From the well log data, we infer that the 4615 ft reflector over the reef is the interface between the A2 Carbonate and the A2 Anhydrite. The parameters for the established rock model were extracted from log and previous seismic (mostly VSP) data. These parameters are listed as "Model 1" in the table shown in Figure 50. The exact Zoeppritz solution for this model is also shown and predicts a near zero amplitude that increases with negative amplitude for increasing angle of incidence, which is not what we observe. The question arises: can we use the crosswell AVA observations to refine the formation parameters of Vp, Vs, and density?

To test this, several exact solutions for the Zoeppritz equation were calibrated for slight modifications to the original "established" set of parameters, all of which fit the observed AVA character of the data fairly well, as shown in Figure 50. These models illustrate the sensitivity of the AVA response to minor changes in Vp, Vs, or density measurements, and its possible use in restricting the range of possible layer parameters.

To refine the model, various layer parameters were used to create a trend that matched the observed AVA data. Attention was primarily paid in varying the Vp and Vs parameters as these had a much higher impact on the large angles of incidence from crosswell data. Density had a larger effect for angles of incidence less than 30°, below the range of available angles within this crosswell environment. Various scenarios were constructed that match the observed data trend of decreasing positive amplitude with increasing angle of incidence at about 50° to 65°. Models were created using re-interpreted well logging measurements (Model 3), and models that held one layer fixed to the established rock model parameters and varied the other (Models 4 and 5). One more model was created by allowing all the velocity parameters to vary (Model 2). This shows that by only slight variations in rock properties, models can be created that accurately fit the observed amplitude trend of the crosswell data.

The main conclusion that we can draw from this exercise is that the crosswell AVA data can provide an extremely robust refinement of the lithologic model of the earth. In this case, very small changes in compressional velocity, shear velocity, and density are required to correctly adjust an initial, somewhat naïve, model in order to fit the AVA data.

Now we turn our attention to a reflection within the reef. Such an interface is most likely the result of fluid contacts or subtle changes in the nature of the reservoir rock such as porosity, density, or change in character of the dolomite, including the presence of anhydrite.

The reflection chosen at 4740 ft depth is very subtle and exhibits a very low amplitude event from 400 to 600 feet from the receiver well, within the producing portion of the reef. The range of angles for which the reflection exists is very narrow, sometimes only a few degrees at a few locations some of which are plotted in Figure 51. Most events within the reef are similarly difficult to track, and exist over small angle ranges making it increasingly difficult to determine how such a window fits in the exact Zoeppritz solution unless the angle data spans the critical angle.

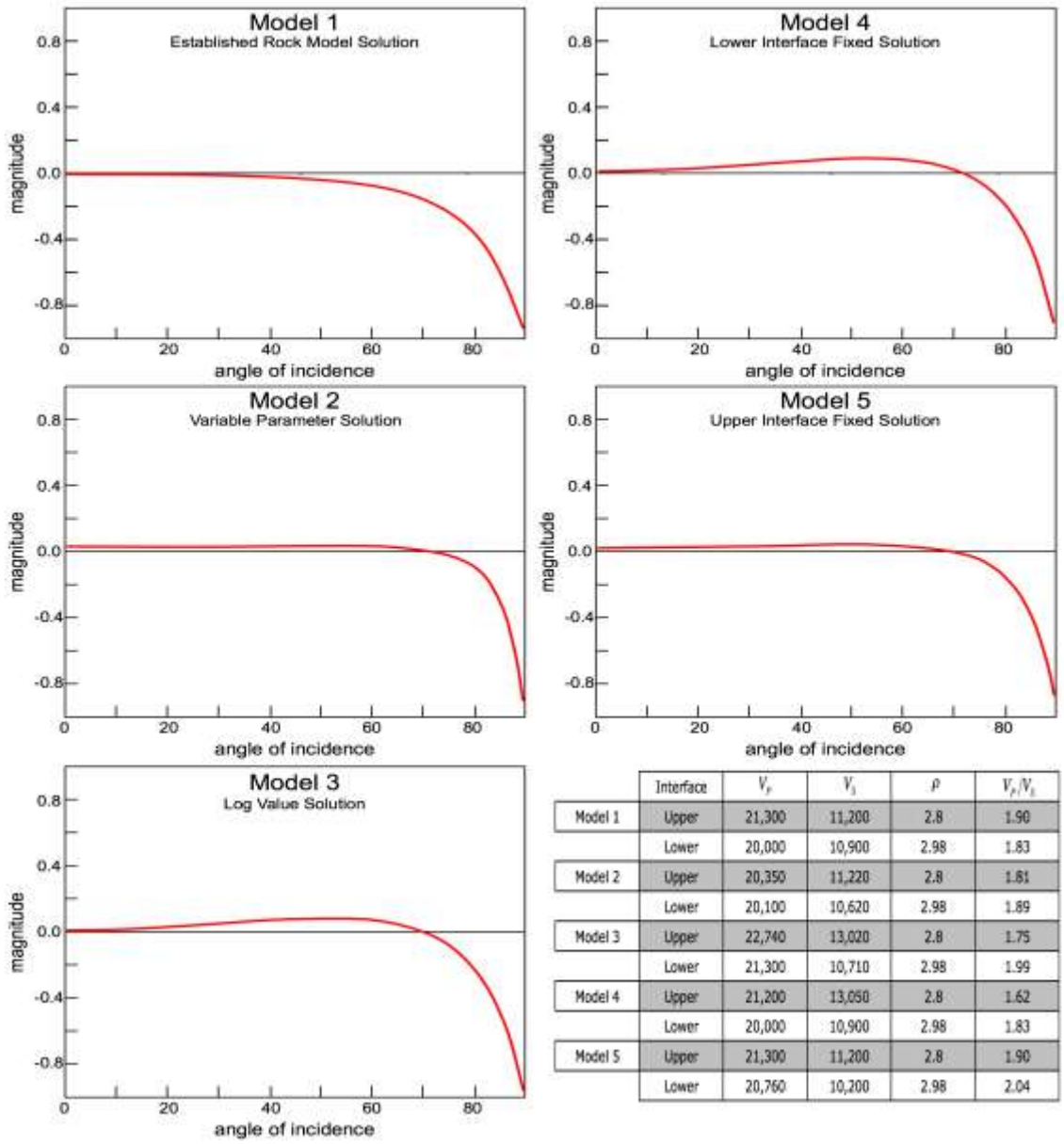

	Interface	V_p	V_s	ρ	V_p/V_s
Model 1	Upper	21,300	11,200	2.8	1.90
	Lower	20,000	10,900	2.98	1.83
Model 2	Upper	20,350	11,220	2.8	1.81
	Lower	20,100	10,620	2.98	1.89
Model 3	Upper	22,740	13,020	2.8	1.75
	Lower	21,300	10,710	2.98	1.99
Model 4	Upper	21,200	13,050	2.8	1.62
	Lower	20,000	10,900	2.98	1.83
Model 5	Upper	21,300	11,200	2.8	1.90
	Lower	20,760	10,200	2.98	2.04

Figure 50: Exact Zoeppritz solutions for the interface between the A2 Carbonate and the A2 Anhydrite for varying layer parameters. Model 1 is the established rock model, and the others are plots for slight variation in Model 1 interface parameters. Descriptions of each model are labeled below model number. Layer properties are listed in table form in the lower right. (Trisch, 2006.)

The seismograms in Figure 51 show no indication of a critical angle response (large increase in amplitude); that is, they are too low amplitude to represent near total reflection. Perhaps this event is similar to the carbonate-anhydrite interface studied over the reef, in the sense that the small positive reflection decreases rapidly to zero (perhaps negative) over the range of angles observed. The reflection itself is very small amplitude measuring perhaps 50 digital counts, where other reflections presented here measure 150

to 250 digital counts. The amplitudes appear to go to zero at wide angles. This is even more apparent when the various interwell distances are combined. This trend fits the same observed trend examined previously with between the carbonate and anhydrite interface, supporting the idea that thin anhydrite layers may exist within Niagaran carbonate reefs. Without a broader angle range, and non-uniqueness of the AVA character makes any interpretation of this interface only speculative. The data could be predicted from a number of Zoeppritz solutions with low positive amplitude trend going to zero for wide angles. While the AVA solution poses no conclusions, other possibilities exist that might explain the nature of the reflection.

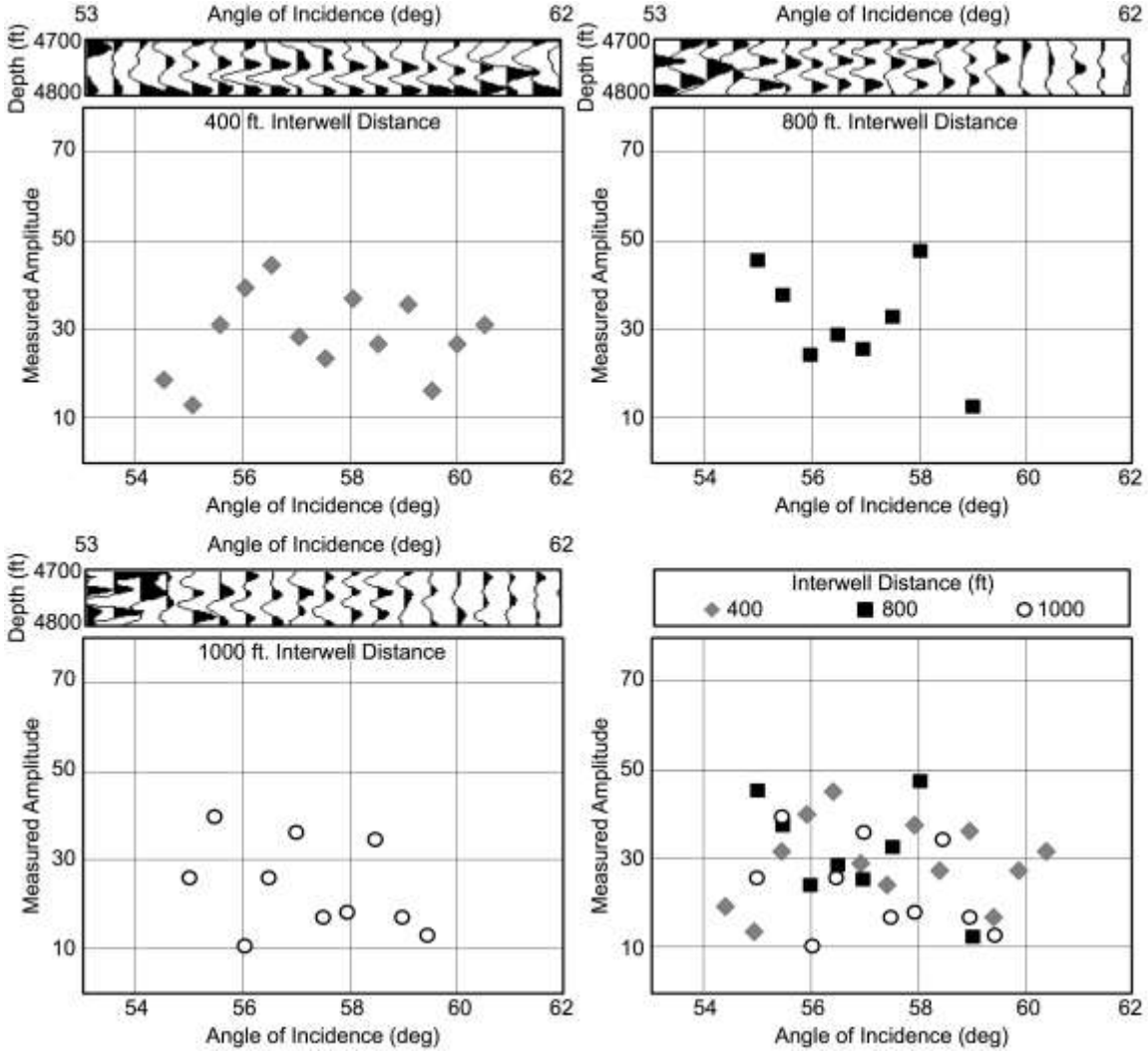

Figure 51: AVA plots (at 0.5° intervals) for the internal reef reflector for interwell distances where the reflector is present. Above each distance is a plot of the reflection character, with residual moveout still apparent. The lower right plot is the combined plot of all distances to show similarities. (Trisch, 2006.)

When the well that is located between the source and receiver wells, the State Springdale 1-20, was first drilled, an oil to water contact was observed at approximately 4787 feet, putting the reflection in Figure 51 in the oil zone of the reef. This zone is now partially

saturated with gas and the reflection may represent the transition of a zone that contains more gas to a patch that contains less gas with more residual oil and water.

Another possibility is that the reflector of Figure 51is a response to change in density and or lithology, and not simply pore fluids. If the geologic interpretation presented earlier is reasonably valid, then the contrast between reef building stages such as carbonate character, dolomitization, and other effects could also produce the subtle contrast that produces a small amplitude reflection at crosswell seismic frequencies.

We do not expect large amplitudes to continue past the critical angle, unless we have been able to properly "track" the reflected event as it passes through large phase changes. Thus, the decrease in amplitude past critical angle may help provide some confidence in our interpretation, rather than casting doubt on it.

In addition, the different raypaths taken by seismic waves at different locations in the profile, even for reflections of identical angle of incidence, can lead to variations in amplitude due to transmission effects. This is shown schematically in Figure 52.

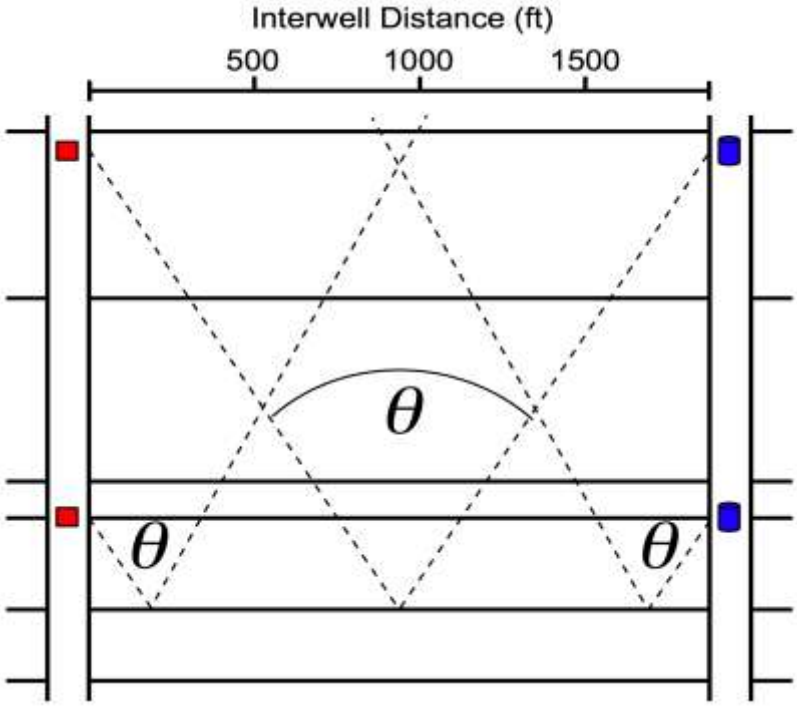

Figure 52: The same angle of incidence at various interwell distances along an interface, is associated with ray paths (dotted lines) that vary greatly in a short horizontal distance. These rays pass through varying lithology as the sources and receivers are located in different beds, even though the angle of incidence is the same. (Trisch, 2006.)

Imaging from Beneath:

One of the most unique aspects of the Springdale dataset was the fact that sources and receivers could be located beneath the target. In virtually all seismic-reflection studies, the sources and receivers are located above the targets being imaged. At the Springdale site, this image is complemented by another one in which the sources and receivers lie beneath the targets being imaged. This is possible because the test wells at this dedicated test site were drilled to extend thousands of feet beneath the reef.

One should not expect the two images to be identical because the reflections should be different when encountering a contrast from one direction or another. In the case of a boundary in which the density and velocity increase with depth, the reflection should have positive polarity and should exhibit a critical angle, when viewed from above. From beneath, however, this same reflection should exhibit negative polarity and no critical angle. Thus, some of the events that we have recognized in previous reports as being due solely to the presence of a critical angle may not be visible at all when viewed from beneath. The AVA character should likewise be different. On the other hand, a model of seismic properties should be able to successfully predict the reflection character from above and from beneath.

There is a reasonable, general, match of seismic reflection events and consistency of reflection polarities for major reflectors. Figure 53(top) shows the (routinely stacked) seismic image of the Springdale site when the sources and receivers are above the reef (the usual case). Figure 53(bottom) shows the same site as imaged when the sources and receivers are beneath the reef. The location of the reef is indicated schematically by the oval on both images for correlation.

It is difficult to compare the two images in detail in a static (paper) report, but a couple of other figures should help. We plotted the "imaged from above" section in black wiggle-trace mode (showing a decimated sample of traces for visibility), and the "imaged from beneath" section in red wiggle traces but with reversed polarity. We then overlaid these sections – once with the red traces on top and once with the black traces on top. Areas extracted from these are shown in Figure 54. It can be seen from these two images that the major reflectors are in fact replicated nicely, and that the reversed polarity display for one of the images is appropriate, as expected.

Some of the similarities and differences in details between the two images are worthy of some speculation, even at this stage of analysis – however, subsequent study may refute this. The reef appears to be an attenuating zone in both cases; this supports the notion that it is a property of the reef that causes the attenuation, whether it be fluid content/ low pressure, or high-density of scatterers. The flanks of the reef are apparently seen on both images, but a Fresnel-zone effect (essentially sideswipe) of a previously suspected "notch" in the reef is only visible from above, which may be compatible with the ray geometry for this situation. Some of the reflectors within the reef are seen on both images while others are not. The absence of reflectors seen on one image from the other image may provide support for the "critical angle" visibility of those reflectors as previously suggested by us.

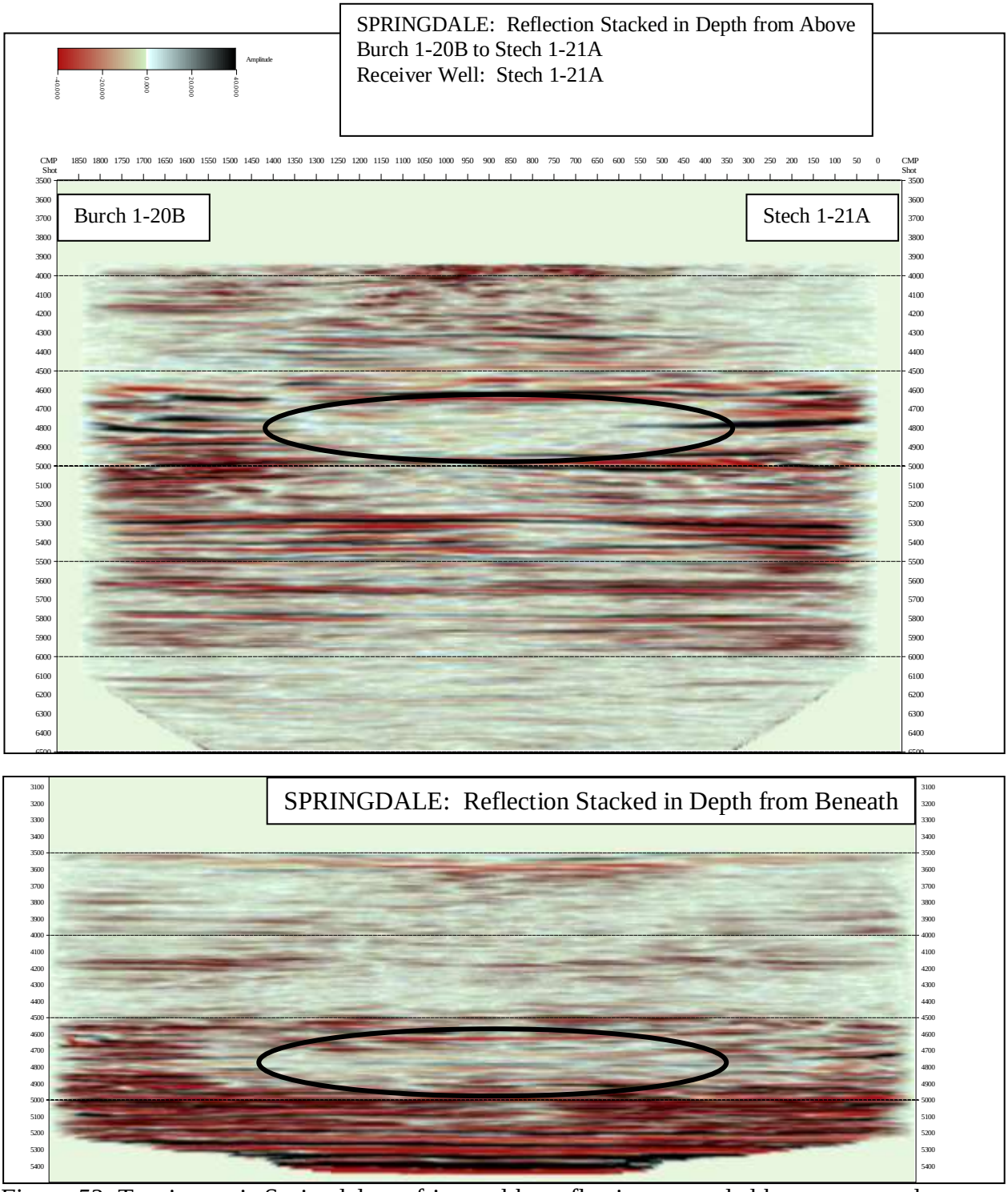

Figure 53: Top image is Springdale reef imaged by reflections recorded by sources and receivers located above the reef; bottom image is the same reef imaged by reflections recorded by sources and receivers located beneath the reef. The general location of the reef is indicated by the oval on both images.

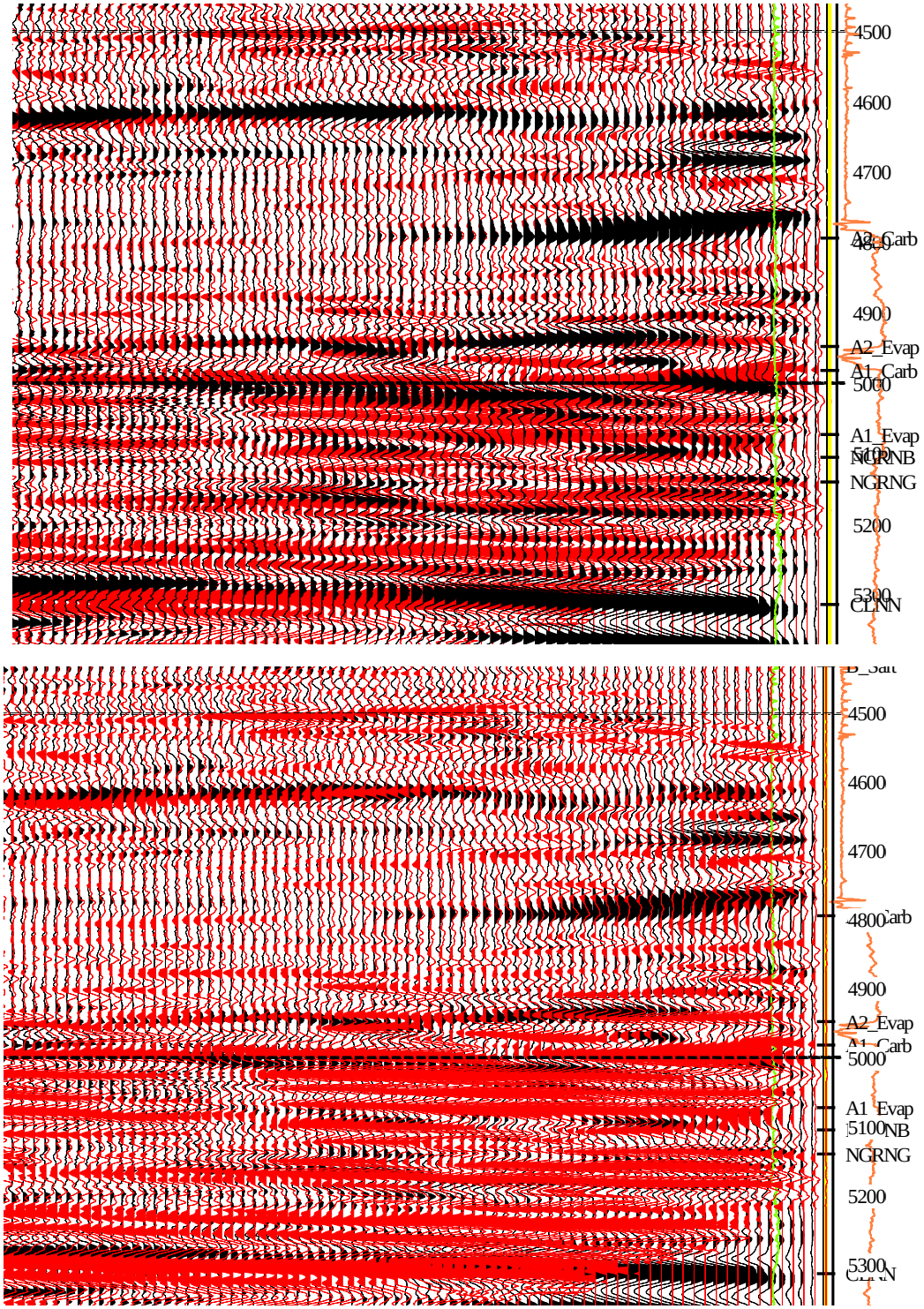

Figure 54: Overlays of Springdale images created from data obtained when the sources and receivers lay above (black) and beneath (red, polarity reversed) the area imaged. The general features and relative polarity (one should be the reverse of the other) are consistent. In the upper figure, the black is laid over the red; in the lower figure, the red is laid over the black.

Inversion of Springdale Seismic Data:

Seismic waves reflect from interfaces exhibiting contrasts in elastic properties (including density). Through a process of integrating the reflection coefficients that are derived from the reflection amplitudes, one can generate an image of acoustic impedance for normal-incidence reflections. This process is known as inversion, and is very useful in converting seismic data into formation properties. In addition, the careful processing required to remove the wavelet from the data results in resolution of extremely fine layering and can identify trends that are difficult to spot on raw seismic data.

This technique can be extended, through the use of a concept called elastic impedance, to non-normal-incidence seismic data. In general, one can create partial stacks of differing angle ranges and invert them, solving simultaneously for an earth model in which the two or three elastic properties (compressional and shear impedances, or compressional and shear velocities plus density) are consistent across all angle ranges.

In crosswell data, we have angles that are far from normal incidence, presenting us with cases not previously encountered in the literature on inversion and interpretation. First, we present results for Springdale from the stacked data, treated in the inversion process as if it were normal-incidence data. Then, we look at inversion of partial stacks and elastic solutions. Finally, we also look at inversion of the stacked data as imaged from beneath (with source and receiver locations located beneath the image).

Figure 55 shows the result of inversion of the stacked crosswell seismic data.

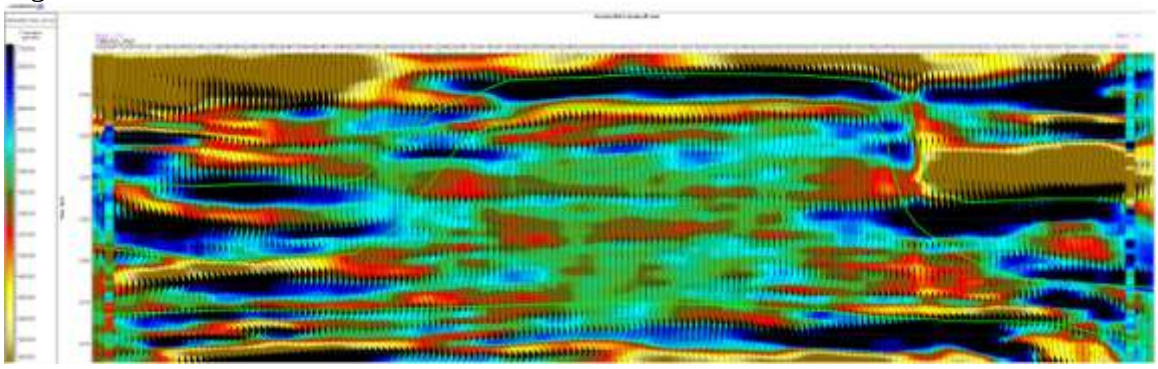

Figure 55: Inverted Springdale seismic data. Only the area around the reef is shown here. The green lines indicate horizons used in guiding the inversion, and show the rough outline of the reef itself. Warmer colors (red, yellow) indicate apparent low impedance, while cooler colors (green, blue) indicate apparent high impedance. Because the data are not normal incidence, the correlation to impedance is not precise, and may have significant errors in places; however, the variations are real.

From the inverted data, we can readily identify the reef and observe several interior layers that are fairly continuous across the reef. In order to take advantage of the range of angles present in the data, inversion of several partial stacks was performed. The input stacked data are shown in Figure 56, and the inversion results are shown in Figure 57.

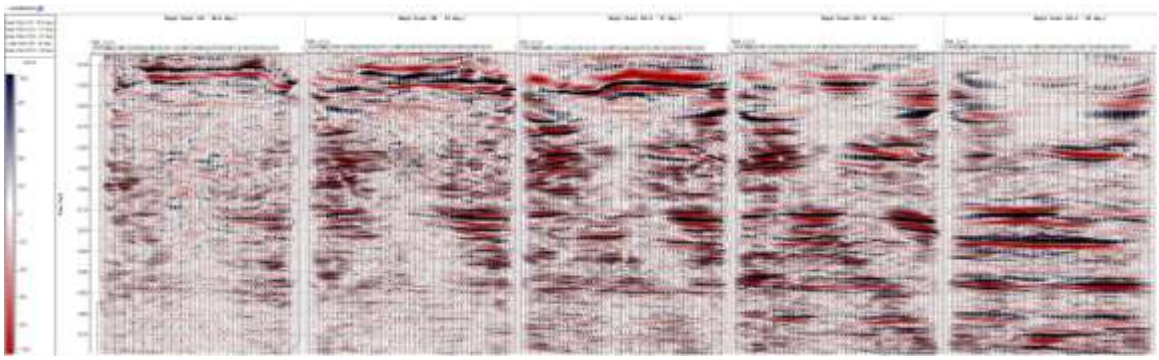

Figure 56: Five angle stacks, representing angles from 36º to 69º. Only the region around the reef is shown here, although the full data set was used.

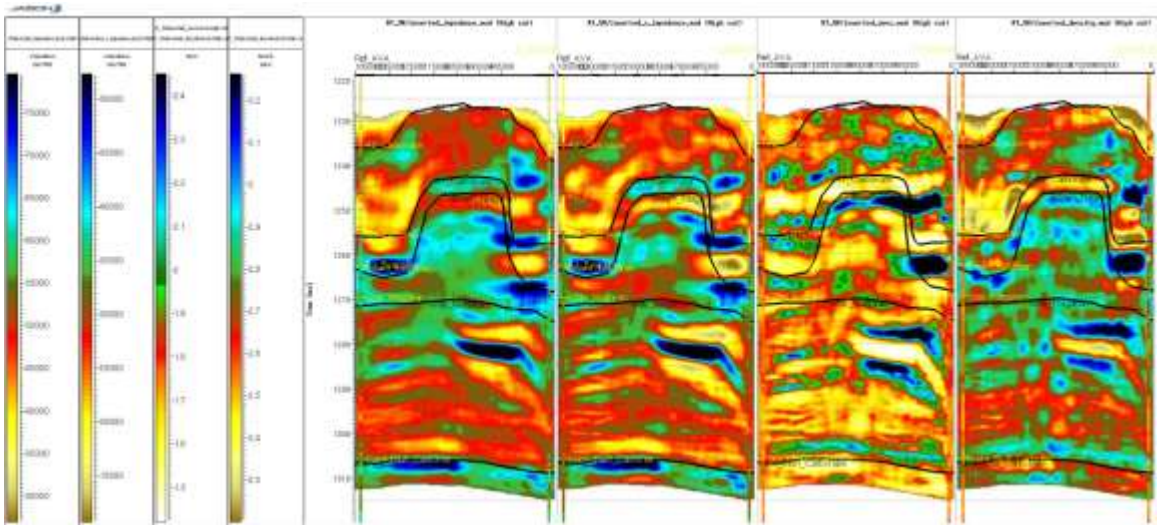

Figure 57: Results of elastic inversion, using the five angle stacks shown in the previous figure. These results are expressed in terms of P-Impedance, S-Impedance, Vp/Vs ratio, and density, from left to right (with scales shown to the left).

The elastic inversion results are products of a simultaneous inversion using the full Zoepprittz equations, and should, therefore, be valid, assuming that our input data contained sufficient breadth of angles to constrain the results. In any case, the results show a distribution of internal layers that is reasonable for this reef.

The use of five angle stacks in the elastic inversion allowed the use of the full range of angles in the data. Many of these angles, however, are likely to be beyond the critical angle for many of the interfaces in the reef, and the phase rotation that occurs beyond critical is not accounted for in our processing. As a result, we also performed elastic inversion for the first three angle stacks, allowing angles only from 36º to 48º. The results for elastic properties are shown in Figure 58.

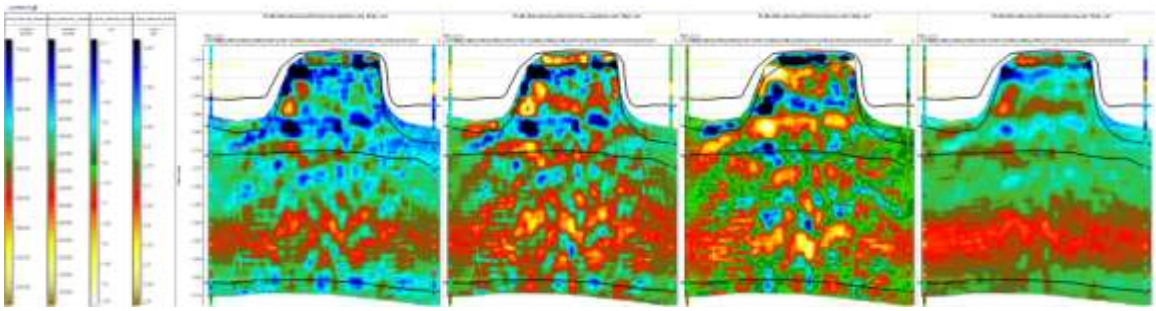

Figure 58: Results of elastic inversion for the first three angle stacks alone. Inversion above the reef was not included, because the A2 carbonate critical angle is less than the maximum angle allowed. Results show P-Impedance, S-Impedance, Vp/Vs ratio, and density, from left to right.

The results of elastic inversion for the limited angle range are probably more reliable than for the complete angle range because it avoids likely critical angles, but the limited angle range also allows for less well-constrained results. Higher density regions are lower porosity, perhaps plugged with anhydrite in the limit, while lower density regions are higher porosity.

The Springdale site allowed for imaging from beneath. Figure 59 shows a comparison of the stacked images, concentrating on the reef area, from above and from beneath.

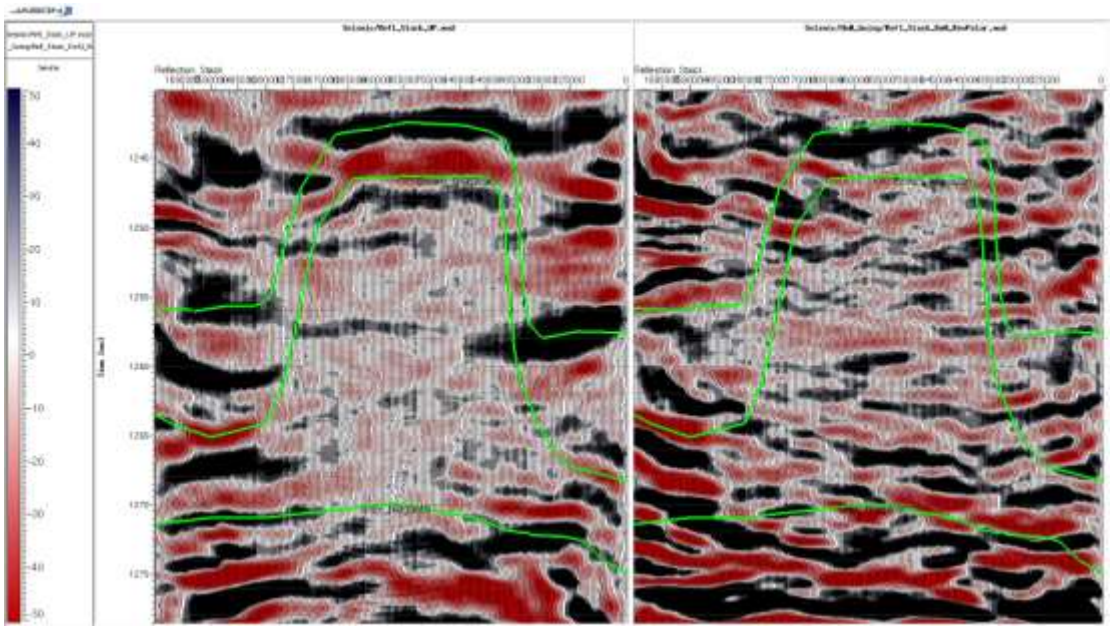

Figure 59: Seismic (stacked) section in the area of the reef, for Springdale. The image on the left shows the stack when sources and receivers are above the image, and the one on the right shows the stack when they are beneath the image.

These stacks were inverted, and the inversions are compared in Figure 60.

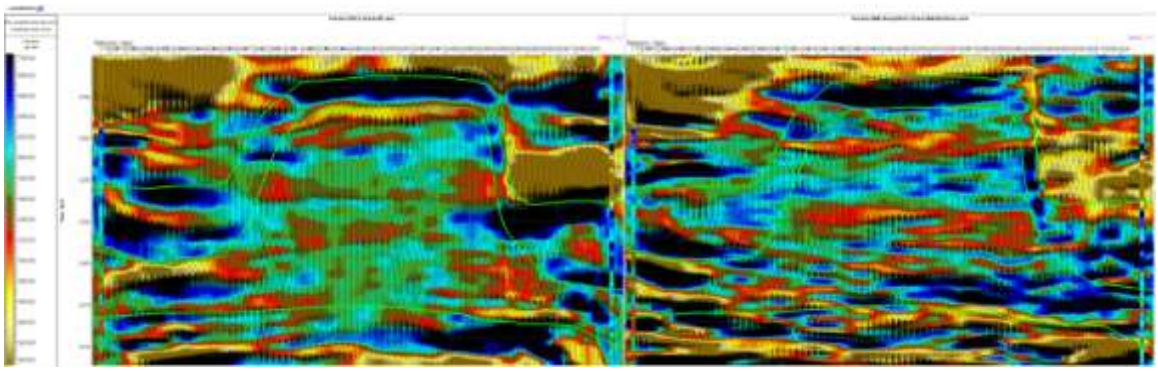

Figure 60: Inverted stacked Springdale images. The left figure is imaged from above (same as shown in Figure 55), and the right figure is imaged from beneath.

The imaging from beneath results in the recognition of layers that are higher resolution and more continuous than imaging from above. This is probably related to the fact that the ray paths connecting sources and receivers beneath the reef with their reflection points do not experience the attenuation and/or scattering that those above the reef because of the simpler geologic structure at the base of the reef. The areas of lower apparent impedance (yellows to reds) indicate higher porosity, while the higher apparent impedance (greens to blues) indicate lower porosity, with anhydrite plugging at the limit.

The bandwidth of signals received beneath the reef is also greater, as indicated in Figure 61, which may also lead to greater fidelity when imaging from beneath.

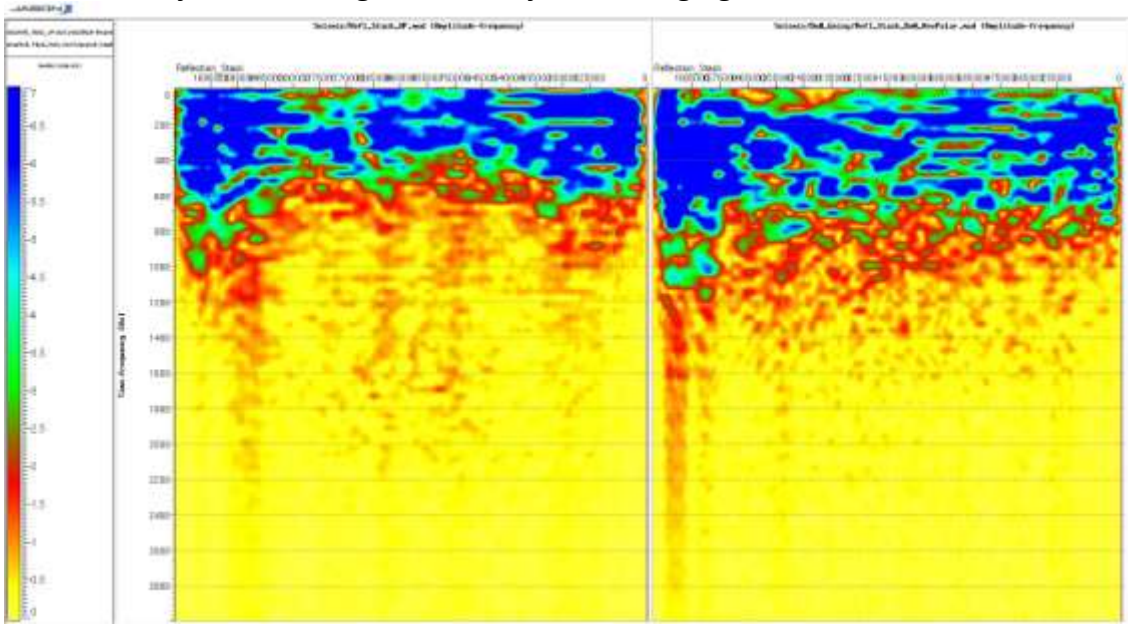

Figure 61: Spectra of seismic data from above (left) and from beneath (right). This shows that the data recorded when sources and receivers are beneath the reef contains higher frequencies, allowing for improved imaging.

Coldspring Site:

The first test site, although well-characterized due to the long operation of test wells outside of the producing reef, suffered from the fact that the source and receiver wells were themselves outside of the target reservoir. The second test site was sought in a field where two wells could be occupied that were both within the producing reef. The Coldspring site met that criterion, as well as having somewhat higher pressure, about 1000 psi (7 MPa). Figure 62 shows a comparison of well locations with respect to a schematic standard reef and log signature.

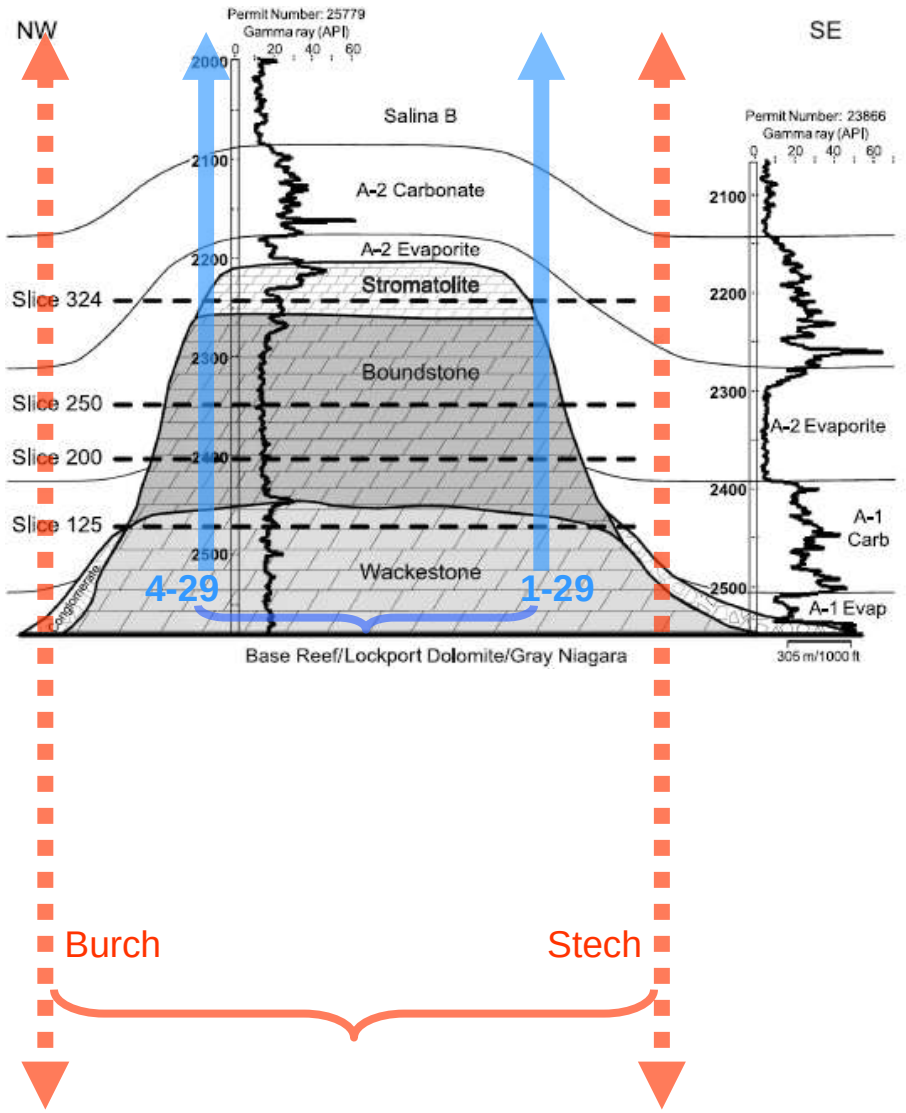

Figure 62: Schematic figure of the sites used in this study. The red dashed lines indicate the general location of the wells used at Springdale, which extended far below the reef, but were outside of the reef. The blue solid lines indicate the general locations of the wells used at Coldspring, where the wells penetrated most of the reef. Notes: vertical exaggeration in this figure is about 10:1; the depths (in feet subsea) are accurate only for the Belle River Mills Reef, not our sites. The image of a reef is taken from the work by Wylie and Wood (2005), under DOE contracts DE-:

AC26-98BC15100,
FC26-00BC15122,
FC22-93BC14983,
FC26-02NT15441.

The overall frequency content of the seismic data was lower than in the first survey, due largely to a source of noise in the receiver borehole that resulted from minor flow through perforations. In spite of this, very good images resulted. At this point, we have only investigated the fully stacked image, and have not yet studied the prestack data. The two wells were drilled at different times, and logs are available from both. For the earliest-drilled well, a set of cased-hole logs run after 25 years of production is also available. These logs are somewhat difficult to fully reconcile, but our current interpretation yields an estimate of an elevated oil-water contact and perhaps a couple of watered-out "stringers" within the oil zone. We will treat the log data first in this report, and then combine that with the seismic image.

A summary of the first-drilled well is provided in Figure 63. The conventional display of saturation reflects the original (1976) open-hole condition, and an overlay shows the later (2001) condition.

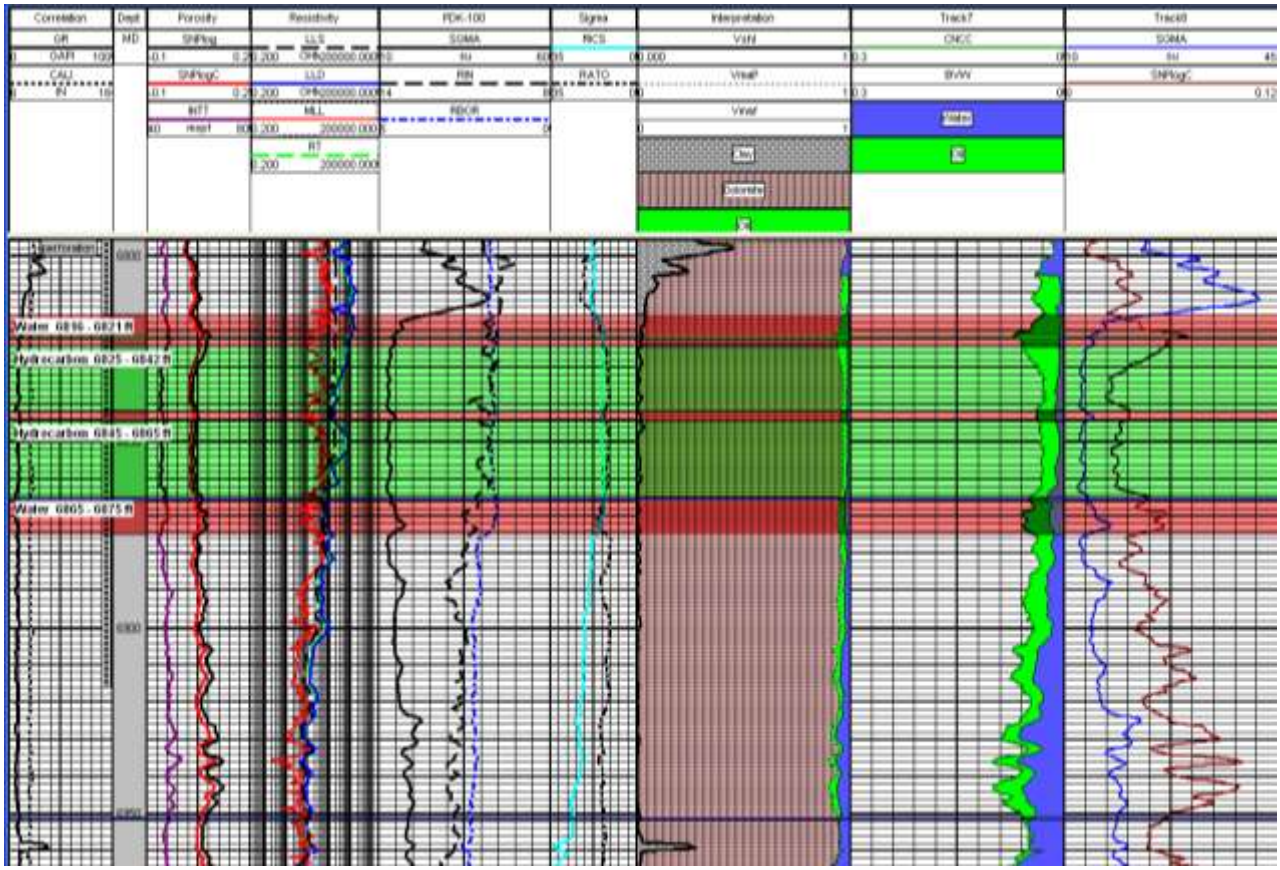

Figure 63: Log display of the first well (1-29) drilled at the second survey site. The track showing the saturation profile is based on the original open-hole logs, while an overlay of red and green bands is based on the cased-hole logs run after 25 years of production. The original oil-water contact was at 6950ft (from KB, not subsea), while the new oil-water

contact is found at 6865ft. Additional possible water streaks at higher levels are indicated by red bands.

The later well, 4-29, was drilled in this same reservoir and logged in 2002. Because of the differential pressure (reservoir pressure was only about 1000 psi at 6800 ft depth), the logging tools experienced sticking, and the radioactive tools could not be run open-hole. After casing was set, a cased-hole suite was run. An interpretation of this suite of logs is shown in Figure 64, although the saturations indicated cannot be trusted, due to the large amount of fresh water used to control the well having invaded the formation.

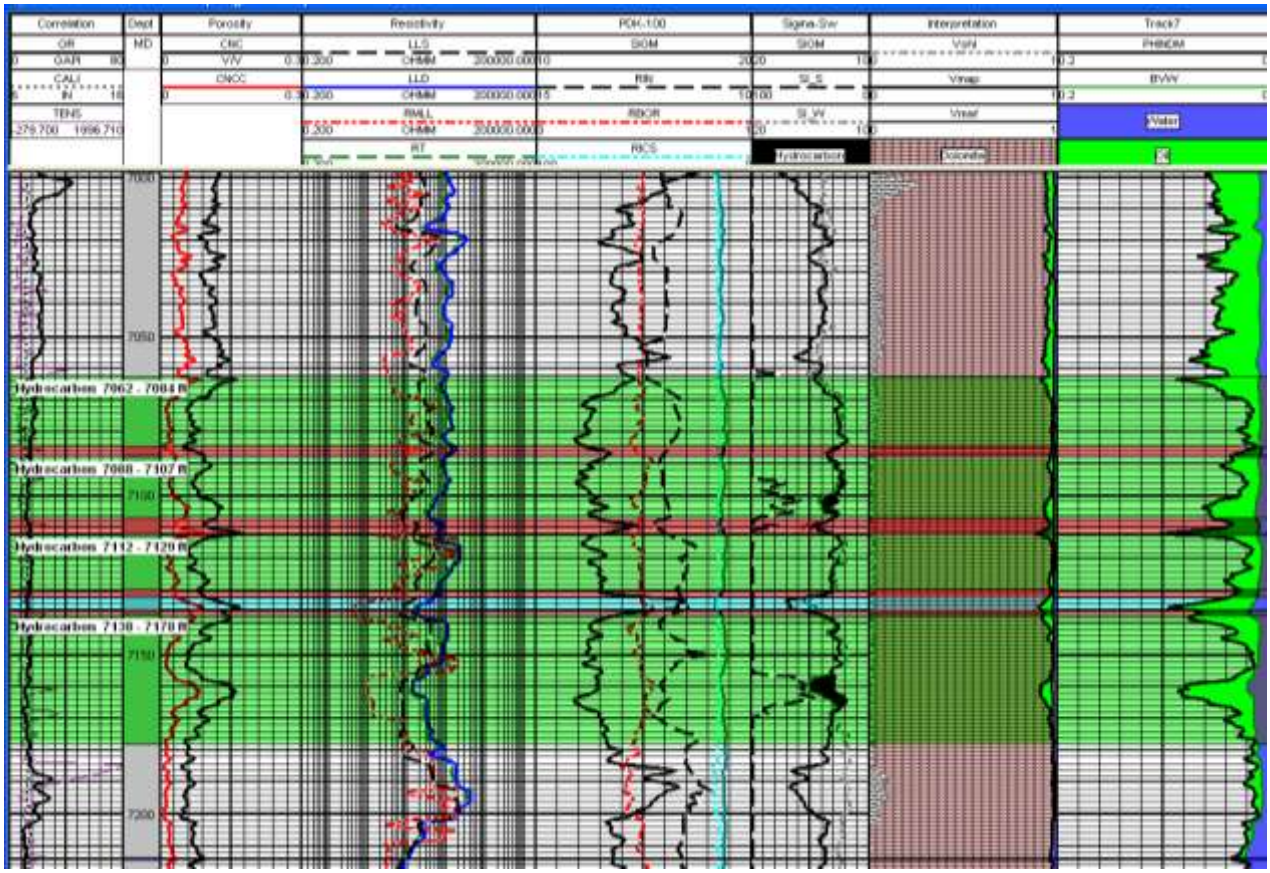

Figure 64: Log display of the last well (4-29) drilled at the second survey site. The previous figure describes the key aspects of the log traces and overlays. The interpretation shown here is not reliable, due to the large amounts of fresh water that had invaded the formation during efforts to control the well. Depths are measured, not true vertical depths and cannot be compared with the previous figure.

The two wells are at the edges of the survey (they were used as source and receiver wells) and can be used to interpret the features evident on the seismic image shown in Figure 65. The dipping upper edge of the reef (and draping sediment layers) can be directly imaged in this data set.

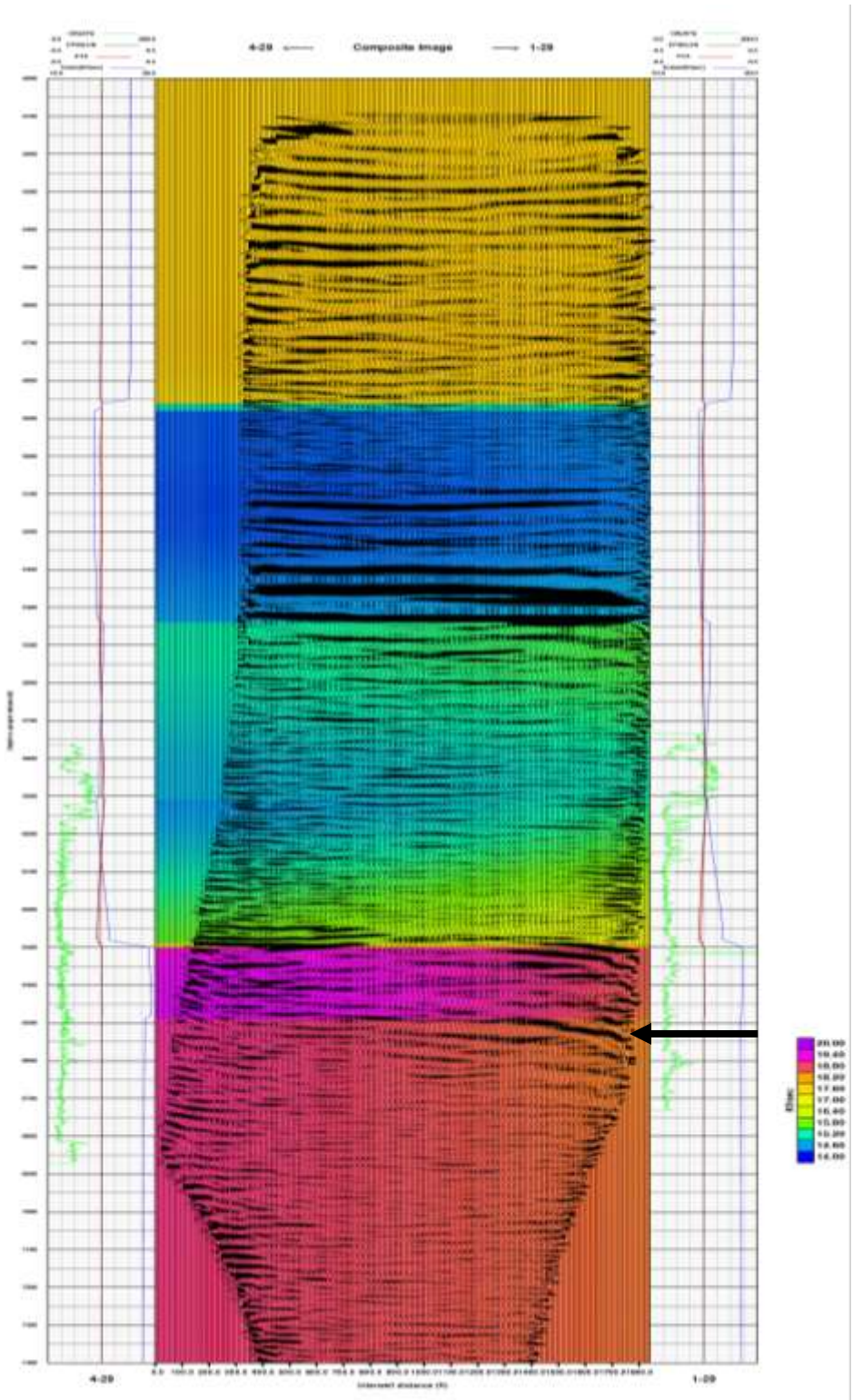

Figure 65: Coldspring image from ZSeis; colors indicate tomographic velocities and wiggle traces are the stacked seismic data. The reef is located beneath the arrow. (Most later figures have left and right reversed from this image.)

Another image of the stacked data is shown in Figure 66.

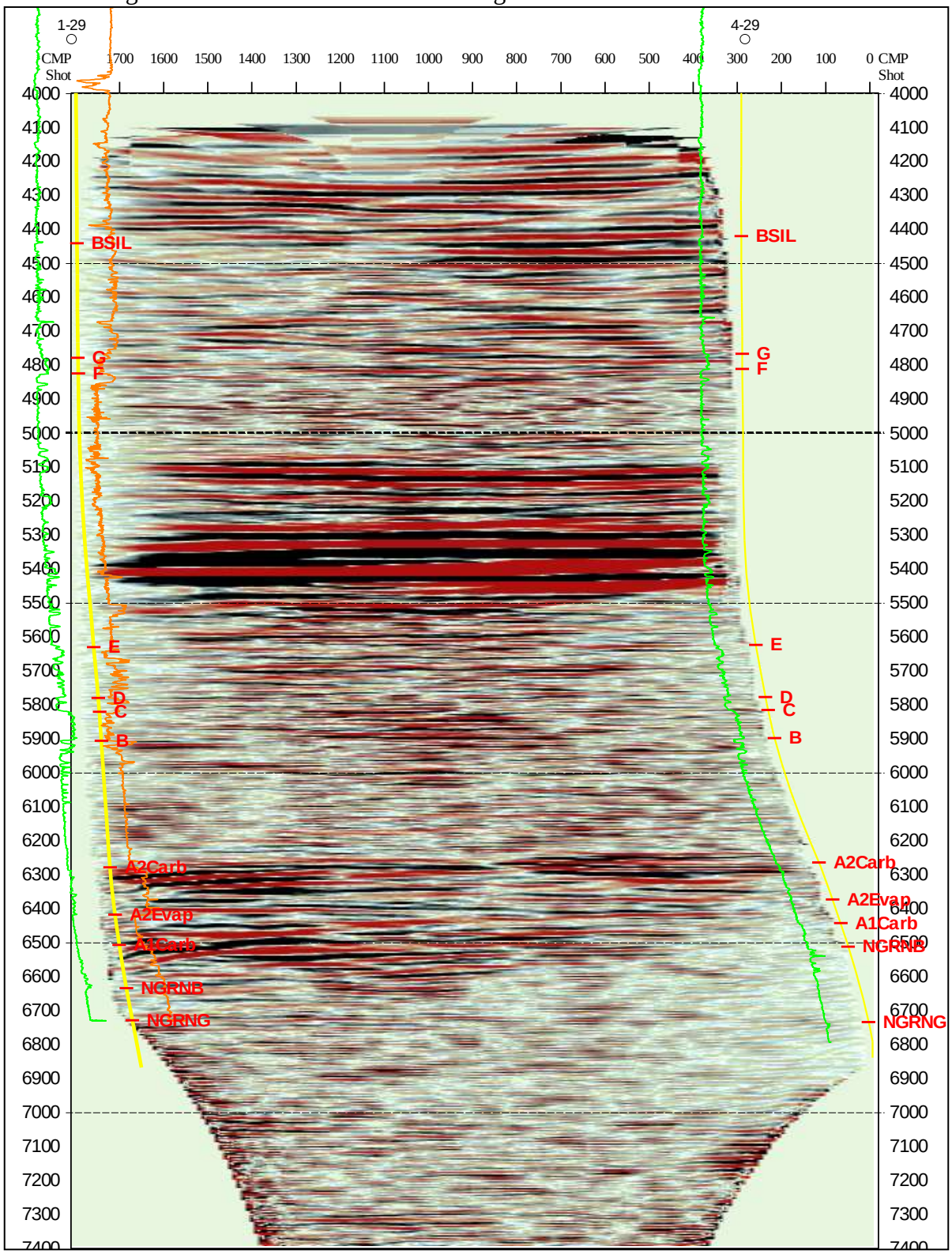

Figure 66: Routinely processed crosswell seismic section for Coldspring. The green logs are GR and the orange log is DT (only available for the 1-29 well). The top of the reef is

indicated by the log pick NGRNB (Niagaran Brown) and its base by NGRNG (Niagaran Gray). (Large reflections at 5400 ft are from the F Salt.)
A log-based cross-section (see Figure 67) shows that the top of the reef exhibits some dip, while most of the other layers are flat.

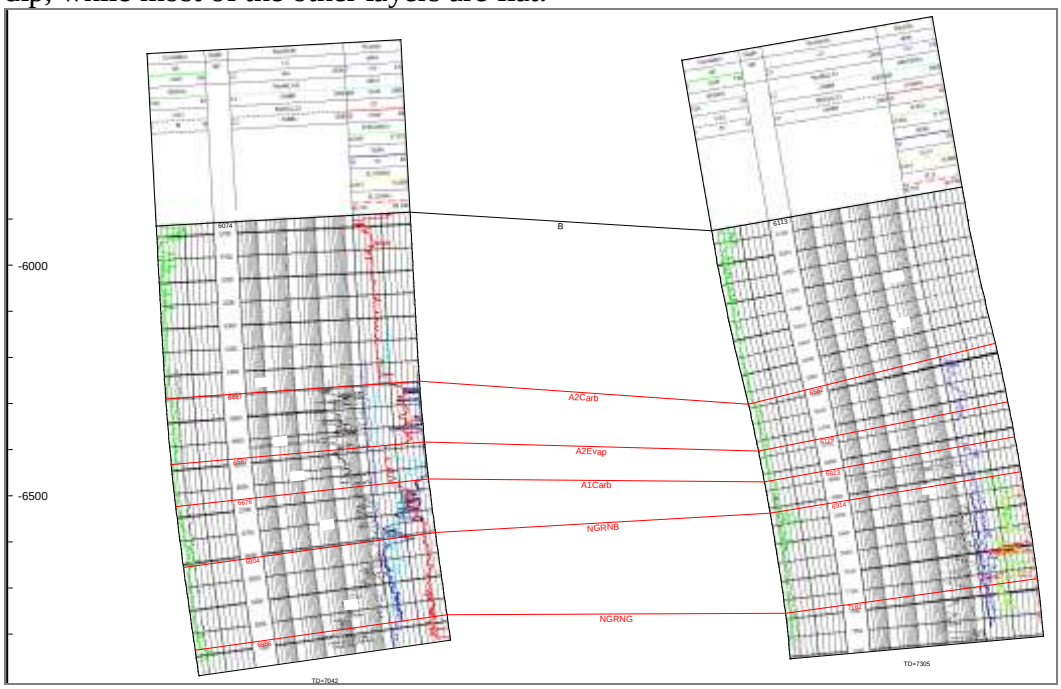

Figure 67: Log-based cross section of Coldspring.

Figure 68 shows a set of slices through the 3D volume of the crosswell data, in which the "y" direction is the angle of incidence (rather than crossline). The following figures are the slices themselves.

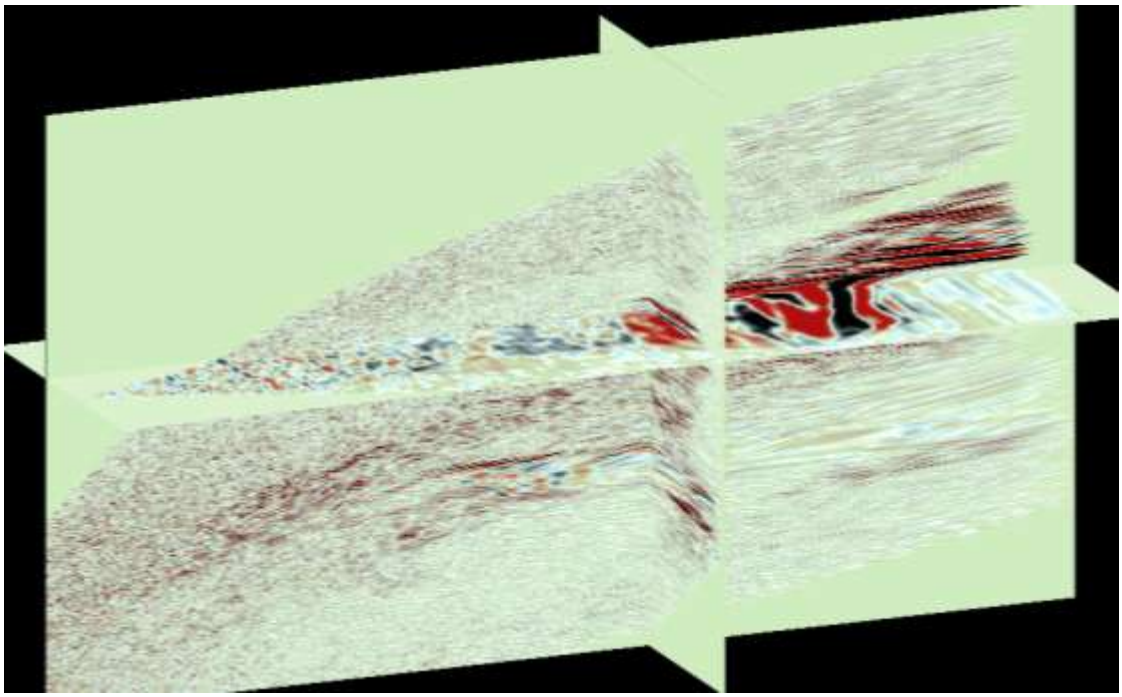

Figure 68: Slices through the "3D" volume generated by loading the angle of incidence prestack data as the "y" direction.
A typical angle gather is shown in Figure 69.

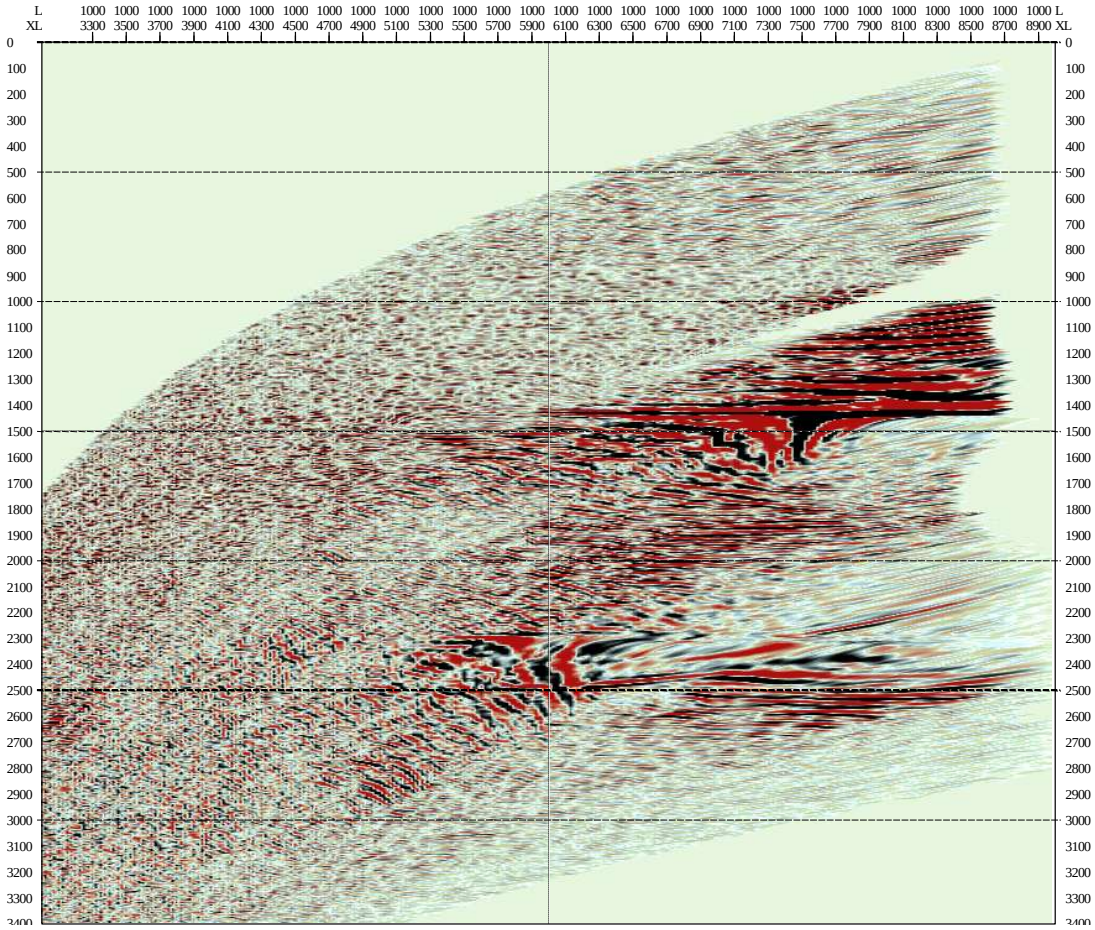

Figure 69: A pre-stack angle gather at one location (1000 ft from one of the wells) showing depth in the vertical dimension and angle of incidence from 30º on the left to 90ºon the right.

In spite of the lower-quality raw data, due to the noise generated by fluid flow through perforations, the image created at Coldspring shows more detail than that created at Springdale. This can be due, in part, to the fact that the wells were within the reef, and distortion due to passage through a complicated set of boundaries is avoided, but it may also be due to the higher pressure within the reef and lack of associated attenuation.

Inversion on this dataset was conducted and led to the following set of results. Figure 70 shows the stacked inversion image with some interpreted horizons. The detail at the top of the reef is remarkable, and it is practical to map the upper surface with confidence.

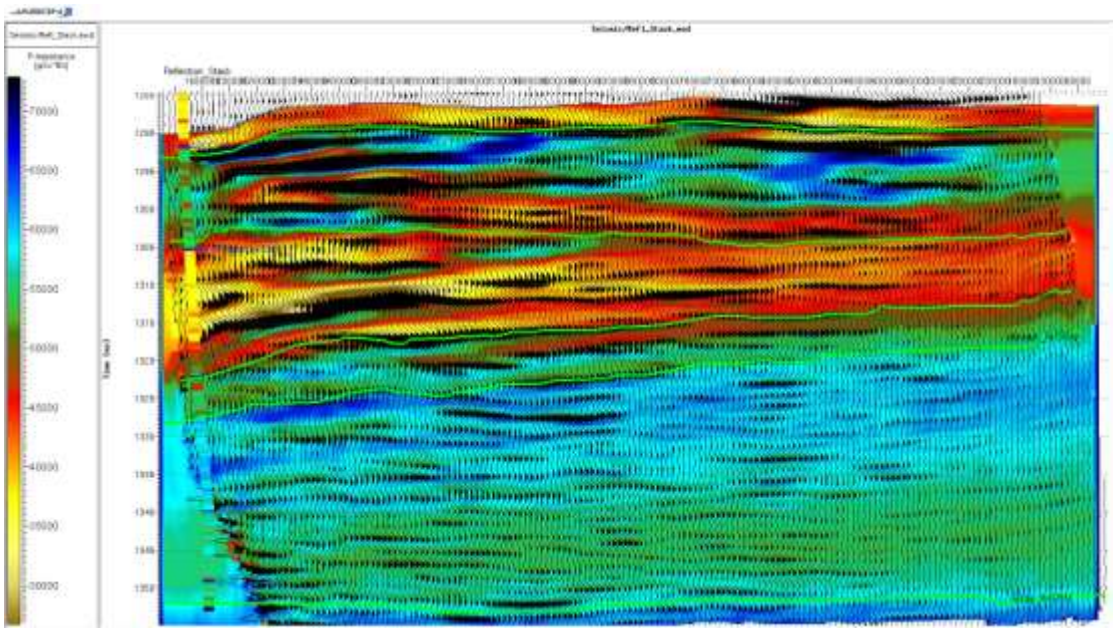

Figure 70: Inversion results for the stacked Coldspring profile, with interpreted horizons. The upper green line is the top of the A2 carbonate; the bottom green line is the top of the Gray Niagaran (base of Brown Niagaran, the reef-forming formation). Horizons in between are discussed in the text.

The flat-lying layers constituting the top of the A2 carbonate and the top of the Gray Niagaran were easy to pick on the seismic section, and these picks agree with the inversion results, as seen in Figure 70. The dipping layers representing the top of the Brown Niagaran and the A1 carbonate are likewise easy to pick, and can be beneficial to reservoir engineering. The green line identified as A2 evaporite is located along a reasonable event as seen on the seismic data, but appears within the "orange-red" layer of lower apparent impedance, rather than at its upper surface. This may indicate that the seismic pick is not appropriate, or it may indicate that the properties of these layers change away from the control well as the reef gains elevation, as may be expected. The inversion process "sees" lithology, while the seismic interpretation is based on boundaries; as rock properties change laterally, inversion makes the change more apparent. The quality of the image degrades slightly as we move from the source well, on the left, to the receiver well, on the right. This is consistent with a decreasing signal-to-noise ratio as expected (Lazaratos, 1993) away from the source well.

We can increase magnification of the image, zooming in on the reef area, and changing the color scale to assist in observing subtle changes within the reef. Such an image is shown in Figure 71. On this image, another horizon has been picked, at the depth indicated by logs as the original oil-water contact. This is also a lithologic contact, where the low-porosity Brown Niagaran increases porosity with depth. Thus, it is seen as a decrease in apparent acoustic impedance with increasing depth, contrary to what might be expected if the contact were purely fluid-based.

We do not see unambiguous indications of any fluid contacts within the reef, and we suspect that all the boundaries apparent in the seismic and inversion images are due to lithologic changes.

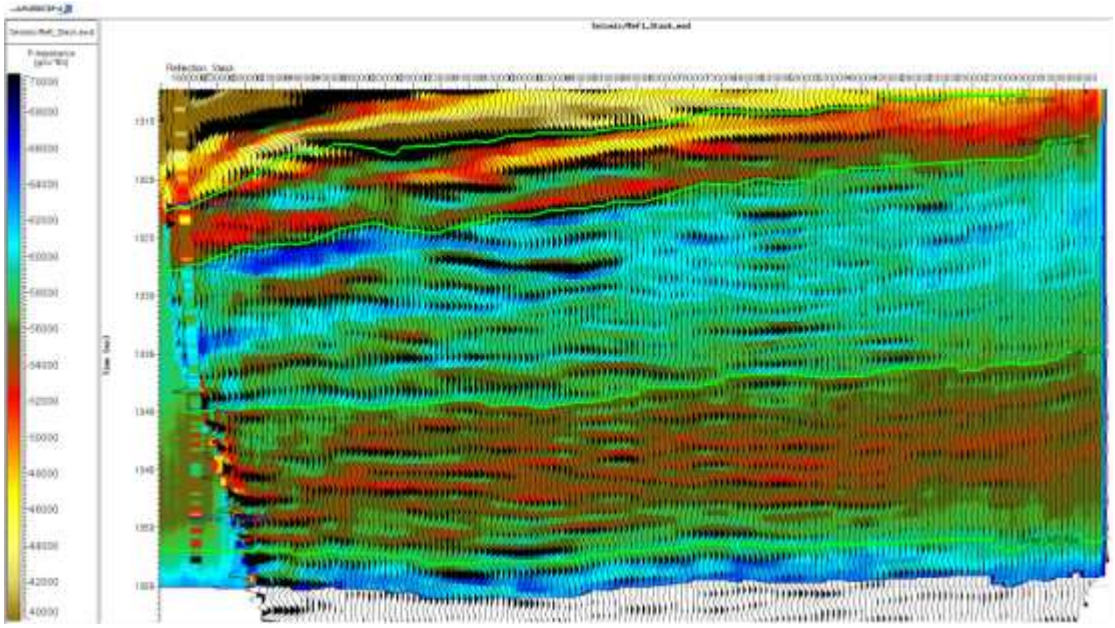

Figure 71: Closeup of the Coldspring crosswell seismic data and inversion results. Note that the color scale has been changed from Figure 71. This image has added another "horizon", picked from logs and at the location of the original oil-water contact.

The images in Figure 71 and 72 clearly demonstrate some of the value of crosswell seismic imaging. The top of the reef is visible as the dipping event, as well as some of the overlying strata, also dipping until the flat-lying sequence of sedimentary layers resumes. This is invisible on surface data, although indirect evidence, through loss of reflection character due to de-tuning, can be used to map rough extent of reefs. Interior to the reef, we observe largely flat-lying reflections, some of which are moderately continuous, but many of which are not continuous across the reef. These are most likely lithologic boundaries, some of them representing inclusions of anhydrite, while others represent variations in reef makeup and porosity. Zones that are demonstrated by inversion to be of lower apparent impedance are likely to be zones of increased porosity. In Figure 72, the lower-most portion of the reef is shown with streaks of orange and red color, mixed in with the green layers. These orange and red layers indicate lower porosity; unfortunately, these are within the water leg of the reef and are not expected to be productive. However, similar, but smaller and less continuous, zones of red and orange can be seen in the productive portion of the reef, appearing to represent higher-porosity intervals within the oil-and-gas-bearing portion. The streaks of anhydrite are most likely encountered where the colors within the productive interval are blue and dark blue, representing higher apparent impedance.

INTERPRETATION AND CONCLUSIONS

Crosswell seismic imaging of the two reefs has provided data that is well beyond any that a reservoir engineer or development geologist has previously had for improved characterization and production. On the other hand, the level of detail provided is almost overwhelming, and not completely unambiguous in its interpretation. Here we provide a summary of the most significant aspects of the reservoirs as gleaned from the crosswell data sets.

Both reservoirs have been produced for many years, and although they originally contained exclusively oil (and connate water), they are now also strongly gas-saturated, and produce gas and water in addition to oil. Both reservoirs are essentially volumetric drive, with minimal water encroachment, if any. Thus, they have been drawn down to very low pressures: 25-50psia (172-345kPa) at Springdale, and about 1000psia (7000kPa) at Coldspring. Many reefs in the Michigan reef trend are known for their volumetric character, and are used as gas storage facilities, because they do not allow water encroachment and they retain pressure changes without diffusing the pressure throughout a large aquifer. As a result, the original oil-water contact rarely moves significantly during production, rather than pulling up as is often seen in water-drive fields. The cased-hole logs run in 2001 (after 25 years of production) at Coldspring demonstrated that the water table has not moved more than three feet during that time. On the other hand, the same logs demonstrated that what was originally an oil-water contact is now a gas-water contact, although some oil is likely still in place.

The original oil-water contact in many reefs coincides roughly with the lithologic boundary where the lower-porosity reef material overlies higher-porosity reef material (perhaps the "boundstone" over "wackestone" interface, using terminology from Wylie and Wood, 2005). The decrease in apparent impedance is consistent with this lithologic difference, and indicates that, at best, the fluid contrast is of secondary importance in imaging.

As a result of these reservoir characteristics, we were not fully able to demonstrate the ability of the crosswell technique to identify fluid contacts, although one reflection in the Springdale reef exhibits characteristics which are consistent with a gas-fluid contact, but without confirmation. In formations with higher porosity and/or weaker rock matrix, the fluid contacts would have been apparent, and in fields under different drives, a time-lapse version of this experiment would have been able to monitor water movement or gas-cap growth.

The crosswell seismic imaging technique has demonstrated that internal features within the reef can be imaged and characterized. The most valuable aspect of this characterization has been the inversion of data. Until techniques are developed that properly account for phase rotations beyond critical angle, it is probably most appropriate to restrict inversion to stacks that do not exceed that angle. Within this limited range, elastic inversion may be conducted, as demonstrated at the Springdale site, with reasonable results, although acoustic inversion also provides meaningful results, as long

as the interpreter recognizes that the resulting image is not truly "acoustic" impedance, but some sort of narrow-angle "elastic" impedance, referred to in this report as "apparent" impedance. Nonetheless, at these lower angle ranges, a decrease in apparent impedance can be interpreted as an increase in porosity within the reef, while an increase in apparent impedance can be interpreted as a decrease in porosity, perhaps anhydrite-plugged at the extreme, within the reef.

The use of Amplitude-versus-Angle can aid in interpretation, and can assist in reducing ambiguity of interpretation, but the main advantage demonstrated here has been in restricting elastic inversion to narrower angles, avoiding the problems associated with phase distortion beyond critical angle. On the other hand, as demonstrated for some internal reflectors at the Springdale site, the complete stack image is improved greatly by including all reasonable angles in that stack. This is due to the possibility of including in the stack events that are only visible over a very narrow range of angles, presumably near the critical angle. These events would normally not appear in seismic data, but when the critical angle is included in the stack, they will show up in the final image and can be used in interpretation.

The differences in signal quality are interesting in their own right. Springdale site exhibited severe attenuation for seismic ray paths that pass through the reef, a feature that may be related to the low pressure and high gas saturation. The image obtained when the sources and receivers were beneath the reef demonstrates low-amplitude arrivals within the reef, but not as subdued as the image from above; it also provided higher resolution and greater continuity of events across the reef. Coldspring site demonstrated the previously known decrease in signal-to-noise as distance increases from the source well. These three observations lead to a series of conclusions: Imaging through a complex structure containing strong contrasts in fluid properties (and pressure) is more difficult than imaging the same feature from another direction, avoiding these transmission effects. In this case, imaging from beneath, where the structure is simple, is better, although rarely practical in the field. Signal-to-noise can be a problem when the source of the noise is erratic and that noise is difficult to remove; at Springdale, the tube-wave noise was highly organized and did not adversely affect the image, while at Coldspring, the noise was generated by fluid flow and was large-amplitude and poorly organized, affecting the data to the point where degradation across the image was observed.

In summary, crosswell seismic imaging provides the highest-quality images possible within the reservoir, and is practical at resolutions and interwell distances not previously tested. The primary structure of the reef is apparent for the first time in seismic images, and internal reflectors are observed with should be useful in planning continued reservoir development.

TECH TRANSFER

This work involved cutting-edge technology, some of which was not previously proven (specifically the AVA characteristics). During discussions with producers (other than those working directly with us), we found that preliminary results could be confusing and misleading. As a result, technology transfer was limited during the time frame of the project to discussions with other experts in the field and presentations at professional-society meetings, including the Seismological Society of America (2007) and Society of Exploration Geophysicists (Carillo et al, 2007). Feedback received as a result of these presentations was found to be very useful. Now that the technical work has been completed, and conclusions can be drawn firmly, presentations will be made at venues where producers will be in attendance, and publications in both the scientific/expert journals and industry trade journals will be prepared.

ACKNOWLEDGMENTS

We thank Merit Energy for access to wells and data. ZSeis contributed beyond their contractual requirements, and were true colleagues in this analysis. Software was provided by Fugro-Jason, Landmark Graphics, GeoTomo, and Schlumberger.

REFERENCES:

Gill, D., 1977, The Belle River Mills Gas Field: Productive Niagaran Reefs Encased by Sabkha Deposits, Michigan Basin, Michigan Basin Geological Society, Spec. Paper No.2, pp. 188.

Lazaratos, S., 1993, Crosswell Reflection Imaging, PhD Dissertation, Stanford University; also printed as Stanford Seismic Tomography Project, Vol. 3 No.2.

Pedro Carrillo, Milagrosa Aldana, Brad Bryans, and Roger Turpening, Attenuation coefficient tomogram and Q distribution image from crosswell survey in the Northern Reef Trend of Michigan Basin; SEG Expanded Abstracts 26, 1252 (2007), DOI:10.1190/1.2792731

Smith, B.A., Gallagher, J.G.,Hoover, G.M., Hufford, J.M.,1993, Characteristics of crosswell wave propagation at varying well offsets, 55th mtg.: Eur. Assn. of Expl. Geophys., Session: C007

Trisch, S.P. 2006, Crosswell Seismic Amplitude Variation with Angle Studies at a Niagaran Reef, MS Thesis, Michigan Technological University.

Wyllie, A.S., Wood, J.R., 2005, Well-log tomography and 3-D imaging of core and log-curve amplitudes in a Niagaran reef, Belle River Mills field, St. Clair County, Michigan, United States, Bull. Amer. Assoc. Petroleum Geologists, 89, 409-433.